10-My history of felidae endogenous retrovirus gamma4 infections

(ネコ科内在性レトロウイルスγ4感染の1000万年の歴史)

Joint Graduate School of Veterinary Medicine

Yamaguchi University

Dimas Arya Abdillah

September 2025

DECLARATION

September 2025, Yamaguchi University, Japan.

I, **Dimas Arya Abdillah,** I hereby declare that the work presented in this dissertation was carried out by me. Any references to the work of others have been properly acknowledged and cited within the dissertation.

ACKNOWLEDGMENT

I am highly grateful to the Government of Japan, the Ministry of Education, Culture, Sports, Science and Technology, for sponsoring my study by providing me the Monbukagakusho (MEXT) Scholarship.

I would like to express my deepest gratitude to my supervisor, Prof. Kazuo Nishigaki, Ph.D., for giving me the opportunity to explore the field of endogenous retroviruses in his laboratory. His invaluable guidance has greatly enriched my understanding of virology, immunology, infectious diseases, and bioinformatics. I am sincerely thankful for his continuous support, not only in providing a positive research environment, but also in supporting life in Japan, especially during the special time when my first child was born.

I would like to express my deepest gratitude to Associate Professor Ariko Miyake, Ph.D., for her kindness and patience in teaching me experimental techniques and guiding me through troubleshooting in the laboratory. I also had the valuable opportunity to learn from her how to prepare practical classes for the Infectious Disease Lab. Moreover, I am sincerely thankful for her generous support with the Japanese language, whether for research-related documents or personal documents while I stay in Japan.

I would like to express my sincere and profound gratitude to Professor Hiroya Kadokawa, Ph.D., for providing me opportunity to pursue my research in the field of endocrinology, with a special emphasis on the anterior pituitary. I am particularly indebted to him for his kind assistance in enabling my wife to join me in Japan. I also extend my heartfelt appreciation to all members of his laboratory and those who have contributed, directly or indirectly, to the successful completion of my research.

I would like to express my heartfelt gratitude to the members of Hirakawa-no-Kazeno Kai, especially Aunty Ryoco Saito, Tokuhisa-san, and Matsumoto-san, for their endless kindness and support throughout my time in Japan. Their warm presence and generous help especially in caring for my first daughter from the time she was a newborn have meant so much to me and my family. I will always treasure the way they extended their hands whenever I faced difficulties and made Japan feel like a second home.

I would like to sincerely thank all past and present members of Prof. Nishigaki's laboratory for their friendship, collaboration, and generous support throughout my time in the lab. I am especially grateful to Dr. Didik Pramono for his kindness, constant support, and thoughtful discussions, which were invaluable whenever I encountered difficulties in my research.

I am sincerely grateful to my mother, father, and mother-in-law for their unwavering support and constant prayers. Their love and encouragement have been a source of strength throughout this journey, and I truly could not have reached this achievement without them.

Lastly, I would like to express my gratitude to my wife, Dinda Andiniga Mayang Sari, and my daughter, Kazuha Dillara Abdillah, who have never stopped encouraging, praying, accompanying, and supporting me during my doctoral studies so that I was able to get the highest degree in my life.

TABLE OF CONTENTS

GENERAL ABSTRACT

Viral protein–host interactions represent a complex and critical aspect of biomedical research, particularly in the context of endocrine regulation and host defense. The anterior pituitary (AP) plays important role in hormone regulation, which is crucial for maintaining immune balance, homeostasis, and reproductive function. However, aging can impair AP function and lower the body's ability to fight disease. Thus, understanding global gene of AP is important. The viral protein interaction to the host may harmful for host. The severe acute respiratory syndrome coronavirus-2 (SARS-CoV-2) is the cause of global pandemic covid-19. The angiotensin-converting enzyme 2 (ACE2), a spike (S) protein receptor has been documented in AP. Therefore, the covid-19 infection potentially disrupts reproductive hormone. On the other hand, Retroviruses, which have unique ability to converts RNA into DNA by reverse transcriptase enzyme, have different fate when enter the host. They can be released and infect to another host horizontally as exogenous retrovirus (exRVs) and integrated into the genome through germline passing down to the offspring (ERVs). The activity of ERVs is typically silenced by methylation and genetic mutations, such as substitutions, deletions, and insertions. Once ERV becomes fixed within a population, it can constitute a significant portion of the host genome, accounting for approximately 8% of the human genome. The feline leukaemia virus (FeLV) is an exogenous gammaretrovirus that causes malignant haematopoietic disorders in domestic cats. FeLV subgroup A (FeLV-A) is transmitted among cats, and FeLV subgroups are known to generate de novo. In our previous study, we identified a new recombinant FeLV containing an X region derived from Felis catus endogenous gamma retrovirus 4 (FcERV-gamma4). These kinds of ERV–XRV exchange can impact the pathogenicity of retroviral infections. Therefore, tracing the FcERV-gamma4 can provide unique models for not only the modern reservoir of new recombinant viruses but also the genetic features shared among ancient retroviruses. Eventually, the mature product of *env* gene consists of SU and TM subunit, in which SU responsible for receptor binding. However, the defective env-ERV is often observed as a consequence of the interaction between the host and the virus. Unlike mature env protein, the defective env may have beneficial function to the host. This dissertation investigates the functional consequences of viral protein interactions with the host endocrine and immune systems, using cattle and domestic cats as mammalian models.

In Chapter One, I investigated how aging influence gene expression in AP. Using RNA sequencing (RNA-seq), I analyzed AP glands from young heifers (~22 months old) and older cows (~120 months old). Of total 20,171 annotated genes expressed in both age groups. The sum expression of seven key AP hormone genes constituted approximately 41.6% of total transcripts in young cattle and 35.5% in older cattle, indicating a significant decline in hormone gene expression with age ($P < 0.05$). Differentially expressed genes (DEG) were identified genes compared young to old 48 genes downregulated and 218 upregulated. Notably, DEGs included cytokines (AIMP1), growth factors (NRG2, PTN, TGFB1), receptor-associated proteins (AGTRAP), and G-protein-coupled receptors (PRLHR, GPR156, GPR176). Metascape analysis revealed enrichment in pathways related to "Peptide metabolic process," "Regulation of hormone levels," and "Peptide hormone processing." Ingenuity Pathway Analysis highlighted networks associated with neurological diseases, organismal injury, and psychological disorders, as well as canonical pathways like "Huntington's disease signaling" and "AMPK signaling. These findings provide valuable insights into the molecular mechanisms underlying age-related endocrine changes and may inform strategies to mitigate reproductive and health issues in aging livestock.

In Chapter Two, I investigate the potential SARS-CoV-2 spike protein influence reproductive hormone. The anterior pituitary (AP) gland plays a pivotal role in regulating reproductive hormones, notably luteinizing hormone (LH) and follicle-stimulating hormone (FSH), through gonadotroph cells. Expression analyses confirmed the presence of angiotensin-converting enzyme 2 (ACE2) mRNA and protein in bovine AP cells. Immunofluorescence microscopy revealed co-localization of ACE2 and gonadotropin-releasing hormone (GnRH) receptors on the plasma membrane of gonadotrophs, with approximately 90% of GnRH receptor-positive cells expressing ACE2. Treatment of cultured bovine AP cells with recombinant SARS-CoV-2 spike protein (0.07–7 pM) resulted in a significant suppression of both basal and GnRH-induced LH secretion, and a dose-dependent suppression of GnRH-induced FSH secretion. Pre-treatment with an ERK1/2/5 pathway inhibitor partially restored LH and FSH secretion levels. These findings suggest that the SARS-CoV-2 spike protein can directly impair gonadotroph function via ACE2-mediated activation of the ERK signaling pathway, potentially disrupting reproductive hormone regulation

In Chapter Three, I examined the evolution of Felis catus endogenous retrovirus gamma4 (FcERV-gamma4) across the Felidae family. A total of 350 related elements were found across seven cat lineages, some retaining full-length, functional envelope genes. The presence of intact full-length proviruses in the Felidae

ERV-gamma4 suggests that they emerged very recently and spread rapidly in each lineage of cats. To explore host restriction for these viruses, functional envelope proteins from domestic cats (*Felis catus*) and Geoffroy's cats (*Leopardus geoffroyi*) were reconstructed. FcERV-gamma4 and LgERV-gamma4 can infect a wide range of mammalian cell lines. Truncated Env proteins from FcERV-gamma4 (called Refrex-2) are secreted by cells and inhibit infection by these viruses, likely through receptor competition. Refrex-2, which lacks the transmembrane domain, is widely expressed in domestic cats and conserved across Felidae species. Genetic evidence suggests Refrex-2 has been maintained by purifying selection, reflecting a long evolutionary battle with retroviral infections and their significant role in shaping animal evolution.

In conclusion, this study examined how viral proteins influence hormone regulation and immune function in cattle and cats. Aging was shown to impair anterior pituitary function in cows, while the SARS-CoV-2 spike protein suppressed reproductive hormone secretion via the ACE2 receptor. In cats, analysis of FeLV and endogenous retroviruses led to the identification of a new infectious FeLV-B clone. Additionally, the evolution of Felidae ERV-gamma4 produced a truncated envelope protein, Refrex-2, which may inhibit viral infection, highlighting the evolutionary dynamics of host–virus interactions.

GENERAL INTRODUCTION

Understanding the interactions between the endocrine system and viral infections remains a significant challenge in both biology and medicine. The endocrine system plays a critical role in regulating immunity and maintaining homeostasis. Hormones can either weaken or strengthen host defenses, making hormonal status a key factor in determining susceptibility to infections. The anterior pituitary (AP) receives signals from the hypothalamus and various peripheral tissues and serves as a central regulator of the endocrine system by controlling the function of multiple organs. It synthesizes a wide range of bioactive peptides involved in endocrine, paracrine, and autocrine signaling (1). Consequently, the AP expresses numerous genes essential for maintaining physiological health. However, aging suppresses AP function, leading to decreased reproductive efficiency and compromised disease resistance (2-4). Studying global gene expression in the AP can deepen our understanding of its regulatory mechanisms. Unlike in humans, fresh bovine AP tissue is more accessible from slaughterhouses (5), making it a practical model for studying the mammalian anterior pituitary.

Global gene expression in the AP has been previously analyzed in various species, including sexually mature fish, high- and low-producing laying hens, and healthy young adult mice, using RNA sequencing (RNA-seq) (6-8). However, those studies typically used pooled or whole pituitary samples rather than individual AP glands, making it challenging to evaluate gene expression at the level of a single AP. In cattle, RNA-seq has been applied to the entire pituitary to investigate genes involved in growth, puberty, and feed intake in bulls, steers, and heifers (9-13). Although RNA-seq has also been used to compare gene expression before and after ovulation in heifers (14), to date, no studies have specifically examined anterior pituitary gene expression in the context of aging.

Infectious agent such as viruses may disrupt hormone regulation system. The spreading of severe acute respiratory syndrome coronavirus-2 (SARS-CoV-2) caused global pandemic corona virus disease (COVID-19). SARS-CoV-2 classified to the genus Betacoronavirus (15). SARS-CoV-2 is an enveloped positive-sense RNA virus. The outer surface of the virus contains spike (S) proteins. Previous studies have shown that the spike protein facilitates the entry of the virus into target host cells by binding to the angiotensin-converting enzyme 2 (ACE2) receptor (16). Moreover, in human, ACE2 is highly expressed in testes, ovaries, and other

reproductive organs (17). Consequently, the virus may affect semen quality and quantity through unknown mechanism (18, 19). However, the effect of virus infection in female infertility remains unclear.

The AP is located outside the blood-brain barrier (20). The AP do express ACE2 and can be viral targets (21). One of the important cells are gonadotroph, located in AP glands. Gonadotrophs secrete luteinizing hormone (LH) and follicle-stimulating hormone (FSH), which important for reproductive organs in animals such as testes and ovaries (22). However, to the best of our knowledge, the effect of the virus on gonadotrophs remains unclear. Gu et al. (23) reported that human gonadotrophs express ACE2. A recent study clarified that the spike protein of SARS-CoV-2 directly activates the cytoplasmic extracellular signal-regulated kinase (ERK) pathway downstream of ACE2 in human platelets (24). However, the mechanism by which spike protein-activated ACE2 affects LH and FSH secretion by gonadotrophs in all species remains unclear

The Retroviridae family comprises two subfamilies, Spumaretrovirinae and Orthoretrovirinae, which are primarily distinguished by differences in how they form infectious particles and infect host cells (25). Retrovirus consist of 3 main protein gene, Gag, Pol, and Env (25, 26). The Gag protein directs the production of internal structural components of the virion, including the matrix (MA), p12, capsid (CA), and nucleocapsid (NC). The Pol region encodes enzymes such as reverse transcriptase and integrase, while the Env gene is responsible for producing the surface and transmembrane subunits of the viral envelope protein (26). The envelope serves as the first point of contact for infection by binding to receptors on the host cell. Envelope gene consist of surface (SU) and transmembrane (TM) subunit. The SU subunit contains the receptor-binding domain (RBD) for receptor-specific binding, while the TM subunit facilitates cell entry for infection. Upon entry the target cells, RNA of the viral genome reverse transcribed into DNA to match the host's genetic material (26, 27). Retroviruses are classified based on their mode of transmission into exogenous retroviruses (exRVs), which spread through horizontal transmission, and endogenous retroviruses (ERVs), which are passed on through vertical transmission (28). Typically, retroviruses infect somatic tissues and are considered exogenous. However, over time, some retroviruses may integrate into germline cells, allowing their genetic material to be inherited through the host's gametes, thus becoming ERV. ERVs may be eliminated from the genome or become permanently integrated, depending on the influences of natural selection and random genetic drift (28). Even ERV has a complete essential open reading frame (ORF) Gag,

Pol, and Env, ERV may inactivated due to accumulation of substitution, deletion, and insertion. In fact, ERV proviruses have the potential to increase their copy number through various mechanisms that occur after endogenization.

ERVs are ancient molecular fossils originated from exogenous retroviruses and constitute approximately 4–10% of the genomes of humans, mice, and cats (29-31). ERVs are documented present in vertebrates such as mammals, fish, squamates, turtle, crocodilians, and bird (32). Consequently, there is a potential for ERV expression in used cell lines, tissues, and model organisms. This phenomenon may interfere with the accurate interpretation of experimental data, particularly in the development of biological samples, vaccine formulations, and pharmacological reagents (33). Most of ERVs are considered as junk DNA. However, instead being silenced or lost, some ERVs have beneficial function to the host through co-option process (34, 35). Specific physiological function has been well documented such as antiviral factor (34, 35), placenta formation ability (36), myoblast fusion ability (37), mRNA transporter in the nervous system (38, 39), or pregnancy regulation (40). In fact, some studies found erv retain replication ability to generate infectious viruses in several species including mice (34), koala (41, 42), pigs (43), cats (44, 45), and mule deer (46, 47).

Feline leukemia virus (FeLV) is one of example of gammaretrovirus that spread in domestic cats and small wild cat in the world (48). FeLV infection can potentially cause various diseases in cats, particularly malignant hematopoietic disorders such as lymphoma, myelodysplastic syndrome, acute myeloid leukemia, aplastic anemia, and immunodeficiency (49). FeLV is capable of infecting cats of all ages, but kittens are at a higher risk of developing a progressive form of the infection than adult cats (50, 51). Based on interference assay and host range, FeLVs classified into several subgroups (52, 53). FeLV-A, -B, -C, -D, -E, and -T subgroups were identified including their receptor (54-63). FeLV-B is generated through recombination in the env gene, involving FeLV-A and endogenous FeLV (enFeLV) sequences present in the feline genome (64, 65). FeLV is primary virus horizontally transmitted among domestic cats. Horizontal transmission of FeLV-B is uncommon, but it can occasionally occur alongside FeLV-A during co-infection (66, 67). FeLV-B is found in approximately 33–68% of cats infected with FeLV-A, likely resulting from recombination events after FeLV-A infection in domestic cats (58, 66, 68).

The selection of FeLV detection method is critical for the accurate interpretation of diagnostic outcomes and the reliable assessment of a cat's FeLV infection status. Diagnosing FeLV remains challenging, as the progression and outcome of infection can shift over time based on the host's immune response (49). In clinical practice, FeLV infection is most commonly identified by detecting soluble viral antigens present in the bloodstream (49). However, antigen detection and antibody tests have not been developed to identify viral subgroups. Polymerase chain reaction (PCR) can be useful in certain cases for identifying recombinant viruses like FeLV-B and FeLV-D (45, 69-71). Conventionally, FeLV subgroups were identified through receptor interference assays using mouse sarcoma virus, alkaline phosphatase, β-galactosidase, and green fluorescent protein (63, 69, 72, 73).

In our previous study, a new recombinant feline leukemia virus (FeLV) containing an X region was discovered (74). The X region is derived from *Felis catus* endogenous gamma-retrovirus 4 (FcERV-gamma4). This recombinant FeLV was named XR-FeLV. XR-FeLV was detected in 6.4% of FeLV-infected cats examined. In addition, XR-FeLV was detected in 12.5% from 32 FeLV-infected cats with lymphoma case. All isolated XR-FeLV clones shared a common X region that incorporated the middle portion of the FcERV-gamma4 5′ leader region. The sequence corresponding to the portion included in all X regions is also present in at least 13 endogenous retroviruses (ERVs) observed in the genomes of cats, humans, primates, and pigs. This shared genetic feature was named the common shared (CS) sequence (74).

In this dissertation, I investigate viral protein-host interactions in mammals, using cattle and cats as animal models. Interestingly, these interactions can have either detrimental or beneficial effects on mammalian physiology.

SCOPE OF THIS DISERTATION

Chapter one:

To demonstrate how aging and viral protein influence the reproduction hormone in AP.

Chapter two:

To demonstrate how viral protein influence the reproduction hormone in AP.

Chapter three:

To demonstrate how envelope protein of ERVs evolve in host genome, highlighting new antiviral molecule.

1. CHAPTER ONE:

Age-associated changes in gene expression in the anterior pituitary glands of female Japanese black cattle

This work has been published as follows:

Dimas Arya Abdillah, Onalenna Kereilwe, Yoichi Mizukami, Kenji Watanabe & Hiroya Kadokawa. 2022. Age-associated changes in gene expression in the anterior pituitary glands of female Japanese black cattle. Mammalian Genome. https://doi.org/10.1007/s00335-022-09958-9

1.1. ABSTRACT

Proper functioning of the anterior pituitary (AP) gland is imperative, however, is suppressed by aging via unclear mechanisms. Therefore, we identified differentially expressed genes (DEGs) in the AP glands of Japanese Black young heifers (approximately 22 months old) compared to old cows (approximately 120 months old) via deep sequencing of the transcriptome (RNA-seq) to characterize potentially important pathways. The young and old AP glands expressed 20,171 annotated genes. Of the total transcripts per million, approximately 41.6% and 35.5% were the sum of seven AP hormone genes in young and old AP glands, respectively, with difference observed in the sum between the young and old AP glands ($P < 0.05$). Moreover, we identified 48 downregulated genes and 218 upregulated genes in old compared to young AP glands ($P < 0.01$, fold change > 120%). The DEGs included 1 cytokine (AIMP1), 3 growth factors (NRG2, PTN, and TGFB1), 1 receptor- associated protein gene (AGTRAP), and 10 receptor genes, including PRLHR and two orphan G-protein-coupled receptors (GPR156 and GPR176). Metascape analysis of the DEGs revealed "Peptide metabolic process," "Regulation of hormone levels," and "Peptide hormone processing" as enriched pathways. Furthermore, Ingenuity Pathway analysis of the DEGs revealed (1) a network of 24 genes (including GPR156 and PRLHR) named "Neurological disease, organismal injury and abnormalities, and psychological disorders", and (2) two canonical pathways ($P < 0.01$), namely "Huntington's disease signaling", and "AMPK signaling". Thus, the findings of the current study revealed relevant DEGs, while identifying important pathways that occur during aging in AP glands of female cattle.

1.2. INTRODUCTION

The anterior pituitary (AP) gland is the central regulator of the endocrine system, coordinating signals from both the hypothalamus and various peripheral tissues to regulate physiological functions in multiple organs. As such, proper functioning of the AP gland is important to maintain human and animal health; however, aging suppresses AP gland functionality, resulting in disease and infertility(2-4, 75).

The AP gland has numerous physiological roles and, thus, is expected to encode many genes. However, little is known regarding global gene expression in the AP glands after aging. Unlike human AP glands, fresh bovine AP glands can be obtained as they can be collected from slaughterhouses (5, 22). Deep sequencing of the transcriptome (RNA-seq) via next-generation sequencing (NGS) technology is a recently developed high-throughput genetic analysis tool for determining global gene expression. NGS methods have certain advantages over microarrays, while RNA-seq has the capacity to identify novel transcript variants without being limited by potential cross-hybridization (76). Meanwhile, few studies have applied this technique to AP gene expression. Specifically, this technique has been utilized to analyze samples comprising multiple whole pituitary glands from sexually immature and mature fish (6), high- or low-yielding laying hens (8), and healthy young adult mice (7), due to the small size of the glands, this makes it challenging to assess the expression levels of genes in single AP glands. In addition, previous studies have used this technique on whole pituitary samples collected from bovine for the purpose of understanding growth, puberty, and feed intake in young bulls, steers, and heifers (9-13). Moreover, the size of the whole bovine pituitary gland (at least 4 cm along its rostrocaudal axis, 3 cm along the lateral axis, and 4 cm along the vertical axis), facilitates easy differentiation of the anterior lobe (light brown or pink color, and hard portion) from the posterior and intermediate lobes (brown color, and softer parts) following sagittal dissection along the midline (77). However, to the best of our knowledge, only one study has previously compared gene expression before and after ovulation in heifers and reported gene expression patterns in an individual bovine AP gland using RNA-seq (14). Meanwhile, no previous studies have used this technique to investigate AP glands from the perspective of aging.

Cattle are important food and dairy source worldwide. The maximum recorded lifespan of dairy and beef cattle is approximately 20 years (78); however, the average lifespan of cattle is only approximately 25% of the recorded maximum lifespan due to culling when health, fertility, or productivity is suppressed (78).

Therefore, in this study, we assessed gene expression patterns in the AP glands of young heifers and old cows via RNA-seq to clarify age-related genes and important-associated pathways.

1.3. MATERIALS AND METHODS

1.3.1. Sample collection

All experiments were performed according to the Guiding Principles for the Care and Use of Experimental Animals in the Field of Physiological Sciences (Physiological Society of Japan) and approved by the Committee on Animal Experiments of the School of Veterinary Medicine, Yamaguchi University (Approval Number, 301). All cattle were obtained from contract farmers in western Japan. Following the disaster of bovine spongiform encephalopathy in 2002, all cattle born in Japan are registered at birth in a national database, with an individual identification number. Consumers can obtain information regarding the breed, date of birth, farm of origin, and slaughter by querying the server of the National Livestock Breeding Centre of Japan. We verified the above information in this study.

We obtained AP samples from healthy, post-pubertal, non-pregnant, non-lactating Japanese Black heifers (22.0 ± 1.5 mo old, n = 5) and old Japanese Black cows (123.8 ± 19.0 mo old; 7.4 ± 1.1 parity; n = 5) managed by our contracted farmer in western Japan. The farms had open free-stall barns, and the animals had free access to water. The cattle were fed twice daily with a total mixed ration according to the Japanese feeding standard (Agriculture, Forestry and Fisheries Research Council Secretariat 2008). The heifers and cows were slaughtered at a local abattoir for harvesting beef according to the regulations of the Ministry of Agriculture, Forestry and Fisheries of Japan. All heifers and cows were non-lactating, non-pregnant, and with no follicular cysts, luteal cysts, or other ovarian disorders based on macroscopic examinations of the ovaries. Old cows were slaughtered after completing parturition a sufficient number of times as planned by farmers to obtain beef, usually after 84 months of age.

The heifers and cows were in the luteal phase, that is, + 9 d to + 16 d from estrus, as determined by macroscopic examination of the ovaries and uterus (79). AP gland samples were collected from the head as previously described (80). Briefly, the heifers and cows were stunned using a captive bolt pistol and subsequently exsanguinated by cutting of the throat. The heads were placed on ice within 5 min of slaughter. AP glands were isolated from other tissues within 15 min of slaughter, immediately frozen in liquid nitrogen, and preserved at − 80 °C until RNA extraction.

1.3.2. Preparation of the transcriptome library for deep sequencing

We followed a previously reported method (14, 80) with slight modification. Total RNA was extracted from the AP glands using a Maxwell RSC simply RNA Kit (Promega, Madison, WI, USA), and subsequently treated samples with ribonuclease-free deoxyribonuclease (Promega) to eliminate possible genomic DNA contamination. The quality was verified using agarose gel electrophoresis and capillary electrophoresis using an Agilent 2100 Bioanalyzer (Agilent Technologies, Santa Clara, CA, USA) and an RNA 6000 Nano Kit (Agilent Technologies) once the concentrations had been determined using a Qubit (Thermo Fisher Scientific, Wilmington, DE, USA). The RNA integrity values were > 7 for all samples, indicating that the samples contained high-quality RNA. The expression libraries were produced using an NEBNext Ultra II RNA Library Prep Kit for Illumina (New England Biolabs, Ipswich, MA, USA). Total RNA (100 ng) was reverse transcribed to cDNA and amplified using the primer provided with the kit. Barcodes were inserted into the amplicons, and adapter sequences were inserted into both ends using a NEB Next Adaptor kit (New England Biolabs). The libraries were amplified by PCR with 11 cycles of denaturation for 10 s at 98 °C, followed by annealing and extension for 75 s at 65 °C using NEB Next multiplex oligos for Illumina. The quality of the products was confirmed with a Bioanalyzer, and the concentrations were determined using Qubit.

The sequence reaction was conducted using an Illumina Next-seq500 DNA sequencer with a 75-bp paired end cycle sequencing kit (Illumina Inc., San Diego, CA, USA). Approximately 30 million reads and 2.2 gigabases were detected from the reaction.

1.3.3. Analysis of read information

Short sequence reads of 75 bp in the fast file created by the Illumina NEXTSeq500 system were assembled and mapped using CLC Genomic Workbench software (ver. 20.0.4, CLC Bio, Aarhus, Denmark) using *Bos taurus* (Hereford) ARS- UCD1.2 (National Center for Biotechnology Information [NCBI] assembly accession GCA_002263795.2) as a reference sequence. The mapping ratio was > 97.5%, and the read count for each sample was > 16 million. Considering that transcripts per million (TPM) is a preferred metric for quantifying gene/transcript abundance rather than the RPKM (81), the TPM value was used to represent gene expression level. The sum of the TPM values for all transcriptomes (total TPM values) was 1,000,000 in each AP sample.

1.3.4. Statistical analysis, and selection of genes for pathway analyses

To calculate significant differences in TPM values for each gene between the two groups, we followed the statisti cal method reported by Shimizu et al. (82). Briefly, the binary logarithm of each TPM value was calculated following the addition of 1. Analysis of significant differences in the expression of each gene between the young and old AP glands was performed using a non-paired *t*-test. We calculated the average TPM values for young AP glands and divided them by the average TPM values of the old AP glands (old/young ratio) to show the differences in the TPM values for each gene. We also calculated the fold change, which was calculated as: [binary logarithm of (old AP TPM + 1)] − [binary logarithm of (young AP TPM + 1)]. Data are expressed as the mean ± SEM.

We selected genes with (1) an average binary logarithm of (TPM + 1) in all AP glands ≥ 0.01, (2) varying expression ($P < 0.01$) between the young and old AforP glands, and (3) fold change increased by > 20% (log2 fold change > 0.263) or decreased by > 20% (log2 fold change < -0.263) for pathway analyses. We also excluded genes not assigned a name in Ensembl gene identifier (ENSBTAG). Pathway analysis was then performed using Metascape (https://metascape.org) (83) on January 14, 2022. Another pathway analysis was performed using Ingenuity Pathways Analysis (IPA) (Qiagen, Valencia, CA, USA) content version 70,750,971 (release date October 22, 2021) on December 22, 2021. The parameters were set to the default values. The molecular activity predictor function was utilized in IPA to predict both upstream and downstream molecules and functions following identification of canonical pathways.

Location and types were decided based on the IPA database, although each expressed protein may have various locations and multiple roles.

1.4. RESULTS

1.4.1. Annotated genes expressed in young and old AP glands

Fig. 1.1. shows a volcano plot of 20,171 annotated genes. The P values of the 18,970 genes shown (gray dots) were ≥ 0.05. Among the remaining genes, 48 (green dots) and 218 (red dots) were significantly ($P < 0.01$) expressed with fold changes > 20% lower and higher, respectively, in the old than young AP glands. Table 1.1.6.1 lists the gene expression of all 48 genes as highly expressed in young AP glands compared to old AP glands, while Table 1.2 lists the gene expression of the top 50 genes among the 218 upregulated genes in old AP glands compared to young AP glands. Table 1.1 shows only nine unnamed genes (ENSBTAG in the Tables, and No-name in Fig. 1.1), whereas 26 appear in Table 1.2. After excluding the unnamed genes, 258 genes were differentially expressed between the young and old AP glands ($P < 0.01$). Table 1.3A summarizes the locations of the proteins encoded by the 258 genes, while Table 1.3B summarizes the protein families encoded by these genes.

Among the 258 genes, one encodes a cytokine [AIMP1 (aminoacyl tRNA synthetase complex interacting multifunctional protein 1; fold change, 0.258)], and three encode growth factors [NRG2 (neuregulin 2; fold change, 0.825) PTN (pleiotrophin; fold change, − 1.545), and TGFB1 (trans- forming growth factor beta 1; fold change, − 1.700)], while 10 encode receptors, and one encodes a receptor-associated protein.

1.4.2. Transcriptomes of AP hormone genes

Table 1.4 lists the TPM values of the seven AP hormone genes (*PRL*, *GH1*, *CGA*, *LHB*, *POMC*, *FSHB*, and *TSHB*). The sum of TPM values accounted for 416,718 or 354,526 of the total TPM of all transcriptomes in the young and old AP glands, respectively. Since the total TPM was 1,000,000 in all individuals, approximately 41.6% and 35.5% of these corresponded to the AP hormones in the young and old AP glands, respectively. Although no significant differences were detected in each AP hormone gene TPM between the young and old AP glands, differences occurred in the sum of the seven AP hormone gene TPMs between the two groups ($P < 0.05$). The old/young ratio of FSHB and CGA were lower than that of the other five AP hormone genes. The TPM value of PRL (prolactin) was the highest among all genes, including those encoding AP hormones in both young and old AP glands.

1.4.3. Transcriptomes of receptor genes

Table 1.5 lists the TPM values of the established five receptor genes in the young and old AP glands. No significant differences were observed between young and old AP glands for any genes. The old/young ratio of *GNRHR* was lower than that of the other five receptor genes.

Table 1.6 shows differentially expressed genes of 1 receptor-associated protein gene, and 10 receptor genes, including *PRLHR* and two orphan G-protein-coupled receptors (GPCRs; *GPR156*, and *GPR176*).

1.4.4. Results of metascape analysis

As shown in Table 1.7, Metascape revealed 20 enriched biological pathways, including "Peptide metabolic process", "Regulation of hormone levels", "Peptide hormone processing", "Regulation of membrane potential", and "Regulation of binding".

1.4.5. Results of IPA

The IPA of the 218 genes (shown as red in Fig. 1.1.6.1) revealed two important canonical pathways. Figure 1.1.6.2 shows that for the first pathway, Huntington's disease signaling ($P = 1.17 \times 10^{-3}$), a 2.8% overlap occurred (8/283 genes). Meanwhile, Fig. 1.1.6.3 shows that for the AMPK signaling ($P = 2.18 \times 10^{-3}$), 2.9% overlap occurred (7/244 genes).

The IPA also revealed five upstream regulators: inosine ($P = 5.34 \times 10{-}5$; activation predicted), dynein axonemal assembly factor 6 (DNAAF6; $P = 1.82 \times 10{-}4$; no predicted effect), zinc finger and BTB domain containing 1 (ZBTB10; $P = 2.51 \times 10{-}4$; activation predicted), TATA-box binding protein-associated factor 12 (TAF12; $P = 3.61 \times 10{-}4$; no predicted effect), and cAMP responsive element binding protein 1 (CREB1; $P = 6.38 \times 10{-}4$; no predicted effect).

IPA further revealed a network of 24 genes, including PRLHR and GPR156, as associated with "Neurological disease, organismal injury, and abnormalities, psychological disorders", where Parkinsonism-associated deglycase (PARK7), AKT serine/threonine kinase 1 (AKT), estrogen receptor, small ubiquitin-like protein (SUMO), and calmodulin were identified as central genes (Fig.1.1.6.4).

1.5. DISCUSSION

We assessed gene expression patterns in the AP glands of young heifers and old cows via RNA-seq to clarify age-related genes and important associated pathways. Significant differences were observed in the sum of seven AP hormone gene TPMs between the young and old AP gland samples, although no differences were detected in the individual mRNA levels of each AP hormone. Moreover, the gene ontology analysis results, performed by Metascape, sug- gested that old AP glands may have suppressed functioning from response to stimulation, translation, and secretion. Indeed, Malhi et al. (75) reported that crossbred Hereford cows (13 to 14 years of age) showed a delayed preovulatory LH surge following estradiol treatment. Therefore, the present data suggests that aging may suppress the function or sensitivity of AP cells to secrete AP hormones. Up to 35.5–41.6% of the total TPM corresponded to the AP hormones in the old and young AP glands, which is similar to data reported previously for heifers before and after ovulation (14). In the current study, the TPM value of PRL was the highest among all genes, including the other six AP hormone genes. Freeman et al. (84) reported that PRL is expressed in both lactotrophs and mammosomatotrophs, which comprise up to 50% of the cellular population in the AP gland. Prolactin has a broad range of functions in the body, apart from its role in promoting lactation (85).

Considering that the present study used non-lactating heifers and cows, the high TPM value of PRL suggests multiple important roles of prolactin. Interestingly, the IPA analyses revealed a gene network, made up of 24 genes including PRLHR, associated with "Neurological disease, organismal injury, and abnormalities, psychological disorders". The gene network also included PARK7encoding SP22 (syn. Of Parkinsonism-associated deglycase). SP22, implicated in fertility and ontogeny of early-onset Parkinson's disease (86), is expressed in somatotropes, thyrotropes, corticotropes, lactotropes, and gonadotropes of rats and hamsters (87). Therefore, the network may be important for addressing age-related disorders, including infertility.

Differences in the TPM values of the established five receptor genes were not significant in the young and old AP glands. The SEM of TPM were large compared to average of TPM, suggesting a large individual difference. The old cows were healthy, and receptor mRNA expression might have been changed in short time. Another possible reason may be attributed to the number of receptor proteins on the cell surface being controlled by not only mRNA expression, but also translational or posttranslational steps. Sensitivities of hormone secretory cells are not only controlled by the number of receptor proteins but also G-proteins and

cytoplasmic pathways. Therefore, we could not definitively conclude that the sensitivities of hormone secretory cells in old cows are not different from young heifers.

The IPA results also Identified Huntington's disease signaling as the top canonical pathway. We previously reported that bovine gonadotroph expresses GPR61 co-localized with GnRH receptors, and the quality of its ligand, ethanolamine plasmalogen, changes after aging, resulting in lowered FSH secretion (5). Moreover, the amount of ethanolamine plasmalogen decreases in the aged human brain leading to Alzheimer's disease (88). Therefore, further studies are required to determine whether animals with brain diseases, e.g., Parkinson's disease, Huntington's disease, or Alzheimer's disease, are infertile and whether additional signals are secreted from the diseased area to suppress AP functions and reduce fertility.

We also discovered 11 differentially expressed receptors, including GPR176, which may be important for understanding age-related diseases and infertility. However, little is known regarding these receptors. GPR176 plays an important role in the circadian clock in the suprachiasmatic nucleus, as reviewed by Nakagawa et al. (89). Thus, further studies are required to clarify the role of these receptors in AP glands.

Although the DEGs included those encoding a cytokine and three growth factors, data on their roles in AP glands remain limited. For example, AIMP1, also known as p43, is the precursor of the multifunctional inflammatory cytokine endothelial monocyte-activating polypeptide II and is secreted by GH-secreting pituitary adenomas (90). Although its role in normal pituitary glands has not been clarified, interestingly, AIMP1 has anti-aging activities in human skin (91). TGFB1 inhibits FSHB transcription in mouse AP cells (92), prolactin secretion from rat AP cells, and growth of lactotropes (93). Meanwhile, CREB has a central role in the control of POMC gene expression in corticotropes (94). CREB is an important pathway for both GnRH and membrane estradiol receptors that controls LHB gene expression and binding of GnRH in gonadotrophs (95-97). Moreover, PTN, also known as HB-GAM, is expressed in neurohypophyseal cells in rat embryonic and adult pituitary glands (98). However, to our knowledge, there are no previous studies on the remaining growth factor (NRG2), and four upstream regulators (inosine, DNAAF6, ZBTB10, and TAF12), hence their roles in AP glands remain unknown. There are two possibilities for the lack of data regarding gene expression in pituitary glands. One is that some genes expressed in bovine AP glands may be cow specific; while the other is that variations in methodology or sampling may cause difference. There are several generations among "next generation sequence" that may affect the sensitivity to detect low expression. Also, it is impossible to obtain only AP gland from whole pituitary gland in mice due to the

small size of the glands (7). Therefore, the genes detected from the RNA-seq data of the whole pituitary must be different from those detected from the RNA-seq data of only the AP gland. This particularly holds true for genes with low TPM values, such as receptors, unlike those with high TPM values, such as secreted hormones.

Improved NGS technology has allowed for an increased number of genes to be annotated using RNA-seq (99). Indeed, by employing this platform, the present study annotated more genes than previous studies (9-14). Research utilizing recently improved RNA-seq techniques has challenged the definition of the term "pseudogenes," which have now been reported as being both transcribed and translated (99). Our study discovered 26 and 9 unnamed genes (ENSBTAGs) among the top genes as being upregulated or downregulated in old/young AP glands, as listed in Tables 1.1 and 1.2. More ENSBTAGs (26) are shown in the heatmap of Table 1.2 compared to those (9) in Table 1.1. A possible reason for the higher number of unnamed genes is that previous studies focused primarily on young and healthy organs assuming that all genes are expressed in young, healthy organs. Therefore, further studies are required to clarify the roles of proteins encoded by these genes as they might be involved in health and fertility during aging.

The results of this study should be interpreted with caution. AP has a heterogeneous cell population; for example, gonadotrophs constitute only 15% of all cells in AP and are scattered among other cell types in rats and humans (100). We have previously shown that gonadotrophs may comprise 27% of AP population in bovine (101). In fetal sheep, each cell type constituted 15–20% (102); however, percentages of other cell types to all cells remain to be determined in adult cows. Also, the results of the pathways and network revealed by Metascape and IPA provide only potential directions for data analysis. Therefore, future studies are required using various method including cell sorter, and proteomics.

The present study clarified the genes differentially expressed in AP glands between young and old female cattle, while also suggesting potentially important pathways in the AP glands. Further studies are required to clarify the roles of the identified upstream regulators, growth factors, and receptors during aging in AP glands.

1.6. TABLES, FIGURES, SUPPLEMENTARY DATA

Tables

Tables 1.1. The 48 significantly downregulated young to old anterior pituitary (AP) glands

Gene symbol	Entrez Gene Name	Location	Type(s)	Log2 of Fold Change	P-value	Young AP 1	Young AP 2	Young AP 3	Young AP 4	Young AP 5	Old AP 1	Old AP 2	Old AP 3	Old AP 4	Old AP 5
ENSBTAG00000027962	*No information*	*No information*	*No information*	-2.37	0.0003										
TGFB1	transforming growth factor beta 1	Extracellular Space	growth factor	-1.70	0.0003										
PTN	pleiotrophin	Extracellular Space	growth factor	-1.55	0.0033										
JAK3	Janus kinase 3	Cytoplasm	kinase	-1.47	0.0048										
NRGN	neurogranin	Cytoplasm	other	-1.34	0.0075										
KIF26A	kinesin family member 6	Nucleus	other	-1.31	0.0007										
COL1A1	collagen type I alpha 1 chain	Extracellular Space	other	-1.22	0.0039										
RF00019	*No information*	*No information*	*No information*	-1.12	0.0056										
FNDC1	fructose-bisphosphatase 1	Cytoplasm	phosphatase	-1.11	0.0096										
ENSBTAG00000054250	*No information*	*No information*	*No information*	-1.05	0.0052										
CSGALNACT1	chondroitin sulfate N-acetylgalactosaminyltransferase 1	Cytoplasm	enzyme	-1.02	0.0034										
ENSBTAG00000052438	*No information*	*No information*	*No information*	-1.02	0.0056										
PLD4	phospholipase D family member 4	Extracellular Space	enzyme	-0.99	0.0062										
FKBP10	FKBP prolyl isomerase 10	Cytoplasm	enzyme	-0.94	0.0064										
AMIGO2	adhesion molecule with Ig like domain 2	Plasma Membrane	other	-0.92	0.0087										
PLEKHA4	pleckstrin homology domain containing A4	Cytoplasm	other	-0.84	0.0075										
ENSBTAG00000022399	*No information*	*No information*	*No information*	-0.80	0.0060										
PRSS27	serine protease 27	Extracellular Space	peptidase	-0.76	0.0096										
IGFBP4	insulin like growth factor binding protein 4	Extracellular Space	other	-0.72	0.0042										
ZNF300	zinc finger protein 300	Nucleus	transcription regulator	-0.71	0.0022										
TERT	telomerase reverse transcriptase	Nucleus	enzyme	-0.70	0.0042										
TNNT1	troponin T1, slow skeletal type	Cytoplasm	other	-0.70	0.0076										
PPP1R16B	protein phosphatase 1 regulatory subunit 16B	Plasma Membrane	phosphatase	-0.70	0.0033										
MIC1	major histocompatibility class I related protein	*No information*	*No information*	-0.65	0.0058										
GRIK4	glutamate ionotropic receptor kainate type subunit 4	Plasma Membrane	ion channel	-0.65	0.0035										
HSPB6	heat shock protein family B (small) member 6	Cytoplasm	other	-0.59	0.0025										
SMC4	structural maintenance of chromosomes 4	Nucleus	transporter	-0.57	0.0004										
METRN	meteorin, glial cell differentiation regulator	Extracellular Space	other	-0.56	0.0033										
SLC29A4	solute carrier family 29 member 4	Plasma Membrane	transporter	-0.52	0.0063										
KCNK4	potassium two pore domain channel subfamily K member 4	Plasma Membrane	ion channel	-0.49	0.0020										
SPAG5	sperm associated antigen 5	Nucleus	peptidase	-0.49	0.0005										
DAPP1	dual adaptor of phosphotyrosine and 3-phosphoinositides 1	Cytoplasm	other	-0.44	0.0008										
STAG3	sperm associated antigen 5	Nucleus	peptidase	-0.44	0.0064										
PIDD1	p53-induced death domain protein 1	Cytoplasm	peptidase	-0.44	0.0074										
SHCBP1	SHC binding and spindle associated 1	Cytoplasm	other	-0.44	0.0035										
COL5A1	collagen type V alpha 1 chain	Extracellular Space	other	-0.43	0.0036										
SLC12A9	solute carrier family 12 member 9	Plasma Membrane	transporter	-0.40	0.0061										
ENSBTAG00000050326	*No information*	*No information*	*No information*	-0.37	0.0005										
ENSBTAG00000050646	*No information*	*No information*	*No information*	-0.37	0.0077										
ENSBTAG00000038204	*No information*	*No information*	*No information*	-0.36	0.0031										
ENSBTAG00000050161	*No information*	*No information*	*No information*	-0.35	0.0088										
ENSBTAG00000015759	*No information*	*No information*	*No information*	-0.34	0.0075										
SPC24	SPC24 component of NDC80 kinetochore complex	Cytoplasm	other	-0.34	0.0099										
IGF2BP3	insulin like growth factor 2 mRNA binding protein 3	Cytoplasm	translation regulator	-0.33	0.0057										
ADPRM	ADP-ribose/CDP-alcohol diphosphatase, manganese dependent	Cytoplasm	enzyme	-0.33	0.0013										
TNNI1	troponin I1, slow skeletal type	Cytoplasm	other	-0.30	0.0061										
DTL	denticleless E3 ubiquitin protein ligase homolog	Nucleus	enzyme	-0.30	0.0073										
SYT5	synaptotagmin 5	Cytoplasm	transporter	-0.28	0.0048										

Tables 1.2. Top 50 upregulated genes from young to old AP glands

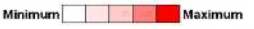

Gene name	Entrez Gene Name	Location	Type(s)	Log2 of Fold Change	P-value	Young AP 1	Young AP 2	Young AP 3	Young AP 4	Young AP 5	Old AP 1	Old AP 2	Old AP 3	Old AP 4	Old AP 5
ENSBTAG00000050136	*No information*	*No information*	*No information*	4.24	0.0003										
ENSBTAG00000052293	*No information*	*No information*	*No information*	3.98	0.0003										
ENSBTAG00000048135	*No information*	*No information*	*No information*	3.91	0.0033										
ENSBTAG00000047121	*No information*	*No information*	*No information*	3.90	0.0048										
ENSBTAG00000055240	*No information*	*No information*	*No information*	3.84	0.0075										
ENSBTAG00000050723	*No information*	*No information*	*No information*	3.82	0.0007										
ENSBTAG00000050495	*No information*	*No information*	*No information*	3.70	0.0039										
ENSBTAG00000050062	*No information*	*No information*	*No information*	3.65	0.0056										
ENSBTAG00000050373	*No information*	*No information*	*No information*	3.36	0.0036										
ENSBTAG00000048030	*No information*	*No information*	*No information*	3.27	0.0052										
ENSBTAG00000051734	*No information*	*No information*	*No information*	3.21	0.0034										
ENSBTAG00000048048	*No information*	*No information*	*No information*	2.97	0.0056										
ENSBTAG00000022502	*No information*	*No information*	*No information*	2.97	0.0082										
ENSBTAG00000052699	*No information*	*No information*	*No information*	2.93	0.0084										
ENSBTAG00000003408	*No information*	*No information*	*No information*	2.75	0.0087										
ENSBTAG00000051010	*No information*	*No information*	*No information*	2.68	0.0075										
APOD	apolipoprotein D	Extracellular Space	transporter	2.36	0.0060										
CARTPT	CART prepropeptide	Extracellular Space	other	2.16	0.0096										
ENSBTAG00000017305	*No information*	*No information*	*No information*	2.07	0.0042										
ENSBTAG00000050098	*No information*	*No information*	*No information*	1.99	0.0022										
ENSBTAG00000047700	*No information*	*No information*	*No information*	1.97	0.0042										
ENSBTAG00000053635	*No information*	*No information*	*No information*	1.79	0.0076										
CBLN1	cerebellin 1 precursor	Cytoplasm	other	1.69	0.0033										
CABP7	calcium binding protein 7	Cytoplasm	other	1.45	0.0058										
C15H11orf88	*chromosome 15 C11orf88 homolog*	*No information*	*No information*	1.40	0.0035										
ENSBTAG00000046322	*No information*	*No information*	*No information*	1.23	0.0025										
RF00108	*No information*	*No information*	*No information*	1.22	0.0004										
METTL7A	methyltransferase like 7A	Cytoplasm	other	1.20	0.0033										
ENSBTAG00000046161	*No information*	*No information*	*No information*	1.18	0.0093										
LHX4	LIM homeobox 4	Nucleus	transcription regulator	1.15	0.0020										
JCHAIN	joining chain of multimeric IgA and IgM	Extracellular Space	other	1.15	0.0005										
ULBP21	UL16 binding protein 21	*No information*	*No information*	1.14	0.0008										
SCGB1D	secretoglobin, family 1D, member 2	*No information*	*No information*	1.12	0.0064										
FNDC7	fibronectin type III domain containing 7	Other	other	1.11	0.0074										
ENSBTAG00000048869	*No information*	*No information*	*No information*	1.05	0.0035										
ENSBTAG00000052931	*No information*	*No information*	*No information*	1.05	0.0036										
PLA2G7	phospholipase A2 group VII	Extracellular Space	enzyme	1.03	0.0061										
PRKCQ	protein kinase C theta	Cytoplasm	kinase	1.02	0.0005										
NTSR2	neurotensin receptor 2	Plasma Membrane	G-protein coupled receptor	0.97	0.0077										
AK7	adenylate kinase 7	Cytoplasm	kinase	0.95	0.0031										
ENSBTAG00000047787	*No information*	*No information*	*No information*	0.91	0.0088										
TMEM176B	transmembrane protein 176B	Other	other	0.89	0.0075										
CD27	CD27 molecule	Plasma Membrane	transmembrane receptor	0.87	0.0099										
ENSBTAG00000049637	*No information*	*No information*	*No information*	0.86	0.0057										
SPA17	sperm autoantigenic protein 17	Plasma Membrane	other	0.86	0.0013										
SLC1A1	solute carrier family 1 member 1	Plasma Membrane	transporter	0.85	0.0051										
NRG2	neuregulin 2	Extracellular Space	growth factor	0.83	0.0073										
CDH13	cadherin 13	Plasma Membrane	other	0.82	0.0048										
BCHE	butyrylcholinesterase	Plasma Membrane	enzyme	0.79	0.0048										
CCDC39	coiled-coil domain containing 39	Cytoplasm	other	0.79	0.0048										

Tables 1.3. Summary of locations (A) and types (B) of proteins encoded by the 258 genes differently expressed between young and old anterior pituitaries ($P < 0.01$)

(A) Location	Number of genes
Cytoplasm	110
Extracellular Space	30
Nucleus	45
Plasma Membrane	24
Other	49
SUM	258
(B) Type(s)	**Number of genes**
cytokine	1
enzyme	51
G-protein-coupled receptor	5
Receptor-associated protein	1
growth factor	3
ion channel	4
kinase	13
peptidase	7
phosphatase	4
transcription regulator	14
translation regulator	4
transmembrane receptor	5
transporter	23
other	123
SUM	258

Table 1.4. Transcripts per million (TPM) values (mean ± SEM) of AP hormone genes in the young and old AP glands, arranged as per the old/ young ratio (average of the TPM values of old AP glands divided by the average of the TPM values of young AP glands).

Gene	Description	Accession	TPM value		Ratio
			Young	Old	
FSHB	follicle stimulating hormone subunit beta	NM_174060	488 ± 188	255 ± 98	0.52
CGA	glycoprotein hormones, alpha polypeptide	NM_173901	10,340 ± 1539	6932 ± 2084	0.67
PRL	prolactin	NM_173953	325,647 ± 33,389	262,679 ± 25,064	0.81
LHB	luteinizing hormone beta polypeptide	NM_173930	2966 ± 464	2547 ± 847	0.86
TSHB	thyroid stimulating hormone subunit beta	NM_174205	1110 ± 262	983 ± 413	0.89
GH1	growth hormone 1	NM_180996	66,881 ± 8364	68,868 ± 14,165	1.03
POMC	proopiomelanocortin	NM_174151	9287 ± 1314	12,263 ± 5075	1.32
TOTAL			416,718 ± 24,686	354,526 ± 10,146	0.85*

There were no overall significant differences between young and old AP glands for any genes; however, a difference ($^{*}P < 0.05$) was noted in the total TPM of seven genes between young and old AP glands

Table 1.5. TPM values (mean ± SEM) of the established receptor genes in young and old AP glands, arranged per the old/young ratio

Gene	Description	Accession	TPM value		Ratio
			Young	Old	
GNRHR	Gonadotropin-releasing hormone receptor	NM_177514	82.2 ± 19.7	46.4 ± 12.0	0.57
GHRHR	growth hormone releasing hormone receptor	NM_181020	74.7 ± 12.5	71.7 ± 16.1	0.96
DRD2	dopamine receptor D2	NM_174043	318.1 ± 33.4	308.6 ± 53.5	0.97
CRHR1	Corticotropin-releasing hormone receptor 1	NM_174287	12.8 ± 2.0	14.4 ± 2.9	1.13
AVPR1B	arginine vasopressin receptor 1B	NM_001192142	2.9 ± 0.6	3.3 ± 2.3	1.13
TRHR	thyrotropin releasing hormone receptor	NM_174203	8.9 ± 2.8	12.0 ± 3.4	1.34

Table 1.6. Transcripts per million (TPM) values (mean ± SEM) for genes of receptor and receptor-associated proteins (indicated with *) expressed differentially ($P < 0.01$) between the young and old anterior pituitaries, arranged per the old/young ratio

Gene	Description	Accession	TPM value		Ratio
			Young	Old	
CD27	CD27 molecule	NM_001082434	0.1 ± 0.0	1.0 ± 0.2	17.5
PRLHR	prolactin releasing hormone receptor	NM_001030300	0.05 ± 0.02	0.80 ± 0.16	16.4
NTSR2	neurotensin receptor 2	XM_002691479	1.2 ± 0.2	3.4 ± 0.6	2.8
CHRNA1	cholinergic receptor nicotinic alpha 1 subunit	NM_176664	0.7 ± 0.1	1.9 ± 0.2	2.7
OMG	oligodendrocyte myelin glycoprotein	NM_001077524	1.1 ± 0.2	2.4 ± 0.3	2.2
GPR176	G-protein-coupled receptor 176	NM_001192616	1.6 ± 0.3	3.4 ± 0.5	2.1
GPR156	G-protein-coupled receptor 156	NM_001205643	0.50 ± 0.05	0.84 ± 0.04	1.7
RELT	RELT TNF receptor	XM_002693451	29.3 ± 2.8	44.3 ± 3.7	1.5
TSPO	translocator protein	NM_175776	27.0 ± 0.7	38.4 ± 1.4	1.4
LGALS3BP	galectin 3 binding protein	NM_001046316	39.6 ± 2.6	56.6 ± 4.4	1.4
*AGTRAP**	angiotensin II receptor-associated protein	NM_001075363	22.7 ± 1.4	29.4 ± 0.9	1.3

Table 1.7. Top 20 clusters revealed by Metascape with their representative enriched terms

Gene ontology	Description	N[a]	%[b]	Log10(P) [c]	Log10(q) [d]
0,006,518	peptide metabolic process	21	8.08	−8.7	−4.65
0,003,351	epithelial cilium movement involved in extracellular fluid movement	8	3.08	−8.69	−4.65
0,010,817	regulation of hormone levels	20	7.69	−7.85	−4.1
0,016,486	peptide hormone processing	6	2.31	−6.38	−2.87
R-HSA-9663891	Selective autophagy	8	3.08	−6.3	−2.85
0,042,391	regulation of membrane potential	15	5.77	−5.31	−2.17
0,007,610	behavior	17	6.54	−5.05	−1.94
1,903,146	regulation of autophagy of mitochondrion	5	1.92	−4.86	−1.84
0,007,268	chemical synaptic transmission	13	5.00	−4.35	−1.44
0,036,473	cell death in response to oxidative stress	4	1.54	−4.3	−1.4
0,051,098	regulation of binding	12	4.62	−4.06	−1.24
0,031,102	neuron projection regeneration	4	1.54	−3.91	−1.13
0,032,770	positive regulation of monooxygenase activity	4	1.54	−3.8	−1.05
0,018,130	heterocycle biosynthetic process	18	6.92	−3.73	−1.02
0,006,301	postreplication repair	4	1.54	−3.69	−1.01
R-HSA-71387	Metabolism of carbohydrates	10	3.85	−3.59	−0.93
hsa05022	Pathways of neurodegeneration—multiple diseases	13	5.00	−3.56	−0.92
0,050,801	ion homeostasis	17	6.54	−3.50	−0.92
hsa04922	Glucagon signalling pathway	6	2.31	−3.47	−0.92
0,007,162	negative regulation of cell adhesion	10	3.85	−3.47	−0.92

[a]number of genes in the provided lists with membership in the given ontology term

[b]percentage of all provided genes found in the given ontology term (only input genes with at least one ontology term annotation are included in the calculation)

[c]*P*-value in log base 10

[d]multi-test adjusted *P*-value in log base 10

Figures

P-value	Fold Change	Number of genes
P < 0.01	Young/Old > 1.2	48 genes
P < 0.01	Old/Young > 1.2	218 genes
P < 0.01	Others	52 genes
0.01 ≤ P < 0.05	All	883 genes
0.05 ≤ P	All	18,970 genes

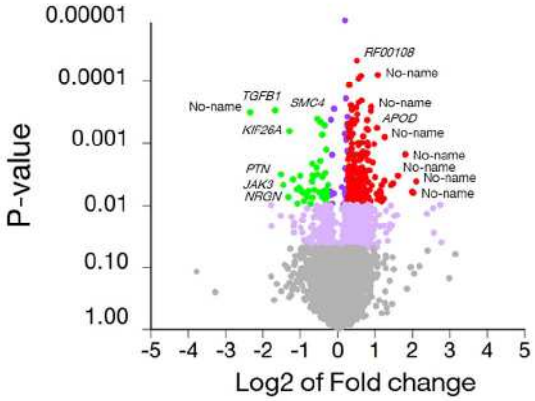

Fig. 1.1. Volcano plot of 20,171 annotated genes in which the X-axis is the binary logarithm of fold change in old anterior pituitary (AP) glands to young ones, and the Y-axis is the P-value of significant difference levels. The gray dots indicate 18,970 genes with *P*-values ≥ 0.05. The green (48 genes) dots indicate genes significantly (P<0.01) downregulated by>20% (log2 fold change<-0.263) in old AP glands compared to the young AP glands. The red (218 genes) dots indicate genes significantly (*P* <0.01) upregulated by>20% (log2 fold change>0.263) in the old AP glands compared to young AP glands. The dark purple (52 genes) dots indicate genes with *P*-values<0.01, but neither up-regulated nor down-regulated (log2 fold change between -0.263 and 0.263). The light purple (883 genes) dots indicate genes with *P*-value≥0.01, and<0.05. Italic font indicates top genes, of which details are shown in Tables 1 and 2.

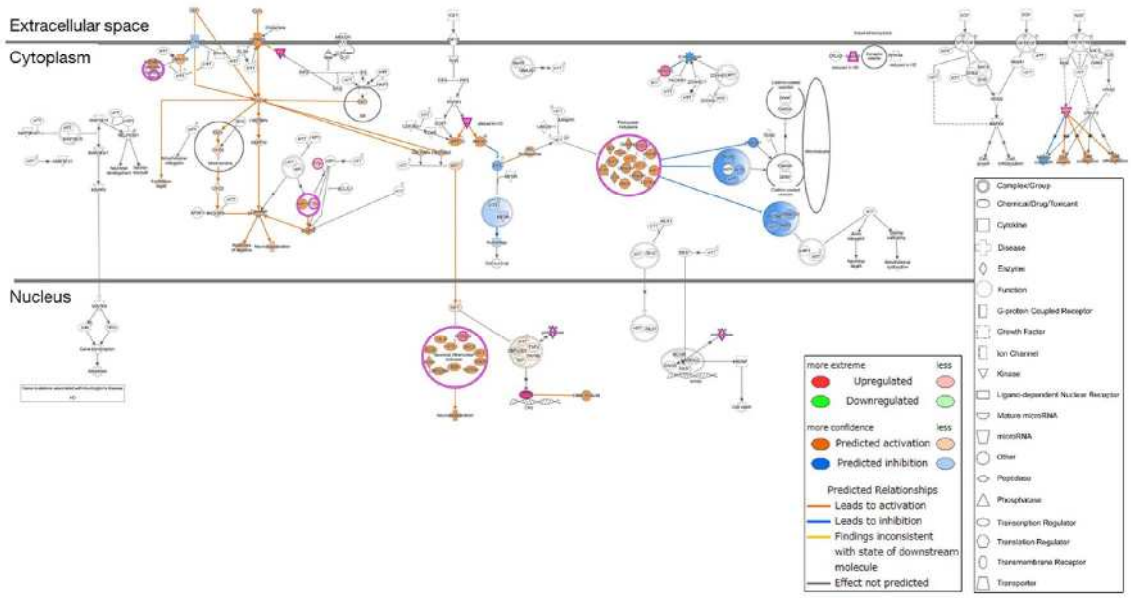

Fig 1.2. Subcellular location of genes in the canonical pathway termed as "Huntington's diseases signaling," as determined using Ingenuity Pathways Analysis (IPA) to compare transcriptomes in the young and old AP glands. Note that the IPA software shows gene names as normal font and not italics. Solid and dotted lines indicate direct or indirect biological relationships between genes, respectively. Bold gray lines indicate the border between the extracellular space, cytoplasm, and nucleus. Purple indicates the upregulated genes identified in this experiment. The results of molecule activity predictor are also shown here. Genes predicted to be stimulated are shown in orange, and those predicted to be inhibited are shown in blue. In total, 283 genes constituted the canonical pathway, and eight of these genes (AKT1, BET1L, CREB3, GNB3, IFT57, POLR2E, PRKCQ, and SH3GL3) were identified in the bovine AP glands used in this study.

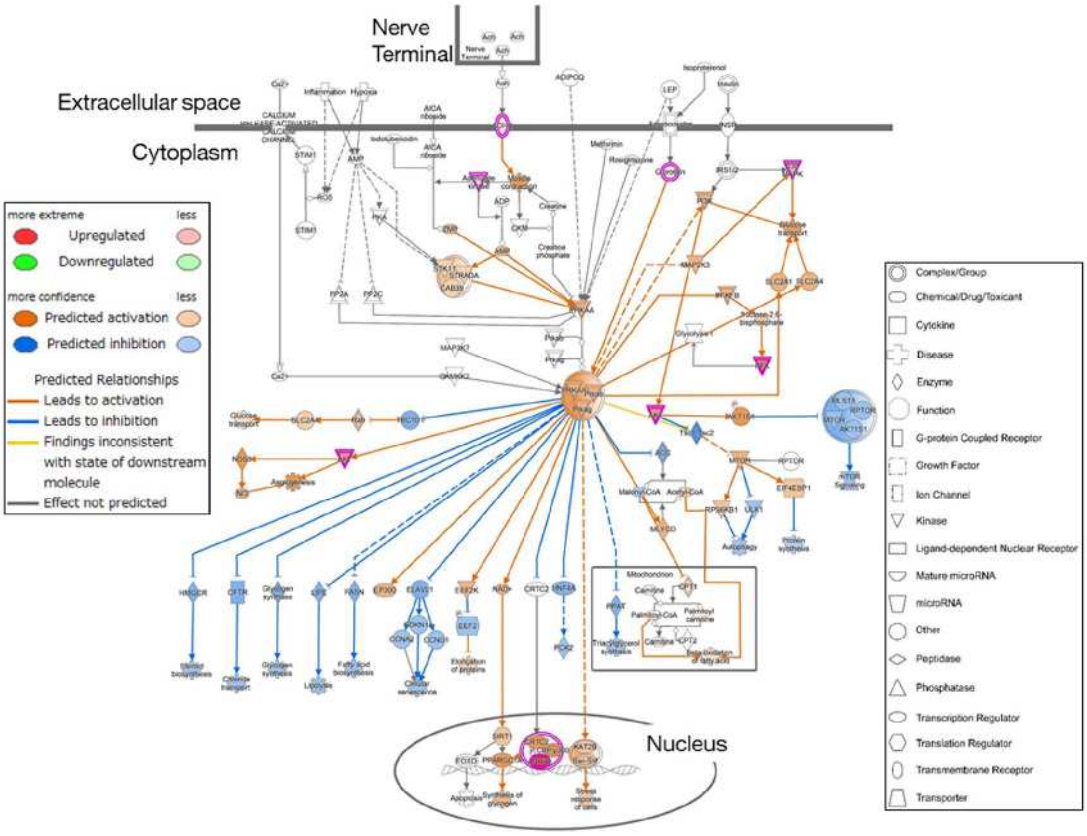

Fig 1.3. Subcellular location of genes in the canonical pathway termed as "AMPK signaling" as determined via IPA analysis to compare transcriptomes in the young and old AP glands. The results of molecule activity predictor are also shown here. In total, 244 genes constituted the canonical pathway, and seven of these genes (AK7, AKT1, CHRNA1, CREB3, GNB3, MAPK13, and PFKL) were identified in the bovine AP glands used in this study.

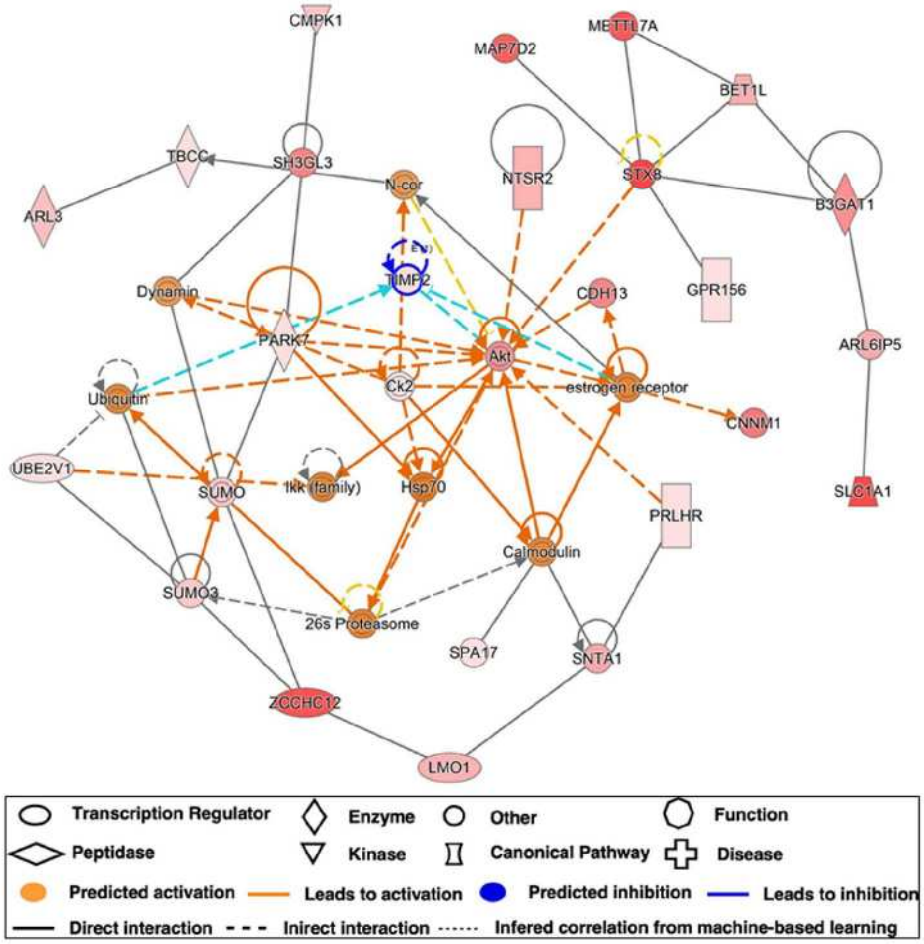

Fig 1.4. A network of 24 genes reveled using Ingenuity Pathways Analysis with name "Neurological disease, organismal injury, and abnormalities, psychological disorders". The 24 genes are 26 s Proteasome, Akt, ARL3, ARL6IP5, B3GAT1, BET1L, Calmodulin, CDH13, Ck2, CMPK1, CNNM1, Dynamin, estrogen receptor, GPR156, Hsp70, Ikk (family), LMO1, MAP7D2, METTL7A, Ncor, NTSR2, PARK7, PRLHR, SH3GL3, SLC1A1, SNTA1, SPA17, STX8, SUMO, SUMO3, TBCC, TIMP2, UBE2V1, Ubiquitin, and ZCCHC12

2. CHAPTER TWO:

Spike protein of SARS-CoV-2 suppresses gonadotrophin secretion from bovine anterior pituitaries

This work has been published as follows:

Dimas Arya Abdillah, Onalenna Kereilwe, Raihana Nasrin Ferdousy, Risa Saito, Hiroya Kadokawa. Spike protein of SARS-CoV-2 suppresses gonadotrophin secretion from bovine anterior pituitaries. 2022. Journal of Reproduction and Development. https://doi.org/10.1262/jrd.2021-126

2.1. ABSTRACT

Coronavirus disease (COVID-19), the ongoing global pandemic, is caused by the severe acute respiratory syndrome coronavirus-2 (SARS-CoV-2). Recent evidence shows that the virus utilizes angiotensin-converting enzyme 2 (ACE2) as a spike protein receptor for entry into target host cells. The bovine ACE2 contains key residues for binding to the spike protein receptor-binding domain. This study evaluated the hypothesis that bovine gonadotroph expresses ACE2, and spike protein suppresses luteinizing hormone (LH) and follicle-stimulating hormone (FSH) secretion from cultured bovine anterior pituitary (AP) cells. ACE2 mRNA expression and ACE2 protein expression were detected in the bovine AP cells using reverse transcription PCR and western blot analysis. Immunofluorescence microscopy analysis with the anti-ACE2 antibody revealed the co-localization of ACE2 and gonadotropin-releasing hormone (GnRH) receptor on the gonadotroph plasma membrane. Approximately 90% of GnRH receptor-positive cells expressed ACE2, and approximately 46% of ACE2-positive cells expressed the GnRH receptor. We cultured bovine AP cells for 3.5 days and treated them with increasing concentrations (0, 0.07, 0.7, or 7 pM) of recombinant spike protein having both S1 and S2 regions. The spike protein (0.07–7 pM) suppressed both basal and GnRH-induced LH secretion ($P < 0.05$). Spike protein (0.7–7 pM) suppressed GnRH-induced ($P < 0.05$), but not basal FSH secretion. In contrast, pre-treatment with ERK 1/2/5 inhibitor (U0126) partially restored the GnRH-induced LH and FSH secretion from the spike protein suppression. Collectively, the results indicate that gonadotrophs express ACE2, a receptor for coronavirus 2 spike protein, which in turn suppresses LH and FSH secretion from AP cells.

2.2. INTRODUCTION

The ongoing global coronavirus disease (COVID-19) pandemic has been caused by the spread of severe acute respiratory syndrome coronavirus-2 (SARS-CoV-2). Recent evidence shows that the virus utilizes angiotensin-converting enzyme 2 (ACE2) as a spike protein receptor to enter target host cells (103); however, the primary role of ACE2 is to convert angiotensin II to angiotensin-(1–7). Cells expressing ACE2 may thus be a target for the virus. ACE2 is highly expressed in the human testes, ovaries, and other reproductive organs (17). Indeed, the virus may be an important cause of infertility in men because of its deleterious effects on semen quality and quantity through unclarified mechanisms, as reviewed by Agolli et al. (18) and Moshrefi et al. (19). However, it remains unclear whether the virus also causes female infertility, especially in domestic animals.

The anterior pituitary (AP) gland lies outside the blood-brain barrier (20), and may be affected by the virus (21). Gonadotrophs are important cells located in the AP glands, and secrete luteinizing hormone (LH) and follicle-stimulating hormone (FSH), which regulate the testes, ovaries, and, via gonadal steroids, other reproductive organs in animals (22). However, to the best of our knowledge, the effect of the virus on gonadotrophs remains unclear. Gu et al. (23) reported that human gonadotrophs express ACE2. A recent study clarified that the spike protein of SARS-CoV-2 directly activates the cytoplasmic extracellular signal-regulated kinase (ERK) pathway downstream of ACE2 in human platelets (24). The ERK pathway is also the cytoplasmic pathway downstream of the membrane estradiol receptor (GPR30), that suppresses LH secretion in bovine gonadotrophs (104). However, the mechanism by which spike protein-activated ACE2 affects LH and FSH secretion by gonadotrophs in all species remains unclear.

Cattle are important domestic animals for food supply worldwide; thus, infertility in cattle is an important issue. Unlike human AP glands, bovine AP glands can be obtained for primary culture as they can be collected from slaughterhouses. Indeed, using bovine gonadotrophs, we discovered new receptors that control LH and FSH secretion, colocalizing with gonadotropin-releasing hormone (GnRH) receptor (GnRHR) in the lipid rafts of bovine gonadotrophs (5, 22, 105, 106). Bovine ACE2 contains most of the key residues for the receptor-binding domain of SARS-CoV-2 (107) (details are shown in Supplementary Fig.1), and SARS-CoV-2 replicates in bovine respiratory tissues (108). Therefore, we tested the hypothesis that gonadotrophs express the spike protein receptor ACE2, colocalizing with GnRHR on the bovine gonadotroph cell surface, and that the recombinant spike protein suppresses LH and FSH secretion from

cultured bovine AP cells. It is also important to clarify the cytoplasmic signaling pathway downstream of ACE2. Therefore, we used an inhibitor to evaluate the contribution of the ERK pathway to the effect of spike protein on gonadotropin secretion from the bovine AP.

2.3. MATERIALS AND METHODS

2.3.1. Anterior pituitary sample collection

All experiments were performed in accordance with the Guiding Principles for the Care and Use of Animals in the Field of Physiological Sciences (Physiological Society of Japan). All experiments involving animals were approved by the Animal Ethics Committee of Yamaguchi University (approval number 301).

We obtained AP tissue from post-pubertal (26 months of age) Japanese Black heifers at a local abattoir, using a previously described method (109). All heifers were in the luteal phase, as determined by macroscopic examination of the ovaries and uterus (105); the AP gland exhibits the highest LH, FSH, and GnRH receptor levels in this phase (110).

The AP samples for RNA or protein extraction (n = 5) were stored at −80°C. The AP samples for immunohistochemistry (n = 5) were fixed with 4% paraformaldehyde at 4°C for 16 h. The AP samples to be used for cell culture followed by immunocytochemical analysis (n = 5), and those that were to be used for cell culture to evaluate the effect of spike on LH and FSH secretion (n = 6) were stored in ice-cold 25 mM HEPES buffer (pH 7.2) containing 10 mM glucose and transported to the laboratory on ice.

2.3.2. RT–PCR, sequencing of amplified products, and homology search in gene databases

Total RNA was extracted using RNAzol RT isolation reagent (Molecular Research Centre, Inc., Cincinnati, OH, USA) and treated with deoxyribonuclease. The concentration and purity of each RNA sample was evaluated using spectrophotometry (acceptable range, 1.8–2.1) and electrophoresis (28S:18S ratios were 2:1). Complementary DNA was synthesized using the Verso cDNA Synthesis Kit (Thermo Fisher Scientific, Waltham, MA, USA).

We used previously reported RT-PCR methods (105) to detect the mRNA levels of ACE2 (NCBI reference sequence, NM_001024502). The expected amplicon size of ACE2 was 470 bp (orange highlighted region in Supplementary Fig. 1; nucleotides 1297-1766; forward primer in 9th exon: 5′-CCGCAGCCACACCTCACTAT- 3′; reverse primer in 13th exon: 5′-GGTCCAGGGTTCTGATTTTCC-3′). PCR was performed using 20 ng of cDNA and polymerase (Tks Gflex DNA Polymerase, Takara Bio Inc., Shiga, Japan) under the following thermocycling conditions: 94°C for 1 min for pre-denaturation, followed by 35 cycles of 98°C for 10 sec, 60°C for 15 sec, and 68°C for 30 sec. The PCR products were separated on 1.5% agarose gel using electrophoresis with a molecular marker (Nippon Gene, Tokyo, Japan), stained with Gelstar (Lonza, Allendale, NJ, USA), and observed using a charge-coupled device (CCD)

imaging system (GelDoc; Bio-Rad, Hercules, CA, USA). The PCR products were purified using a NucleoSpin Extract II kit (Takara Bio Inc.) and then sequenced using PCR primers and the Dye Terminator v3.1 Cycle Sequencing Kit (Thermo Fisher Scientific). The sequences obtained were used as query terms to search the homologous sequences using the basic nucleotide local alignment search tool (BLAST) (available on the NCBI website).

2.3.3. Antibodies used in this study

We used a specific anti-ACE2 rabbit polyclonal antibody (HPA000288; Sigma-Aldrich, St. Louis, MO, USA). The antigen sequence that produces the antibody has 86% homology with the corresponding region of bovine ACE2, as shown by the green highlighted region in Supplementary Fig. 1. In particular, ACE2 has a single transmembrane region (111), as indicated by the blue highlighted region in Supplementary Fig. 1. There is 91% homology between the extracellular regions of bovine and human ACE2 (the NCBI reference sequences of bovine and human ACE2 are NP_001019673.2 and BAB40370, respectively).

We also used a guinea pig polyclonal antibody that recognizes the N-terminal extracellular domain of the bovine GnRH receptor (anti-GnRHR). The specificity of the anti-GnRHR antibody has been verified previously (109). We used a mouse monoclonal anti-LH antibody (clone 518-B7) (112) and a mouse monoclonal anti-FSH antibody (clone A3C12) (113) for immunohistochemical analysis of AP tissue and cultured AP cells. These antibodies do not cross-react with other pituitary hormones (113, 114).

2.3.4. Western blot analysis for ACE2

We extracted proteins from AP tissue and performed western blotting using a previously described method (109). Briefly, total proteins were extracted from frozen stock AP tissue using a tissue protein extraction reagent containing Halt Protease Inhibitor Cocktail (Thermo Fisher Scientific). The extracted protein sample was boiled with Sample Buffer Solution containing Reducing Reagent (6x) for SDS-PAGE (09499-14; Nacalai Tesque, Kyoto, Japan) for 3 min at 100°C. The protein samples (8,000 ng of total protein) were loaded onto a polyacrylamide gel (Any KD Criterion TGX gel, Bio-Rad) along with the whole-cell lysate of human liver-derived HepG2 cells (sc-2227, Santa Cruz, Heidelberg, Germany) as positive controls (115), and a molecular weight marker (Precision Plus Protein All Blue Standards; Bio-Rad). The proteins were resolved by sodium dodecyl sulfate-polyacrylamide gel electrophoresis at 100 V for 90 min. The proteins were transferred onto polyvinylidene fluoride (PVDF) membranes (Trans-blot turbo PVDF, Bio-Rad) with electroblotting at 2.5 A, 25 V, for 7 min using a Trans-blot Turbo system (Bio-Rad).

A Can Get Signal kit (Toyobo Co., Ltd., Osaka, Japan) was used to block the membrane (1 h at 25°C), primary antibody reaction (1 h at 25°C) with the anti-ACE2 rabbit antibody (1:400,000 dilution with immunoreaction enhancer solution), and secondary antibody reaction (1 h at 25°C) with a goat anti-rabbit IgG horseradish peroxidase- conjugated antibody (Bethyl Laboratories, Inc., Montgomery, TX, USA; 1:400,000 dilution with immunoreaction enhancer solution). The protein bands were visualized using an ECL-Prime chemiluminescence kit (GE Healthcare, Amersham, UK) and a CCD imaging system (LAS-3000 Mini; Fujifilm, Tokyo, Japan). To verify the specificity of the signals, we included several negative controls in which the primary antibodies were omitted, or normal rabbit IgG (Wako Pure Chemicals, Osaka, Japan) antibodies were used instead of the specific primary antibodies. Signal specificity was also confirmed using negative controls in which the primary antibodies were pre-absorbed with 4 nM of the antigen peptide (PrEST Antigen ACE2, APREST74018, Sigma-Aldrich).

The antibodies were removed from the PVDF membrane using a stripping solution (Nacalai Tesque) before blocking and subsequent immunoblotting with an anti-β-actin mouse monoclonal antibody (1:400,000 dilution; Sigma-Aldrich).

2.3.5. Fluorescence immunohistochemistry and confocal microscopy

We followed our previously reported method (109) for the immunofluorescence analysis of AP tissue (n = 5) after storage in 4% paraformaldehyde PBS at 4°C for 16 h, and 30% sucrose PBS until the blocks were infiltrated with sucrose. The blocks were frozen in an embedding medium (Tissue-Tek OCT compound Sakura Finetechnical Co., Ltd., Tokyo, Japan) and maintained at −80°C. Briefly, 15-μm sections were prepared using a cryostat, mounted on slides for treatment with 0.3% Triton X-100 in PBS for 15 min, and blocked with 10% normal goat serum in PBS for 1 h. Incubation with a cocktail of primary antibodies (anti-ACE2 rabbit antibody, anti-GnRHR guinea pig antibody, and either anti-LH or anti-FSH mouse antibody [all diluted 1:1,000]) for 12 h at 4°C was followed by incubation with secondary antibodies (Alexa Fluor 488 goat anti-rabbit IgG, Alexa Fluor 546 goat anti-mouse IgG, and Alexa Fluor 647 goat anti-guinea pig IgG [all from Thermo Fisher Scientific and diluted as 1 μg/ml]) for 2 h at room temperature, and counterstaining with 1 μg/ml of 4, 6-diamino-2-phenylindole (DAPI; Wako Pure Chemicals).

The stained sections were observed using a confocal microscope (LSM710; Carl Zeiss, Göttingen, Germany) equipped with diode (405 nm), argon (488 nm), HeNe (533 nm), and HeNe (633 nm) lasers. Images obtained by fluorescence microscopy were scanned with a 40 × or 63 × oil-immersion objective and recorded using a CCD camera system controlled by ZEN2012 black edition software (Carl Zeiss). To verify the specificity of

the signals, we included several negative controls in which the primary antiserum had been omitted or pre-absorbed with 4 nM of the antigen peptide, or in which normal rabbit IgG (Wako Pure Chemicals) was used instead of the primary antibody. Ratios of ACE2 positive gonadotrophs were calculated from 12 representative confocal images per AP gland.

2.3.6. AP cell culture and immunocytochemical analysis of cells

We followed our previously reported method (109) for the enzymatic preparation of AP cells (n = 6) and their culture. Cell viability was confirmed to be greater than 90% by trypan blue exclusion. Total cell yield was 19.8 × 106 ± 0.8 × 106 cells per AP gland. Dispersed cells were then suspended in Dulbecco's modified Eagle's medium (DMEM; Thermo Fisher Scientific) containing 1 × nonessential amino acids (Thermo Fisher Scientific), 100 U/ml penicillin, 50 μg/ml streptomycin, 10% horse serum (Thermo Fisher Scientific), and 2.5% fetal bovine serum (Thermo Fisher Scientific). The cells (2.5 × 105 cells/mL, total = 0.15 ml per lane) were cultured in the culture medium at 37°C in 5% CO2 for 82 h, using a microscopy chamber (μ-Slide VI 0.4, Ibidi, Planegg, Germany). Recombinant human activin A (final concentration, 10 ng/ml; R&D Systems, Minneapolis, MN, USA) was used to stimulate FSH synthesis at 24 h before fixation (105). FSH secretion from cultured AP cells is weak in ovine and bovine AP cells, and the pre-treatment time and final concentration have already been established in previous studies (116).

The cultured cells were fixed with either 4% paraformaldehyde for 3 min followed by treatment with 0.1% Triton X-100 for 1 min (PFA-Triton method), or with CellCover (Anacyte Laboratories UG, Kuhreder, Hamburg) for 2 min without Triton X-100 treatment (CellCover method), as described by Kadokawa et al. (109). For the PFA-Triton method, fixed cells were incubated with 0.1 ml of the same cocktail of primary antibodies for 2 h at room temperature. Incubation with Triton X-100 allowed anti-GnRHR and anti-ACE2 antibodies to bind to target proteins in the cytoplasm and at the cell surface. For the CellCover method, the fixed cells were incubated with guinea pig anti-GnRHR and rabbit anti-ACE2 (both 1:1,000) for 2 h at room temperature. As the cells were not treated with Triton X-100, the antibodies could only bind to the extracellular domains of the respective receptors in most cells. For both the PFA-Triton and CellCover methods, cells were incubated with the fluorochrome-conjugated secondary antibody cocktail and DAPI and subjected to confocal microscopy. Signal specificity was confirmed using negative controls in which the primary antibody was omitted or pre-absorbed at 4 nM with the same antigen peptide. Normal rabbit IgG was used as the primary antibody. Eight randomly selected images of cells prepared with the CellCover

method were analyzed for co-localization using the ZEN 2012 black edition software (Carl Zeiss) to calculate overlap coefficients (117) for Alexa Fluor 488 and Alexa Fluor 647.

2.3.7. Effects of the recombinant spike protein of SARS-COV-2 on LH and FSH secretion

AP cells derived from six post-pubertal heifers were plated in 48-well cell culture plates (Sumitomo Bakelite, Tokyo, Japan) and incubated at 37°C and 5% CO2 for 82 h. Recombinant human activin A (final concentration, 10 ng/ml) was added to the plates 24 h before the test to stimulate FSH synthesis.

The medium was replaced with 270 µl of DMEM containing 0.1% BSA (IgG-free Protease-free culture grade, 032-22364, Wako Pure Chemicals) and 10 ng/ml activin A (base medium) and incubated for 2 h to evaluate the effect of spike protein in the absence of GnRH. Treatment was performed by adding 30 µl of base medium alone or 30 µl of base medium with different concentrations of spike protein (final concentrations of 0, 0.07, 0.7, and 7 pM). We used a recombinant spike protein of SARS-CoV-2 containing both the S1 and S2 regions (40589-V08H4; Sino Biological US Inc., Wayne, PA, USA). After incubation for 2 h, the medium from each well was collected for radioimmunoassay (RIA) analyses of LH and FSH levels.

The old medium was replaced with 240 µl of base medium and incubated at 37°C for 2 h to evaluate the effect of the spike protein in the presence of GnRH. The cells were pre-treated by adding 30 µl of base medium containing different concentrations of the recombinant spiked protein (final concentrations of 0, 0.07, 0.7, and 7 pM). The cells were incubated with gentle shaking for 5 min, and then treated with 30 µl GnRH (Peptide Institute Inc., Osaka, Japan; final concentration of 1 nM (109)) dissolved in the base medium for 2 h. As previously reported (109), gonadotropin secretion was stimulated by increasing the amounts of GnRH, with a peak at 1 nM of GnRH, and reduced secretion at GnRH concentrations higher than 1 nM. Therefore, the final concentration of GnRH used in this study was 1 nM in all treatments, except in the controls. After incubation for 2 h, the medium from each well was collected for LH and FSH RIAs.

2.3.8. Effect of ERK pathway inhibitor on the suppression of secretion

We evaluated the effect of the ERK1/2/5 pathway inhibitor, U0126, on spike-mediated suppression of secretion from bovine AP cells. AP cells obtained from a different set of post-pubertal Japanese Black heifers (n = 8, in the middle of the luteal phase, 26 months of age), were cultured for 82 h in the medium described in the previous section. Each experiment was repeated eight times with each of the eight AP glands, using four wells per treatment. The wells were washed twice with PBS and then incubated with 287 µl of DMEM

containing 0.1% BSA and 10 ng/ml activin A for 2 h. Cells were pre-treated with 3 μl of DMEM alone or 3 μl of DMEM containing U0126 (final concentration, 1,000 nM; Enzo Biochem, Inc., New York, USA). After 30 min of incubation, either 5 μl of DMEM alone or 5 μl of DMEM containing spike protein (final concentration of 7 pM, which showed a significant inhibitory effect on gonadotropin secretion) was added to each culture well. The cells were incubated with gentle shaking for 5 min, after which they were incubated for 2 h with 5 μl of DMEM containing GnRH (final concentration, 1 nM) to stimulate gonadotropin secretion. After 2 h of incubation, the medium was collected for RIA. We previously confirmed that pre-treatment with 1,000 nM U0126 alone had no effect on GnRH-induced gonadotropin secretion, but inhibited the ability of estradiol to suppress GnRH-induced gonadotropin secretion from cultured bovine AP cells (104).

2.3.9. RIAs to measure gonadotropin concentration in culture media

The concentration of LH was measured in duplicate samples of culture media using double-antibody RIA using ^{125}I-labeled bLH and anti-oLH-antiserum (AFP11743B and AFP192279, National Hormone and Pituitary Program of the National Institute of Diabetes and Digestive and Kidney Diseases, Bethesda, CA, USA). The intra- and inter-assay coefficients of variation (CV) were 3.6% and 6.2%, respectively. The concentration of FSH was measured by double-antibody RIA using bFSH and anti-oFSH antiserum (AFP5318C, AFP5346D, and AFPC5288113, NIDDK). The intra- and inter-assay CVs were 4.3% and 7.1%, respectively.

2.3.10. Statistical analysis

The statistical significance of differences in LH or FSH concentration was analyzed by one-factor ANOVA followed by *post-hoc* comparisons using Fisher's protected least significant difference test in StatView version 5.0, for Windows (SAS Institute, Inc., Cary, NC, USA). The level of significance was set at $P < 0.05$. Data are expressed as the mean ± standard error of the mean (SEM).

2.4. RESULTS

2.4.1. Expression of ACE2 in AP of post-pubertal heifers

The expected PCR products were obtained by electrophoresis (Fig. 2.1A). Homology searching for the amplified product sequences revealed that the best match alignment was bovine ACE2 (NM_001024502), which was identical (identities were 100% (470/470) with no gaps). No other bovine genes were found to have any homology with the obtained sequences of the amplified products, suggesting that the sequences of the amplified products were identical to the sequence of bovine ACE2.

Western blotting revealed similar bands for AP and HepG2-cells (Fig. 2.1B). One difference was the band size of 42 kDa for AP and 50 kDa for HepG2. Another difference was that a 100-kDa band was observed in the AP sample, but not in HepG2. No bands were observed in the negative control membranes, where the primary antiserum was pre-absorbed with the antigen peptide.

2.4.2. Immunofluorescence analysis of ACE2 expression in bovine AP tissue

ACE2 and GnRHR were colocalized in the majority of LH-positive (Fig. 2.2A) and FSH-positive (Fig. 2.2B) cells in bovine AP tissue. The percentages of single- and double-labeled ACE2- and GnRHR-positive cells were determined from 15 representative confocal images per AP gland. In each AP gland, there was an average of 54.4 ± 2.4 GnRHR-positive cells, 105.2 ± 1.1 ACE2-positive cells, and 48.6 ± 1.7 double-positive cells; further, 89.5 ± 1.6% of GnRHR-positive cells were ACE2-positive, and 46.3 ± 1.9% of ACE2-positive cells were GnRHR-positive. No immunostaining signals were observed in the negative control tissues, where the primary antiserum was pre-absorbed with the antigen peptide.

2.4.3. ACE2 and GnRHR on the cell surface

Among the AP cells prepared using the PFA-Triton method, we observed ACE2 expression in LH-positive (Fig. 2.3A) and FSH-positive cells (Fig. 2.3B).

The AP cells prepared using the cell cover method showed that ACE2 was colocalized on the surface of GnRHR-positive cells (Fig. 2.4). The overlap coefficient of the cultured AP cell surface between ACE2 and GnRHR was 0.73 ± 0.01.

2.4.4. Effects of spike protein on gonadotropin secretion from cultured AP cells

Figure 5 shows the effect of various concentrations of spike protein on LH or FSH secretion from AP cells derived from post-pubertal heifers cultured in the absence (A, C) or presence (B, D) of GnRH. In the absence of GnRH (Fig. 2.5A), 0.07 pM ($P < 0.05$), 0.7 pM ($P < 0.05$), and 7 pM ($P < 0.01$) of spike protein suppressed

LH secretion compared to the controls. Moreover, 0.07 pM ($P < 0.05$), 0.7 pM ($P < 0.01$), and 7 pM ($P < 0.01$) of spike protein suppressed GnRH-induced LH secretion (Fig. 2.5B).

In the absence of GnRH (Fig. 2.5C), none of the tested concentrations of spike protein was found to suppress FSH secretion compared to the controls. However, 0.7 pM ($P < 0.01$) and 7 pM ($P < 0.01$), but not 0.07 pM the spike protein suppressed GnRH-induced FSH secretion (Fig. 2.5D).

Figure 2.6 shows that 7 pM of spike protein suppressed GnRH- induced LH secretion, and that pre-treatment with U0126 partially recovered GnRH-induced LH and FSH secretion.

2.5. DISCUSSION

Cultured bovine gonadotroph cells express ACE2, and addition of recombinant spike protein to the culture medium suppressed the secretion of LH and FSH, providing clear evidence that the spike protein, containing both S1 (attachment to ACE2) and S2 (fusion with host membrane) regions, affects the cytoplasmic ERK pathways (24) that play important roles in the control of LH and FSH secretion (104). ACE2 colocalizes with GnRHR on the lipid rafts of gonadotrophs (22), suggesting that the S2 region suppresses LH and FSH secretion by fusing with the lipid rafts (118) to affect heteromer receptors.

We found that approximately 90% of gonadotroph cells in bovine AP were ACE2-positive. Similar to other GPCRs [26], GnRHR forms functionally active homomers and heteromers with different receptors (22, 119). We obtained a strong positive overlap coefficient between ACE2 and GnRHR on the cell surface of bovine gonadotrophs. Therefore, ACE2 may form a heteromer with GnRHR in gonadotrophs.

However, the results of this study must be interpreted with some caution. Gu et al. (23) reported ACE2 expression in the human AP gland, but found no significant difference in blood LH and FSH concentrations between and SARS-CoV-2-infected and uninfected patients. However, in another study, male patients with COVID-19 showed lower blood concentrations of testosterone and higher blood concentrations of LH and prolactin (120). ACE2 is expressed at higher levels in the human testis and ovary than in the AP gland (121). Therefore, one possible reason is that gonadal ACE2 may bind spike proteins rather than ACE2, and the direct and indirect suppression of steroidogenesis by the virus and immune system, respectively, may then induce hypogonadism, which reduces the negative feedback of steroid hormones to gonadotrophs (122). Another possible reason could be that the measurements were performed on a one-point sample and not repeated to measure the parameter of pulsatile secretion of LH and FSH.

Bovine ACE2 can bind the spike protein of SARS-CoV-2 (107) and SARS-CoV-2 replicates in bovine respiratory tissues (108). Intratracheal and intravenous inoculation with SARS-CoV-2 resulted in only minor replication in colostrum-deprived Holstein bull calves (123). However, white-tailed deer (Odocoileus virginianus), a ruminant species, are highly susceptible to infection (124). Therefore, caution is needed against the spillover of SARS-CoV-2, especially of new variants, among humans, domestic animals, and wild animals.

The primary role of ACE2 is to convert angiotensin II to angiotensin-(1–7). Although gonadotrophs are the likely site of angiotensin II production in rat AP glands (125), little is known about the roles of ACE2,

angiotensin II, and angiotensin-(1–7) in gonadotrophs. Therefore, further studies are required to clarify these roles.

There are no previous reports of bovine ACE2 protein size using western blotting. As determined by western blotting, the bovine ACE2 protein was approximately 100 kDa. However, this was larger than the 91 kDa predicted from the amino acid sequence. Additionally, human ACE2 shows a band at approximately 100 kDa along with a 50-kDa band (126). In a previous study (112), HepG2 cells showed an approximately 100-kDa band using the same anti-ACE2 antibody, but showed a 50-kDa band in this study. This difference in band size may be due to experimental conditions in the culture or sample preparation for western blot. This is because band sizes in western blotting often differ from expected sizes in the case of membrane-bound proteins such as cell-surface receptors, owing to their complex three-dimensional structures, which can include hydrophilic and lipophilic regions that form extracellular, transmembrane, and cytoplasmic domains (127).

Primary AP cell culture was used to evaluate rapidly activated (within 30 min) pathways that altered LH and FSH secretion from bovine gonadotrophs, without alterations in the mRNA expression of LHα, LHβ, or FSHβ subunits. Thus, we did not perform RT-qPCR for LH and FSH genes. We previously found that the small interfering RNA method could not be used in this system because secretion was suppressed even in control RNA (unpublished data). Therefore, we evaluated the contribution of ERK pathway using an inhibitor. We could not exclude any other pathway as U0126 partially recovered gonadotropin secretion. In particular, Smad7 pathway suppresses cell function downstream of ACE2 in diabetic nephropathy (128), and inhibits FSHB gene expression in mouse gonadotroph-derived LβT2 cells (129). However, to the best of our knowledge, a SMAD7-specific inhibitor has not yet been developed. Therefore, further studies are required in the future to investigate this aspect.

Angiotensin II activates the type 1 receptor (AT1R) and ERK pathways in rat tubular epithelial cells (130). Thus, if ACE2 is inhibited by the spike protein, angiotensin II may be increased and stimulate the AT1R and ERK pathways. However, to the best of our knowledge, there are no reports on the expression of AT1R in gonadotrophs. In addition, the culture medium did not contain angiotensin II. Therefore, it is unlikely that the angiotensin II-AT1R system contributed to the observed suppression by spike protein.

Moreover, non-gonadotroph cells were also ACE2-positive. Mice that ubiquitously overexpress ACE2 have reduced the expression of proopiomelanocortin and plasma corticosterone in the AP (131). ACE2 activation

by diminazene aceturate increases ACTH secretion from AtT-20 cells but not prolactin secretion from MMQ and GH3 cells (23). Therefore, ACE2-positive non-gonadotroph cells may be corticotrophs.

In conclusion, ACE2 is expressed in gonadotrophs, and the SARS-CoV-2 spike protein significantly suppresses LH and FSH secretion via the ERK pathway. This effect may constitute a cause of infertility in cows; however, further long-term in vivo studies are required to validate these results.

2.6. TABLES, FIGURES, SUPPLEMENTARY DATA

Figures

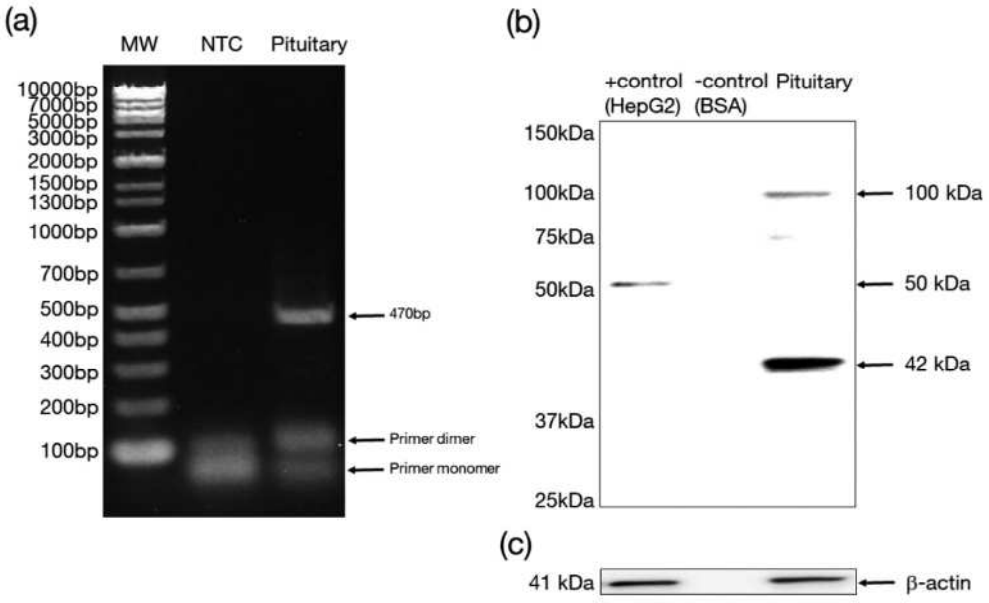

Fig 2.1. Expression of *Angiotensin-converting enzyme 2 (ACE2)* detected using RT-PCR and western blotting. Electrophoresis of PCR-amplified DNA products using primers for bovine *ACE2* and cDNA from bovine anterior pituitary (AP) glands; the band was 470 bp (A). Two bands (100 kDa and 42 kDa) appeared on the AP sample, whereas a 50-kDa band was observed in HepG2 cells, which were used as the positive control (B). The relative band of β-actin (41 kDa) was used as a control for both HepG2 and AP (C).

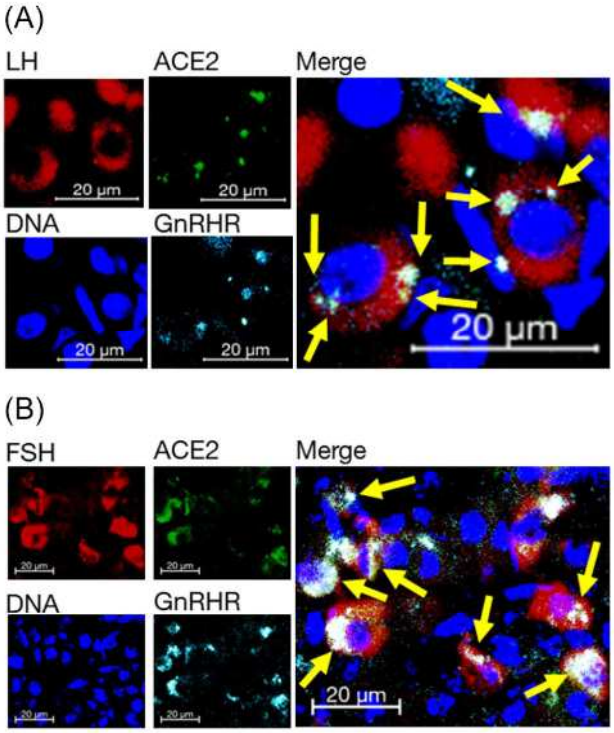

Fig 2.2. Triple-fluorescence immunohistochemistry of bovine AP tissue for ACE2, gonadotropin-releasing hormone receptor (GnRHR), and either luteinizing hormone (LH) (A) or follicle stimulating hormone (FSH) (B). Images were captured using laser confocal microscopy for LH or FSH (red), ACE2 (green), and GnRHR (light blue) with counter-staining using DAPI (dark blue). The yellow arrows indicate the colocalisation of ACE2 with GnRHR. Scale bars are 20 µm.

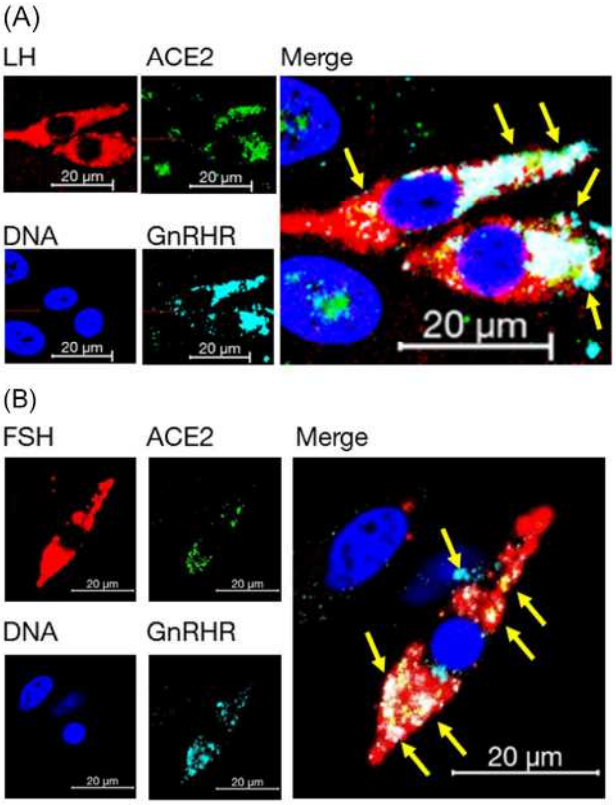

Fig 2.3. Triple-fluorescence immunocytochemistry of cultured AP cells (prepared using PFA-Triton method) of post-pubertal heifers for ACE2, GnRHR, and either LH (A) or FSH (B). Images were captured using laser confocal microscopy for LH or FSH (red), ACE2 (green), and GnRHR (light blue) with counter-staining using DAPI (dark blue). The yellow arrows indicate the colocalisation of ACE2 with GnRHR. Scale bars are 20 µm.

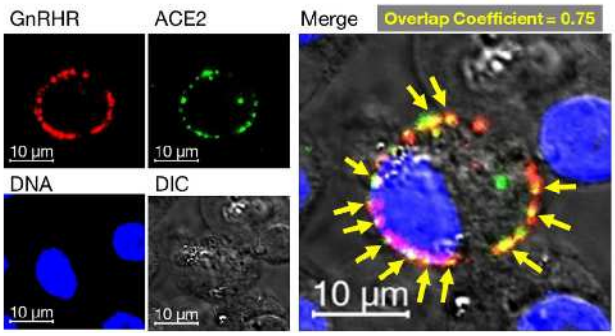

Fig 2.4. Fluorescence immunocytochemistry was used to confirm the colocalisation (yellow in the merge panel) of ACE2 and GnRHR on the surface of cultured AP cells (prepared using the Cell Cover method) of post-pubertal heifers. Images were captured using a laser confocal microscope for GnRHR (red), ACE2 (green), DNA (dark blue), and differential interference contrast (DIC) on cultured AP cells which did not receive Triton X-100 treatment for antibody penetration. Thus, the antibody could only bind ACE2 and GnRHR on the surface of gonadotrophs. The arrows indicate the colocalisation of ACE2 with GnRHR. Note that cells prepared using the Cell Cover method are thicker than those prepared using the PFA-Triton method. Scale bars are 10 µm.

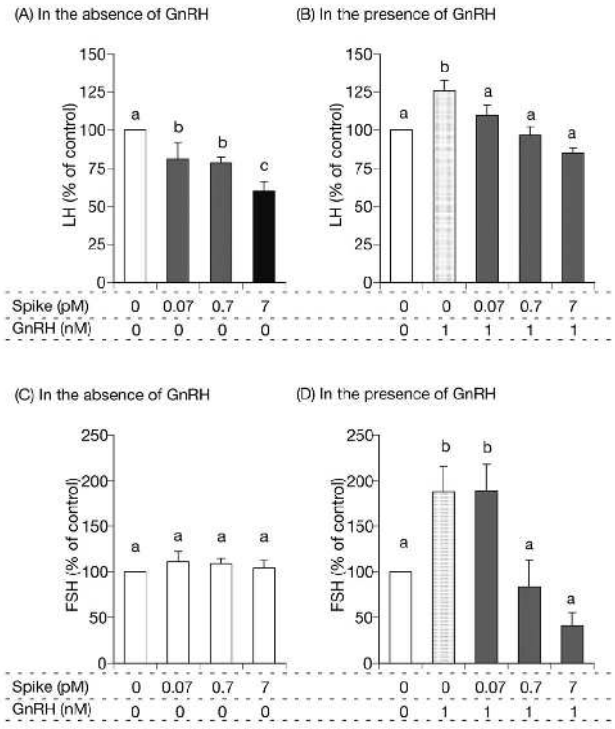

Fig 2.5. Comparison of the effects of various concentrations of spike protein in media without (A, C) and with (B, D) 1 nM GnRH on LH or FSH secretion from cultured AP cells of post-pubertal heifers. All cultured cells were pre-treated with activin. The concentrations of LH or FSH in control cells (cultured in medium alone without spike protein and GnRH) were averaged and set at 100%; the mean LH or FSH concentration for each treatment group is expressed as a percentage of the control value. Different letters indicate statistically significant differences ($P < 0.05$).

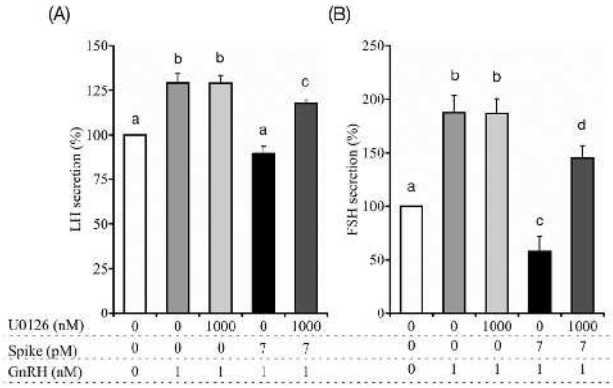

Fig 2.6. Effect of the ERK pathway inhibitor, U0126, on spike protein-mediated suppression of GnRH-induced secretion of LH (A) and FSH (B) from cultured bovine AP cells. All cultured cells were pre-treated with activin. The mean LH or FSH concentration for each treatment group is expressed as a percentage of the control value. Different letters indicate statistically significant differences ($P < 0.05$).

3. CHAPTER THREE:

Refrex-2 is a restriction factor for Felidae Endogenous Retrovirus gamma4 infection

This work will be submitted as follows:

Dimas Arya Abdillah, Miyu Tanaka, Didik Pramono, Loay Abu Eed, Ariko Miyake, Kazuo Nishigaki. 2025. Refrex-2 is a restriction factor for Felidae Endogenous Retrovirus gamma4 infection.

3.1 ABSTRACT

Endogenous retroviruses (ERVs) are remnants of retroviral infection found in vertebrate genomes. ERVs provide valuable molecular fossils records of ancient retroviruses to investigate viral-host interactions over a deep time scale. On occasions, evolutionary selection pressure led host to repurpose retroviral genes to serve their biological function, a phenomenon known as co-option/exaptation. In this study, we focused on FcERV-gamma4, an *Felis catus* endogenous gammaretrovirus 4 which often recombined with FeLV, and traced the infection history of FcERV-gamma4 retrovirus, over approximately 10 million years of feline evolution. Homologues of FcERV-gamma4 viral sequences referred to as Felidae ERV-gamma4 were analyzed from the genomes of 21 species in 7 lineages of cats, and 350 Felidae ERV-gamma4 proviruses were detected. The presence of intact full-length proviruses in the Felidae ERV-gamma4 suggests that they emerged very recently and spread rapidly in each lineage of cats. The spread of this virus shows both interspecies and intraspecies modes of transmission. During the history of these infections, new viruses were shown to arise by viral recombination in addition to their appearance by interspecies transmission. To investigate the host restriction for these viruses, we attempted to reconstruct functional envelopes proteins from domestic cats (*Felis catus*) and Geoffory's cats (*Leopardus geoffroyi*). FcERV-gamma4 and *Lepardus geoffroyi* (Lg)ERV-gamma4 enveloped MLV particles could infect cell lines from a wide range of mammalian species. Notably, the truncated envelope proteins derived from FcERV-gamma4- A1 and -C1, which termed Refrex-2, were secreted from cells, and they specifically inhibited FcERV-gamma4 and *Lepardus geoffroyi* (Lg)ERV-gamma4 infection, probably due to competitive interference on the receptor. Refrex-2 consists of a signal peptide and the 5' N-terminal region of Env SU, but lacks the transmembrane region. Refrex-2 was identified to express in broad tissues of domestic cat. Orthologues of FcERV-gamma4-A1 and -C1 have been identified in Felidae species, where they function as Refrex-2. Genetic analysis showed that Refrex-2 has been under purifying selection in Felidae species. These results highlight the hidden history of viral infection over a long period of time, from prehistory to the present day. Furthermore, they expose the major influence of viral infections on the history of animal evolution. This study provides insights into the history of viral infection on a geological scale that cannot be inferred from extant viral traces, and will enhance our understanding of life events related to virus-host co-evolution.

3.2. INTRODUCTION

Retroviruses are a group of RNA viruses that exhibit a distinctive replication mechanism, which involves a process of reverse transcription and subsequent integration into the host genome (26). These viruses are broadly classified into two categories: exogenous retroviruses (exRV) and endogenous retroviruses (ERV), based on the mode of viral transmission (28). ExRVs are horizontally transmitted among hosts and have been observed to induce malignant diseases in susceptible hosts (132-134). In contrast, ERVs represent molecular vestiges of ancestral germline infection with retroviruses. They are transmitted vertically from parent to child in accordance with the principles of Mendelian inheritance principles (30). ERVs constitute a significant proportion of the mammalian genome, with estimates suggesting that they account for 8-10% of the human and mouse genome (29, 31). The majority of ERVs are inactivated as a result of accumulated mutations or internal recombination, which can impair protein function (9-12). Indeed, the majority of retroviral genes have lost their replication capacity, with only a few still retaining this ability (43, 135). Moreover, reassortment and recombination interactions between partially inactivated retroviral genes and extant viral genomes may precipitate accelerated retroviral evolution, resulting in augmented genetic diversity and the perilous reemergence of viral diseases (132, 136, 137).

The existence of retroviral genes has given rise to concerns regarding their potential influence on genome function (138). However, there is mounting evidence that specific viral genetic material may have been integrated into the host genome over time and may be performing beneficial functions. Indeed, during the process of domestication of ERVs, some retroviral genes (ERVs) have undergone physiological evolution, acquiring new functions such as placentation (139), viral resistance (140-142), and sex-specific muscle development (143). As a result of domestication, ERV non-coding domain (LTR) also have function such as target for epigenetic silencing and may exert regulatory of neighboring genes (144).

Some ERV Envelope (Env) proteins may have a potent evolutionary significance in the immunological response by acting as restriction factors against exogenous retroviruses. Existing research recognized the critical role played by the env gene derived from ERVs (env-ERV), which reportedly exhibits restrictive activity against retroviruses in mice (Fv4, Rmcf, and Rmcf2) (145-147), domestic cats (Refrex-1, Felix) (140, 141), and humans (Suppressyn) (139). The antiviral activity of env-ERV genes is likely owing to their ability to interfere with the entry of exogenous retroviruses into host cells and re-spread of ERV in the hosts (140, 141). The retroviral envelope binds to receptors on the host cell surface and mediates cell entry. Env-ERV

proteins compete with exogenous retroviral Env proteins for binding to these receptors, thereby blocking viral entry and replication. To give an example of domestic cat, Refrex-1 and Felix are present in domestic cat, and are restriction factors against feline retrovirus infection, FeLV-D and ERV-DC, and FeLV-B and enFeLV, respectively. They are encoded by defective Env genes derived from ERV-DC and enFeLV, respectively. Structurally, Refrex-1 and FeLIX consist of a signal peptide and the 5' N-terminal region of Env SU, but lack a transmembrane region. Consequently, they are extracellularly secreted proteins, where they impede viral infection via due to competitive interference on the receptor. Moreover, Fv4 has a defect in its endogenous MuLV envelope fusion peptide. As a result, virus-infected cells expressing Fv4 produce Ecotropic-MuLV virions that incorporate this faulty envelope, leading to reduced infectivity (145).

Feline leukemia virus (FeLV), a Gammaretrovirus endemic to domestic cats worldwide, was identified as the infectious agent responsible for feline leukemia and lymphoma in the early 1960s (52). FeLV induces malignant hematopoietic disorders, including lymphoma, myelodysplastic syndrome, acute myeloid leukemia, aplastic anemia, and immunodeficiency in cats (49). FeLVs can be categorized into several subgroups based on viral receptor interference and host range. FeLV subgroups and their FeLV-A, -B, -C, -D, -E, and -T receptors have been identified (52-54, 56, 57, 59-61, 63, 148, 149). FeLV subgroup are generated from FeLV-A de novo in infected animals as a result of envelope (env) gene recombination, point mutations, or insertions (64, 65).

We previously discovered a new recombinant feline leukemia virus (FeLV) gag gene harboring an unrelated insertion, termed the X region, which was derived from Felis catus endogenous gammaretrovirus 4 (FcERV-gamma4) (74). The recombinat FeLV was termed as XR-FeLV. The identified FcERV-gamma4 proviruses have lost their coding capabilities. Although the X-region-carrying recombinant FeLVs (XR-FeLVs) appeared to be replication-defective viruses, they were detected in 6.4% of tested FeLV-infected cats. All isolated XR-FeLV clones commonly incorporated a middle part of the FcERV-gamma4 5'-leader region as an X region. A sequence corresponding to the portion contained in all X regions is also present in at least 13 endogenous retroviruses (ERVs) observed in the cat, human, primate, and pig genomes. We termed this shared genetic feature the commonly shared (CS) sequence. Notably, the CS sequence of human endogenous retrovirus T had 73.8% similarity with that of FcERV-gamma4. The biological function of the X-region or CS-sequence remains unknown (74). A novel recombinant FeLV hijacked the CS sequence from FcERV-gamma4 as the X region. Tracing the FcERV-gamma4 can provide unique models for not only the modern

reservoir of new recombinant viruses but also the genetic features shared among ancient retroviruses. Therefore, a comprehensive study of the evolutionary history of FcERV-gamma4 in Felidae could provide a deeper understanding of viral evolution and host-virus interaction.

In this study, we traced the infection of FcERV-gamma4 and its homologous genes in cats. We have revealed the hidden history of viral infection over a long period of time, from prehistoric times to the present day. Furthermore, it has revealed the significant impact of viral infection on the history of animal evolution. In the process of feline evolution, we have discovered records of intraspecific and interspecific viral transmission, as well as the emergence of recombinant viruses. By reconstructing ancient viruses, we have identified infectious viruses and clarified their properties, which show a wide range of host infection. Furthermore, we discovered a restriction factor Refrex-2 which is a soluble truncated Env protein encoded by proviruses FcERV-Gamma4-C1 and FcERV-Gamma4-A1 It inhibits FcERV-Gamma4 and related virus infections in vitro. It is thought that these are molecules that have emerged through the process of co-evolution between the host and the virus.

3.3. MATERIALS AND METHODS

3.3.1. Homology search in NCBI database

BLAST with NCBI using the pol nucleotide sequence of FcERV-gamma4 as a query (https://blast.ncbi.nlm.nih.gov/Blast.cgi) search was performed. The feline database used is listed in Table 2.3.6.1. Those with 90% or more homology to the query sequence were defined as FcERV-gamma4 homologous proviruses, and sequences around the POL region were obtained. The provirus was then manually sequenced in full length. The FcERV gamma5 in this study was obtained from Pol nucleotide in NCBI then used for outgroup for phylogenetic analysis (150).

3.3.2. Identification of orthologous insertion sites

1000 bp each of the sequenced provirus upstream and downstream were extracted and manually isolated. The ortholog insertion site was confirmed. A 3-6 bp sequence of the non-proviral host genome 5' and 3' to the site where the retrovirus integrates into the host genome, respectively, is called a **TSD**. The 5' and 3' **TSD** sequences are identical. When the retrovirus integrates, the TSD sequence is duplicated and becomes two. Between these two TSDs, the 5'LTR to 3'LTR provirus integrates into the genome (151)

3.3.3. Nomenclature of ERV-gamma 4 in Felidae

FcERV-gamma4 is an ERV found in *Felis catus* (domestic cats). FcERV-gamma4 and its orthologous proviruses were named by taking one letter from the genus and species name of the feline scientific name as shown in Table 1. FcERV-gamma4; *Felis catus* ERV-gamma4, FsERV-gamma4; *Felis silvestris* ERV-gamma4, FchERV-gamma4; *Felis chaus* ERV-gamma4, OmERV-gamma4; *Otocolobus manul* ERV-gamma4, PvERV-gamma4; *Prionailurus viverrinus* ERV-gamma4, PbERV-gamma4; *Prionailurus bengalensis* ERV-gamma4, LcERV-gamma4; *Lynx canadensis* ERV-gamma4, LrERV-gamma4; *Lynx rufus* ERV-gamma4, AjERV-gamma4; *Acinonyx jubatus* ERV-gamma4, LgERV-gamma4; *Leopardus geoffroyi* ERV-gamma4, PyERV-gamma4; *Puma yagouaroudi* ERV-gamma4.. In case the orthologues ERV sequences obtained by PCR, sample name were included. For example: FsERV-gamma4-3 Fsi-52 (*Felis silvestris*) and FchERV-gamma4-3 Fch-3 (*Felis chaus*). Orthologues provirus were found in felinae subfamily refered as Feline-ERV-gamma4. For orthologues that found in pantherinae subfamily, the first three letters correspond to the species' name. For example: PlERV-gamma4; *Panthera leo*, PpERV-gamma4; *Panthera pardus,* PtERV-gamma4; *Panthera tigris.* Additionally, Abbreviations of scientific names for FcERV-gamma4 homologous proviruses are shown in Table 3.1.

In addition to FcERV-gamma4 homologs, multiple ERV-gamma4 sequences were identified. They were named using a three-letter abbreviation derived from the genus and species names, along with the chromosome name (when known), followed by an ordinal number. In case, species without chromosome, we wrote chromosome name as Unk.

3.3.4. PCR Sample

Tissues of European wildcat (*Felis silvestris*), Tsushima wildcat (*Prionailurus bengalensis euptilurus*), Manul cat (*Otocolobus manul*), jungle cat (*Felis silvestris*), and Iriomote wildcat (*Prionailurus bengalensis iriomotensis*) were used. Information about the samples is given in Table 3.2. Purify DNA from tissue or blood according to protocol using the DNeasy Blood & Tissue Kit.

3.3.5. Cell lines

The Dulbecco's modified Eagle's medium (DMEM, FUJIFILM Wako Pure Chemical Corporation, Osaka, Japan) supplemented with 10% fetal calf serum (FCS) and 1X penicillin-streptomycin were used to cultured cell in this study. Cells were incubated in a CO2 incubator at 37 °C. We used following cell lines: HEK293T (152), MDTF (*Mus dunni* fibroblast tail) (153), CHO (154), AH927 (feline fibroblast cells) (155), CRFK (Crandell-Rees feline kidney) (156), Canine liver cancer cell, MDCK, KWDM (45), HeLA (157), NIH3T3 (158), Vero (159), 208F (160), GPLac (an *env*-negative packaging cell line containing murine leukemia virus (MuLV) *gag-pol* gene and beta-galactosidase (LacZ)-coding pMXs retroviral vector).

3.3.6 PCR

KOD-ONE Blue (Toyobo, Japan), KOD FX Neo, KOD plus Neo (Toyobo, Osaka, Japan), and GoTaq (Promega, Madison, WI, USA) polymerases were used according to the manufacturer's protocol.

3.3.7. PCR cloning

The pCR4Blunt-TOPO (Invitrogen, Carlsbad, CA, USA) was used to directly clone the PCR products. The pFUΔss expression vector was utilized to insert the intact env gene and truncated env gene (45). Sequencing was carried out by a Contracted Service (Fasmac Corporation, Atsugi, Japan).

3.3.8. PCR product cloning

Intact provirus gamma4 was isolated from cat DNA sample. The specific primer was used to perform this experiment (Supplementary table 3.1 and 3.2). In order to investigate the Fca 508 D3: 88351199 (Fca D3-2), we successfully isolate from CB18 sample, we used specific primer pairs, Fe-771S and Fe-796R. To

isolate envelope from CB18 provirus we use Fe-797S and Fe-819R was myc-tagged at the C-terminus and inserted into the pFUΔss vector (termed CB18 env).

Additionally, we constructed the Truncated env of FcERV-Gamma4-A1 using a two-step PCR approach. The first PCR utilized the Fe-406S and Fe-899S primers, while the second PCR utilized the Fe-924R primer to complete the amplification process. FcERV-gamma4-A1 was isolated from MS4 cell lines. This enabled us to obtain a truncated version of the env gene for further analysis.

To extract orthologue Felidae ERV-gamma4 in felidae genome, we used specific primers in Supplementary table 3.1. Briefly, we targeted Pol to 3'flanking region, then inserted into topovector. All amplicons were cloned into pCR4 blunt-TOPO (Invitrogen, Carlsbad, CA, USA) and sequenced (Fasmac Corporation, Atsugi, Japan).

3.3.9. Construction of truncated env

The gene was amplified through PCR with specific primers that contained enzyme sites. The resulting PCR products were then digested using their respective enzymes and cloned into the pFUΔss expression plasmid. To construct the truncated FcERV-Gamma4-A1 (termed trunc Gamma4-A1), Fe-912S and Fe-935R were used from previous pcr sample. To construct Gamma4-C1 from template (74), we used Fe-941S and Fe-957R. We also construct Gamma4-A1 and Gamma4-C1 from different species of felidae by using site directed mutagenesis.

Next, we extend our research in some species felidae genome to investigate antiviral effect of Felidae ERV-Gamma4-A1 and Gamma4-C1. LcERV-gamma4-A1, PvERV-gamma4-A1, LrERV-gamma4-C1, and PvERV-gamma4-C1 were synthesized (Eurofins Genomics, Tokyo, Japan) with myc-tagged at the C-terminus. We constructed FsERV-gamma4-A1, PcERV-gamma4-A1, PiERV-gamma4-A1 by using Fe-912S and Fe-935R. To construct OmERV-Gamma4-A1 we used Fe-912S and Fe-969R. We used primer pairs Fe-946S and Fe-968R to construct FchERV-gamma4-C1. Furthermore, we constructed AjERV-gamma4-C1 (Fe-947S and Fe-970R), LcERV-gamma4-C1 (Fe-948S and Fe-971R), and PyERV-gamma4-C1 (Fe-949S and Fe-972R) by using site directed mutagenesis technique. The primer pairs Fe-961S and Fe-1001R were used to construct OmERV-gamma4-C1 and PiERV-gamma4-C1. FsERV-gamma4-C1 were constructed by using primer Fe-960S and FE-981R. All constructs were then inserted into the pFUΔss plasmid between the BamHI and EcoRI restriction sites. The truncated Env expression plasmids were confirmed using sequencing (Fasmac Corporation, Atsugi, Japan).

3.3.10. Construction of infectious env and mutant env

The optimized Lge A1-4 env was synthesized (Eurofins Genomics, Tokyo, Japan). Env genes were myc-tagged at the C-terminus and inserted into the pFUΔss vector. Env mutant of CB18 was constructed based on alignment with Infectious Lge A1-4 env to identify amino acid candidate for reconstruction of CB18 env. Mutant_1 to 7 were derived from from CB18 env by using site-directed mutagenesis or infusion technique according manufacture protocol. Mutant_1 (Fe-864R and Fe-828S; Fe-833S and Pfu-1R), Mutant 2 (FE-951R, Fe-828S, Fe-934S, and Pfu-1R) were constructed from Cb18 and Lge A1-4 by using infusion technique. Mutant_3 (Fe-867S and FE-897R) were constructed from the CB18 by using site directed technique. Based on Mutant_1, the following Mutants were made, the primer pairs for Mutant_4 (Fe-867S and Fe-897R). Based on Mutant_4, Mutant_5 (Fe-848S, Fe-913R, Fe-892S, Pfu-1R, Fe-828S, Fe-879R) and Mutant_6 (Fe-848S, Fe-917R, Fe-893S, and Pfu-1R) were made. Mutant_7 (Fe-910R, Fe-828S, Fe-885S, and Pfu-1R) was made from Mutant_3. All mutant were made by using infusion technique except Mutant_3.

3.3.11. Env-pseudotyped virus preparation

To generate Env-pseudotyped viruses carrying the LacZ marker, we follow the procedure outlined by previous paper (45). This involves seeding approximately 1×10^6 GPLac cells in a six-well plate one day before transfection. The plasmids utilized for viral preparation were as follows: Mutant_1 until Mutant_7, CB18 env, and Optimized Lge chrA1:194722361 (Lge env). The optimized Lge env were synthesized by Eurofins Genomics, Tokyo, Japan. All of the env were inserted into pFUΔss vector before transfected into GPLac cells. The culture supernatant were collected 48 hours after transfection using TransIT-293, transfection reagent. Then, they were then filtered through 0.22- μm or centrifuged 15,400 × g for 2 min at 4 °C, and the virus stock was stored at -80°C for further experiments. In case of The truncated env of gamma4-3 and Gamma4-A1, the HEK 293T cells were used for transfection using TransIT-293, transfection reagent. After 48 h, the sup was collected and filtered or centrifuged at 15,400 × g for 2 min at 4 °C, then stored at -80°C for further experiments.

3.3.12. Infection assay

To infect the target cells, we seeded 3 × 105 cells in 24-well plates one day before infection. We infected them with Env-pseudotyped virus (250 μL) and Polybrene (10 μg/mL) for 2 hours. After 2 days, we removed the cell supernatants and fixed the cells with 2% glutaraldehyde (250 μL) for 15 minutes at room temperature.

We stained them with X-Gal (5-bromo-4- chloro-3-indolyl-β-D-galactopyranoside) and counted them as blue-stained nuclei under a microscope. We determined the viral titers (IU/mL) with standard deviations.

3.3.13. Viral inhibition assay in the presence of truncated Env proteins

HEK293T cells were seeded at a concentration of approximately 1×10^6 cells in a six-well plate 1 day prior to transfection with truncated Env expression plasmids. The supernatants of HEK293T cells transfected with pFUΔss FcERV-Gamma4-A1, FcERV-Gamma4-C1, and pFUΔss empty vector (negative control) for approximately 48 h were the source of truncated Env proteins. The infection assay was conducted as described previously. In 24-well plates, target cells were treated with 250 µL of cell supernatant (source of truncated Env protein) for 2 h. Subsequently, 250 µL of Env-pseudotyped viruses or replication-competent viruses were inoculated into the target cells with 10 µg/mL polybrene for 2 h, after which 250 µL of fresh medium was added. Two days post-infection, the cells were stained with X-Gal. Single-cycle infectivity was determined by counting blue-stained nuclei under a microscope. IU per milliliter and standard deviations were used to represent the viral titers. Truncated env-overexpression constructs using TransIT-293, transfection reagent and incubated 24 hours. After that, harvesting the cells and seeding in 24-well plates, then infection assays was conducted as described previously.

3.3.14. Expression of Refrex-2

Total RNA was extracted from the tissues of a specific pathogen-free cat (Kyoto-SPF1) described in our previous study (7), using an RNAiso Plus kit (Takara), in accordance with the manufacturer's instructions. Thereafter, cDNA was synthesized using a PrimeScript II first-strand cDNA synthesis kit (Takara) according to the manufacturer's instructions. Prior to reverse transcription, the RNA samples were treated with recombinant DNase I (TaKaRa). FcERV-gamma4-C1 then was amplified using the primer Fc-962S and Fc-982R. FcERV-Gamma4-A1 was amplified using the primers Fc-989S and Fc-954R. Thermal cycling was performed according to the manufacturer's instructions. We determined the expression of FcERV-Gamma4-A1 env genes in feline tissues. The pcr products were sequenced (Fasmac Corporation, Atsugi, Japan).

3.3.15. RNA-seq analysis

RNA-seq data from the AH927 cell line were used to analyze the expression levels of the endogenous gamma envelope gene. The quality of raw reads was assessed using FastQC (version 0.12.1), and raw data trimming was performed with Cutadapt (version 5.1). Reads were aligned to the Felis catus reference genome (F.catus_Fca126_mat1.0) using STAR (version 2.7.11b) with default parameters. Gene annotations were

obtained from NCBI release 105. Expression levels were quantified as transcripts per million (TPM), and read counts were normalized to reads per kilobase of exon per million mapped reads (RPKM) using featureCounts (version 2.0.1).

3.3.16. Immunoprecipitation and immunoblotting

To achieve successful gene transfer, we employed the use of TransIT®-293 (Mirus) reagent to perform plasmid transfection in six-well plates containing either GPLac or HEK293T cells. Two days after transfection, the cell pellets were acquired through the process of being washed with phosphate-buffered saline (PBS) solution thrice. Cells were resuspended in lysis buffer in lysis buffer (20 mM Tris-HCl [pH 7.5], 150 mM NaCl, 10% glycerol, 1% Triton X-100, 2 mM EDTA, 1 mM Na3VO4, and 1 μg/ml each of aprotinin and leupeptin) to prepare cell lysates, then incubate for 20 min on ice. Top-speed centrifugation for 20 min at 4°C was used to remove the insoluble components, and a protein assay kit (Bio-Rad Laboratories, Carlsbad, CA) was used to calculate the protein concentrations.

Cell supernatants were filtered through a 0.22-μm filter and were incubated overnight at 4°C with the desired antibody. The protein that underwent purification from the cell lysate and supernatant was combined with Sample Buffer Solution, a product of Nacalai Tesque, and subjected to a heating process at a temperature range of 95-100°C for a duration of 5 min. SDS-PAGE was conducted using 4-20% gels (Invitrogen, Carlsbad, CA, USA) at 100V for 2 h, then transferred to nitrocellulose filters for western blotting with the following primary antibodies used in the assays: anti-Myc monoclonal antibody conjugated with horseradish peroxidase (FUJIFILM Wako Pure Chemical Corporation; dilution 1:1000). The substrate was LumiGLO® Reagent (20x) and 20X peroxide (Cell Signaling Technology in Danvers, Massachusetts). For Imaging, the blots were performed using Amersham ImageQuant 800 (Cytiva, Shinjuku, Japan).

3.3.17. Phylogenetic tree analysis

Sequences were compared using SEAVIEW (161), Bioedit 75(162), and Genetyx 16 software (Genetyx Corporation, Tokyo, Japan). The phylogenetic tree was constructed using the sequences MEGA11 software package (163). Alignment was performed using MUSCLE. A phylogenetic tree was constructed using maximum likelihood (ML) method, with robustness evaluated by bootstrapping (1,000 times). The substitution models were selected based on the lowest BIC score (164).

3.3.18. Estimation of the integration timings of Felidae ERV-gamma4

The estimated integration timing based on the orthologue-dating method (165) of Felidae ERV-gamma4 provirus. To determine the orthologue, we extracted 300bp upstream and downstream of the provirus from the NCBI database to identify a 3-6 bp sequence of target site duplication (TSD) or the nearest gene. Between these two TSDs, the 5'LTR to 3'LTR provirus integrates into the genome (13). The sequence similarities were compared by Genetyx 16 software (Genetyx Corporation, Tokyo, Japan). After the finding the orthologous gamma4, the dates of gamma4 integration events were assigned according to a vertebrate evolutionary tree from TimeTree database (166).

3.3.19. Selection pressure analysis

Genomic data that was accessible to the public was utilized to perform evolutionary analyses of Gamma4-A1 and C1 using the BLAST method and PCR using specific primer. The database of felidae genomes was scanned with the env ORF of Gamma4-A1 and C1 env nucleotide sequences as guides. Sequences from felidae were then aligned using MUSCLE (167). The amino acid p-distance values were computed to show the proportion of sites where the two sequences differ. Using the Nei-Gojobori method, the non-synonymous substitutions (dN) and synonymous substitutions (dS) per site were calculated (168). The bioinformatics analyses were performed utilizing MEGA11 (169). The amino acids of Gamma4-A1 and C1 felidae were aligned using MUSCLE to analyze amino acid similarity. Genetyx 16 was used to calculate the amino acid identity (%) of all felidae representatives.

3.4. RESULTS

3.4.1 Identification of homologues of FcERV-Gamma4 in Felidae

In this study, Homologue provirus sequences of FcERV-gamma4 were searched in Felidae genome database using FcERV-gamma4 *pol* gene. Total 351 provirus sequences from 14 species were identified, by the following genome data base; *Felis catus, Felis chaus, Prionailurus bengalensis, Prionailurus viverrinus, Puma yagouaroundi, Puma concolor, Acinonyx jubatus, Lynx canadensis, Lynx rufus, Leopardus geoffroyi, Panthera leo, Panthera Pardus, Panthera tigris, and Panthera once* (Table 3.1). Furthermore, orthologue sequences of FcERV-gamma4 were obtained by PCR method from genomic DNAs from 4 species (*Felis silvestris, Otocolobus manul, Prionailurus bengalensis, euptilurus, and Prionailurus bengalensis iriomotensis*) (Table 3.2). In this study, homologous ERVs of FcERV-gamma4 were named Felidae ERV-Gamma4. Furthermore, scientific name of felidae species was named by taking one letter from the genus

and species name of the feline scientific name following chromosome and ordinal number (For example, *Leopardus geoffroyi* chromosome A1 is abbreviated as Lge A1-1, *Felis catus* chromosome X is abbreviated Fca X, and *Panthera leo* in chromosome F2 is abbreviated Ple F2) (Table 3.1 and 3.2). Then, for the provirus orthologs that were isolated from our samples, we put the name of the sample after the name of the provirus.

3.4.2. Structure of Gamma4 in Felidae

The structural organization of Felidae ERV-gamma4 consists of 5'LTR, *gag*, *pol*, *env*, and 3'LTR. In addition to intact proviruses, various deletion variants, including solo LTRs, were also identified. This analysis provided detailed structural information, including nucleotide length variations across each region, based on the alignment of all identified proviruses.

The Gamma4 proviruses were classified into seven distinct structural categories. The first category includes intact proviruses containing the complete structure (5'LTR, *gag*, *pol*, *env*, and 3'LTR), with 22 copies identified. The second category consists of proviruses that retain a full *env* gene but exhibit deletions in the gag and pol regions, referred to as intact-env proviruses, with 37 copies observed. The third category includes proviruses with deletions in *gag* and *pol*, along with a premature stop codon in env, classified as truncated-env proviruses, with 116 copies. The fourth category comprises *env*-less proviruses, which lack the env region entirely and exhibit deletions in *gag* and *pol*, accounting for 155 copies. The fifth category includes *pol* proviruses, characterized by deletions in pol along with the absence of *gag* and *env*, with only three copies identified. The sixth category consists of proviruses with deletions in gag and pol, as well as the absence of the region downstream of pol region, with a single copy detected. Lastly, the seventh category consists of solo LTR structures, with 15 copies observed (Fig. 3.1A). This classification highlights the structural diversity of ERV-gamma4 within the *Felidae* genome, providing insights into its evolutionary dynamics.

A more detailed analysis revealed that Geoffroy's cat and the Leopard cat exhibited the highest copy numbers of Gamma4 proviruses, with 95 and 76 copies, respectively. These species also displayed greater structural variation compared to others. Notably, both species also harbored a substantial number of env-less proviruses, with 35 copies identified in Geoffroy's cat and 55 copies in the Leopard (Fig. 3.1B and 3.1C). This suggests the presence of diverse Gamma4 variants within these populations. Interestingly, type F provirus was exclusively found in the Jungle cat.

3.4.3. Phylogenetic analysis

Phylogenetic analysis of Felidae ERV-gamma4 sequences was performed using the Maximum Likelihood method, with FcERV-gamma5 included as an outgroup. The phylogenetic tree revealed that Gag (Fig. 3.2A) and Pol (Fig. 3.2B) sequences converged on a single node representing Felidae ERV-gamma4. The Leopardus (ocelot lineage), Panthera, and Lynx lineages formed distinct clusters. Further analysis of the surface unit (SU) of Env successfully classified Felidae ERV-gamma4 into ten genotypes (Fig. 3.3).

Genotypes 1 and 7 were highly conserved in both the Felinae and Panthera subfamilies, indicating widespread infection among various feline species. Genotype 3 was detected in the domestic cat (Felis catus), leopard cat (Prionailurus), and Panthera lineages, while Genotype 6 was found exclusively in the Felinae lineage and Genotype 4 only in Panthera. Interestingly, Geoffroy's cat (*Leopardus geoffroyi*), belonging to the ocelot lineage, harbored six different genotypes. Genotypes 2, 5, 8, and 9 were unique to Geoffroy's cat, whereas Genotype 10 was found exclusively in jaguarundi (*Puma yagouaroundi*), suggesting that these genotypes may have independently arisen and remained species-specific (Fig. 3.4). Conversely, Genotypes 1, 3, 4, 6, and 7 were detected across multiple species, indicating the potential for interspecies transmission. Notably, the Geoffroy's cat-specific genotypes (2, 8, and 9) and the jaguarundi-specific genotype (10) exhibited shorter branch lengths in the phylogenetic tree, suggesting lower sequence divergence. This reduced variation implies that these proviral insertions are relatively recent compared to other genotypes. Collectively, these findings suggest that genotype classification could serve as a valuable tool for tracking viral spread. The presence of shared and species-specific genotypes further supports the hypothesis that ERV-gamma4 has undergone both intra- and interspecies transmission during feline evolution.

3.4.4. Intact full-length provirus Felidae ERV-gamma4

Sequence analysis identified 22 intact proviruses containing full-length open reading frames (ORFs) for the gag, pol, and env genes, along with 5'LTR and 3'LTR, in Felis catus (1 provirus), Leopardus geoffroyi (14 proviruses), Lynx canadensis (1 provirus), Panthera pardus (2 proviruses), and Panthera leo (1 provirus). The 5'LTR and 3'LTR sequences were 100% identical across all intact Felidae ERV-Gamma4 proviruses, except for Lge A3-3 and Lge A1-2, which exhibited 99.8% and 99.5% identity, respectively. This high level of sequence conservation suggests that these proviruses represent relatively young ERVs. Additionally, the Lge (B1-4, B1-3, and A3-2) proviruses shared the same target site duplication (TSD) sequence, GTGAC (Table 3.3), further supporting their recent integration.

To investigate the possibility of interspecies transmission among these intact full-length proviruses, we constructed a phylogenetic tree based on the amino acid sequences of gag, pol, and env using the maximum likelihood method (Fig. 3.5A, B, and C). As an outgroup, we included sequences from beta-retroviruses for comparative analysis. Phylogenetic analysis based on the env gene strongly suggests cross-species transmission events. Furthermore, intact proviruses were successfully classified into distinct genotypes. We identified three major genotypes: Genotype 1 was found in domestic cats, Canadian lynx, leopards, and lions, while genotypes 2, 6, and 9 were exclusively identified in Geoffroy's cat. These findings indicate that Felidae Gamma4 has spread through interspecies and/or intraspecies transmission

3.4.5 5'-Leader Sequence of Gamma4

The 5'-leader sequences, known as the untranslated region between 5'LTR and Gag gene, were characterized in FcERV-gamma4, and they have the long 5'-leader sequences, and direct repeats (74). The structural features of the 5'-leader sequences in Felidae ERV-gamma4 were analyzed (Fig 3.6A and B), and structural polymorphisms were assessed using consensus sequences from each species to understand their variations.

The 5'-leader sequence was successfully identified in multiple Felidae species, including domestic cat, jungle cat, leopard cat, fishing cat, jaguarundi, cheetah, Canadian lynx, bobcat, Geoffroy's cat, lion, leopard, and tiger. However, its structure could not be analyzed in puma and jaguar due to poor genome assembly quality in the available databases. In most species, the 5'-leader sequence exceeded 1000 bp in length (Fig. 3.6A). When compared to other retroviruses such as FeLV 61E (423 bp), enFeLV (432 bp), KoRVA (456 bp), and GaLV (505 bp), the 5'-leader in domestic cat ERV-gamma4 was notably longer, reaching 1462 bp (Fig. 3.6B).

Additionally, we analyzed the X-region, a subregion within the 5'-leader sequence. X-region lengths exceeding 500 bp were found in domestic cat (522 bp) and Canadian lynx (541 bp), whereas the X-region was significantly shorter in jungle cat, fishing cat, and leopard cat, measuring 83 bp, 83 bp, and 84 bp, respectively. Further analysis of the X-region revealed the presence of direct repeats across all species, with each lineage exhibiting distinct repeat sizes (Fig 3.6A). Domestic cats and Canadian lynxes had the highest repeat counts, with 25 and 26 repeats, respectively, while the shortest repeats were observed in jungle cat, leopard cat, and fishing cat, each with only four repeats.

Taken together, these findings indicate that the 5'-leader sequence in Felidae ERV-gamma4 is significantly longer than that of other retroviruses. Moreover, X-region size varies among species, suggesting lineage-specific structural adaptations.

3.4.6. Integration time of Felidae ERV-gamma4

Nine loci of FcERV-gamma4 were previously identified in domestic cat such as FcERV-gamma4-A1, FcERV-gamma4-C1, FcERV-gamma4-E2, FcERV-gamma4-B3, FcERV-gamma4-1, FcERV-gamma4-3, FcERV-gamma4-B4, FcERV-gamma4-X, and FcERV-gamma4-X2 (74). Present study, The integration times of Felidae ERV-gamma4 sequences were estimated using the ortholog-dating method (149). A 5-kbp region upstream and downstream of each genomic locus, flanking the proviral integration sites, was analyzed to identify Target Site Duplications (TSDs), which are genomic duplications that occur upon retroviral integration. TSD is DNA duplication in the genome when the retrovirus first integrated.

Orthologous FcERV-gamma4 proviruses were detected in the lineages of domestic cat (23), leopard (10), puma (7), lynx (8), and ocelot (2), but were absent in the Panthera lineage (Fig. 3.7). Among these, FcERV-gamma4-C1, FcERV-gamma4-B3, FcERV-gamma4-3, and FcERV-gamma4-A1 were the most widely distributed orthologs, detected in 11, 10, 10, and 7 species, respectively. Notably, FcERV-gamma4-X2 was exclusive to the domestic cat and was not found in any other species.

Following the acquisition of provirus orthologue data, the age of the provirus was estimated by utilizing the provirus's position within the evolutionary timeline of the time tree (Fig. 3.7 and Fig. 3.8). FcERV-gamma4-3 and FcERV-gamma4-B3 were estimated 12MYA as the oldest integration in ancestors of domestic cats. FcERV-gamma4-C1 and FcERV-gamma4-A1 were estimated 8.94MYA and 7.35MYA, respectively. The FcERV-gamma4-X2 is the youngest provirus that endogenized about 2.98 mya-recently. Interestingly, the panthera lineage showed its own distinct endogenization pattern (Fig. 3.7 and Fig. 3.8). The orthologue of FcERV-gamma4 were not present in Panthera lineage. However, the orthologues of PlERV-gamma4 were detected in panthera species. Ple gamma4-C2 has been widely observed in Tiger, Lion, and Leopard, but not Jaguar. It is because the quality assembly in database is not good. It was estimated ~7MYA as the oldest integration in ancestors of Panthera lineage. In the evolutionary process of animal species other than the Pantera lineage, it seems that FcERV-gamma4 orthologs are detected in various patterns, which could suggest that the endogenization of FcERV-gamma4 into the ancestor of the domestic cat may have occurred during the speciation of the feline species. The detection of FcERV-gamma4 orthologs in multiple Felidae

species, except for Panthera, suggests that the endogenization of FcERV-gamma4 likely occurred during the diversification of Felinae. The absence of FcERV-gamma4 in Panthera species implies that ERV-gamma4 was not present in the common ancestor of Felidae (which includes both Felinae and Pantherinae lineages), but rather integrated into the genome after the divergence of Felinae and Pantherinae.

3.4.7. Infectivity of Felidae ERV-gamma4 Env-pseudotyped viruses

To evaluate the infectivity of Felidae ERV-gamma4, we focused on LgeA1-4 from *Leopardus geoffroyi* and FcaD3-2 from *Felis catus*, which show intact proviruses. The expression vectors of LgeA1-4 Env and Fca D3-2 Env were transfected into GP Lac cells, containing MLV Gag-Pol and MuLV retroviral vector carrying LacZ as a marker, to produce the Gamma4 Env-pseudotyped virus. The supernatants of the transfected cells were tested for their infectivity, and the results showed that Lge A1-4 infected HEK 293T cells with high titer. In contrast, Fca D3-2 had no infectivity. The Lge A1-4 env-pseudotyped virus were able to infect mammal cells broadly such as human cells (HeLa and HEK 293T), Cat cells (CRFK), Hamster cells (CHO), Dog cells (KwDM and Canine liver cancer), and Rat cells (208F). However, the virus could not infect Mouse cells (MDTF and NIH3T3), Cat cells (AH927), and Dog cells (MDCK), and Monkey cells (Vero Monkey) (Table 3.4).

Next, to determine the amino acid that has critical role for infection of Fca D3-2, we constructed several *env* mutants of Fca D3-2 from domestic cats based on Lge A1-4 sequences (Fig 3.9A and Fig 3.10). The substitution of amino acid Histidine (H) to Arginine (R) at position 97 could make Fca D3-2 infect Canine liver cancer (CLC) cells, while HEK 293T did not (Fig 3.9B and C). Furthermore, in experiments using a series of mutants, it was found that Fca D3-2 has high infectivity due to the substitution of at least six amino acids (H97R, I272M, M273I, V308T, L402F, and T410A) created as mutant_5 (Table 3.4, Fig. 3.9B). The infectivity of FcaD3-2 (Mutant_3 and Mutant_5) was observed to exhibit a relatively diverse host range when determined by several cell lines. The host range of Fca D3-2 is similar to that of LgeA-1 (Table 3.4). However, compared to LgeA-1, Mutant5 showed very high infectivity to KWDM, but did not show infectivity to 208F cells (Table 3.4). Therefore, we found infectivity of Felidae ERV-gamma4 from *Leopardus geoffroyi* and *Felis catus*. Furthermore, evidence suggests that Felidae ERV-gamma4 may be capable of infecting a diverse range of species.

3.4.8. Inhibitory effect of Truncated gamma4 env

ERVs are known to function as antiviral molecules through co-evolution with their hosts. To determine whether there are molecules in domestic cats that suppress the infectivity of ERV-gamma4, we explored such molecules by examining the expression of Felidae ERV-gamma4 in domestic cats. The Env genes of FcERV-gamma4-A1, FcERV-gamma4-3, and FcERV-gamma4 -C1 were found to express in MS4 cells (B-cell lymphoma) cells, 3281 (feline lymphoma) cells and thymus, and PBMC, respectively, by RT-PCR with specific primers. Analysis of the gene sequence suggests that FcERV-gamma4-A1, C1 and 4-3 are truncated envelope proteins consisting of 266 AA, 246 AA and 246 AA in length, respectively (Fig. 3.11). Since there is a stop codon in the Surface unit (SU) region of the Env gene, it was predicted that these proteins lack transmembrane (TM) units, but, have signal peptides and a partial SU as the N-terminal region of the SU protein.

The expression of these proteins was then examined. After transfection of HEK293T cells with Env expression vectors, the culture supernatants were immunoprecipitated with Myc-tag antibodies. Western blot analysis revealed the proteins to be approximately 50 kd (Fig. 3.12A). The characteristic structures of Env suggested that they were secreted protein. The inhibitory effect of Gamma4-A1, 4-3 and Gamma4-C1 Env proteins on target cell lines was tested for Felidae ERV-gamma4 Env pseudotyped viruses. Supernatants from transfection of expression plasmids into HEK 293T cells were used as a source of Env proteins. The supernatant was incubated with target cells for 2 hours, and the target cells were then infected with pseudotyped virus for 2 days before infectivity was analysed using the LacZ assay.

Env proteins derived from FcERV-gamma 4-A1 and 4-C1 significantly inhibited infection for Lge A1-4 and Fca D3-2 (mutant_5) Env pseudotyped viruses in cell lines, but gamma4-3 Env protein did not (Fig. 3.12B and C). Moreover, the inhibitory effects of FcERV-gamma4A-1 and FcERV-gamma4-C1 Env proteins on the infection of FeLV-B and FeLV-D were investigated. The findings revealed that only LgeA1-4 was inhibited by these proteins (Fig. 3.12D). The objective of the subsequent investigation was to ascertain whether LgeA1-4 was affected by Felix and Refrex-1, which inhibit infection with FeLV-B and FeLV-D, respectively. Consequently, LgeA1-4 was not affected by Felix and Refrex-1 (Fig 3.12E). The inhibitory effect was found to be dose-dependent for their infection (Fig. 3.12F and G). These findings demonstrate that Felidae ERV-gamma4 infection is specifically inhibited by the Env proteins encoded by FcERV-

gamma4-A1 and 4-C1. The specific function of the Env proteins encoded by FcERV-gamma4-A1 and 4-C1 had been designated as Refrex-2.

3.4.9. Expression of FcERV-gamma4-A1 and FcERV-gamma4-C1 in domestic cats tissue

As mentioned in the section above, we first confirmed the expression of the FcERV-gamma4 subset by PCR amplification and sequencing of the Env gene. As a result, we confirmed that FcERV-gamma4-A1 is expressed in MS4 cells and that 4-C1 is expressed in peripheral blood. Both of them had unique splicing form. FcERV-gamma4-A1 splicing form start after 829bp until before 6733bp, while FcERV-gamma4-C1 start after 707bp until before 6575bp (Fig. 3.13A and B). Gamma4-C1 was widely expressed in various tissues and we found that it is particularly expressed in the spleen, thymus, uterus, ovary, cerebellum and pancreas (Table 3.5).

In case of gamma4-A1, based on our RNA seq data, FcERV-gamma4-A1 was not well expressed in cat tissue. To further investigate its expression, we utilized primers Fe-989S and Fe-954R to detect FcERV-gamma4-A1 transcripts in cat tissues and cell lines. The PCR products were confirmed by sequencing, revealing FcERV-gamma4-A1 expression in the liver, kidney, pancreas, large intestine, mandibular lymph node, and placenta.

To investigate the inhibitory effect of Refrex-2 in cell lines, we evaluated the supernatant from both feline and non-feline cells. Our results showed that supernatants from MS4 and AH927 cell lines exhibited complete inhibition (Fig. 3.14A). RNA-seq data from the AH927 cell line were used to analyze the expression levels of the endogenous gamma envelope gene. The expression level of FcERV-gamma4-A1 and FcERV-gamma4-C1 were 18 and 57 TPM, respectively. FcERV-gamma4-B3, FcERV-gamma4-1, FcERV-gamma4-E2, and FcERV-gamma4-X were considered low, 8, 2, 6 TPM, respectively (Fig. 3.14B). Additionally, heat activation revealed that Refrex-2 loss the activity at 56°C (Fig, 3.14C). Furthermore, to confirm the role of Refrex-2, we utilized a specific antibody to bind Refrex-2 (gamma4-C1 and -A1) protein in cell lines (Fig. 3.14D and E). The anti-Refrex-2 Rabbit was successfully bind into following antibody depletion, Gamma4 infection titers were partially restored (Fig. 3.14F), indicating that Refrex-2 plays a crucial role in restricting Gamma4 infection.

3.4.10. Conservation and evolution of Felidae ERV-gamma4-A1 and C1 genes among Felidae

Since the Env proteins encoded by FcERV-gamma4-A1 and C1 were found to have antiviral activity as Refrex-2, the evolution of FcERV-gamma4-A1 and FcERV-gamma4-C1 was investigated in Felidae. The

orthologues of FcERV-gamma4-A1 and FcERV-gamma4-C1 are named Felidae ERV-gamma4-A1 and Felidae ERV-gamma4-C1 in Felidae species, respectively. We searched the *env* genes from Felidae ERV-gamma4-A1 and Felidae ERV-gamma4-C1 based on NCBI database of Felidae. Felidae ERV-gamma4-C1 and A1 is present in domestic cat lineage (European wild cat, Jungle cat), leopard lineage (Manul cat, and Fishing cat), and Lynx lineage (Canada lynx, and Bobcat). Felidae ERV-gamma4-A1 is present in Puma lineage (Puma, Jaguarundi, and Cheetah), but Felidae ERV-gamma4-A1 is not. Neither of them exists in the Ocelot (Geoffroy's cat) or the Panthera (Tiger, Jaguar, Lion, and Leopard) lineage.

The amino acid sequences of Felidae gamma4-A1 Env among wild cats exhibit a high degree of similarity to that of FcERV-gamma4-A1 Env in Felis catus, comprising 267 amino acids in length. However, notable exceptions are observed in the Manul cat (Oma) and Canadian lynx (Lca). The LcaERV-gamma4-A1 Env has 258 amino acids in length and is slightly shorter due to the absence of an amino acid at the C-terminus. The OmaERV-gamma4-A1Env sequence exhibited a frameshift from the 280th nucleotide position, resulting in the appearance of a stop codon, and thus comprises 127 amino acids (Fig. 3.15). The amino acid sequences of Felidae gamma4-C1 Env among wild cats exhibit a high degree of similarity to that of FcERV-gamma4-C1 Env in Felis catus, comprising 239-249 amino acids in length. The omaERV-gamma4-C1 Env is 239 amino acids in length due to the absence of an amino acid at the C-terminus (Fig. 3.16). The Felidae ERV-gamma4-A1 and C1 Env proteins were predicted that their proteins lack transmembrane (TM) units, but, have signal peptides and a partial SU as the N-terminal region of the SU protein.

Next, we then tested whether Felidae ERV-gamma4-A1 and gamma4-C1 had the same inhibitory effect on Felidae ERV-gamma4 infection as Refrex-2. The expression vectors of Felidae ERV-gamma4-A1 (Fsi, TWC, Pcu, Lca, Pvi, Pir,and Oma), and Felidae ERV-gamm4-C1 (Fsi, Fch, Oma, Pir, Lca, Lru, Pya, Aju, and Pvi) were transfected into HEK 293T cells, and the supernatants of them were immunoprecipitated and conducted the Western blot analysis using anti-Myc antibody. Felidae ERV-gamma4-A1 Env proteins and Felidae ERV-gamma4-C1 Env proteins are well expressed in the supernatant of cells (Fig 3.17A and 3.18A). When these proteins were tested in an inhibition assay, all of them suppressed LgeA1-4 and mutant 5 infection (Fig. 3.17B and 3.18B). However, only the omaERV-gamma4-A1 Env protein showed no effect on infection suppression. These results suggest that Felidae ERV-gamma4-A1 and C1 have potential antiviral activity as Refrex-2.

The evolution of Refrex-2 was then analyzed. The evolution of Felidae ERV-gamma4-A1 and Felidae ERV-gamma4-C1 can be investigated by comparing the rates of dN and dS changes in the orthologue sequences (170). ERV genes, such as host genes, can be conserved in two ways: (a) when the dN/dS rate is < 1, the genes are under purifying selection and retain a beneficial function, or (b) if the dN/dS rate is > 1, the genes are classified under positive selection. The dN-to-dS mutation ratio (dN/dS) was accurately computed according to previously established methods (ref). The dN/dS ratios of Gamma4-A1 ranged from 0.103 to 0.723, and Gamma4-C1 ranged from 0 to 0.632 among felidae (Fig. 3.17C and 3.18C). These findings suggest that both are subject to purifying selection in all Felidae species.

3.5. DISCUSSION

XR-FeLV, Recombinant FeLV containing X region, which derived from the 5'-Leader sequence of FcERV-gamma4 have been identified in lymphoma/leukemia in domestic cats. The 5'-leader sequences of FcERV gamma4 proviruses are unique in that they are longer than those of other retroviruses and contain direct repeats. They also have a CS sequence, which is common to many species, including humans and chimpanzees. However, the function of the 5'-leader sequences of FcERV gamma4 being transduced into FeLV, and the role of CS-sequence are still unknown. XR-FeLV has been isolated from domestic cats with lymphoma and leukemia. This phenomenon suggests that although FcERV-gamma4 is an endogenous retrovirus, it may pose a threat to domestic cats. It raises the question of how FcERV-gamma4 has maintained its existence during animal evolution. In this study, we present new evidence that Felidae ERV-gamma4 maintains its presence in the Felidae genomes through retrotransposition and reinfection. We have discovered a novel antiviral molecule, Refrex-2, that has co-opted between Felidae ERV-gamma4 and hosts. Refrex-2 is thought to play a role in protecting against the threat of Felidae ERV-gamma4. This research highlights the hidden history of viral infection over a long period of time, from prehistoric times to the present day. By using this research approch, we are able to clarify the significant impact of viral infection on the history of animal evolution. This research will provide insights into the history of viral infection on a geological scale that cannot be inferred from the traces of existing viruses, and will deepen our understanding of the biological phenomena related to the co-evolution of viruses and hosts.

Our study revealed that Felidae ERV-gamma4 proviruses were found in only Felidae. However, in baycat and caracal lineage were not detected. This is due to their assembly quality in NCBI database was not good. Furthermore, the analysis of viral integration time of Felidae ERV-gamma4 suggests that endogenization of Felidae ERV-gamma4 had been occurred after divergence between Felid and Panthera lineage (171). This is a reason that the common orthologue of Felidae ERV-gamma4 was not present in Felid and Panthera lineages. We speculate that the disappearance of viruses in the genome was influenced by migration processes during cat evolution. It is consistent with the previous report which Geoffroy's cat, Puma, Lynx, and Leopard cat were shared common ancestor because of second felidae migration (M2) (171). The presence of young provirus in Geoffroy's cat and Jaguarundi might be result of recombination event. However, we speculated that those proviruses came from same ancestor, which is likely from Genotype 1.

In addition, the presence of intact full-length proviruses from different species, including Lynx, Lion, Domestic cat, and Leopard, within genotype 1 suggests the potential for inter-species transmission.

During our search for ERV-gamma4 proviruses, we identified a large number of env-less ERV-gamma4 sequences. This loss of the envelope gene is likely driven by immune pressure from the host, allowing the provirus to persist in the genome. As previously reported, the immunosuppressive domain within the transmembrane region of Env may be detrimental to the host (172, 173). The removal of the envelope protein reduces the pathogenicity of ERV-gamma4, potentially facilitating its widespread dissemination within the host genome, leading to superspreader events (174). Thus, the loss of the env gene represents an adaptive strategy that enables ERV-gamma4 to expand within the host genome while minimizing negative impacts on host fitness. However, although env-deficient proviruses are generally inactive, the possibility remains that recombination with another virus could restore envelope functionality, potentially reactivating viral propagation.

The envelope (Env) gene has undergone stronger selective pressure due to host-virus conflict during evolution. This evolutionary pressure explains why the Gag and Pol genes do not exhibit strong bootstrap support across all species. However, the Gag and Pol regions remain conserved in certain lineages, such as Leopardus (ocelot), Lynx, and Panthera (Fig. 3.2 and Fig. 3.3). The classification of Gamma4 Env SU into 10 distinct genotypes suggests that host-specific adaptation has occurred over time. Additionally, we speculate that the presence of younger genotypes in Geoffroy's cat and Puma may result from Env adaptation to new environments during Felidae evolution. The geographical shift from North America to South America may have contributed to the genetic diversity observed in Geoffroy's cat, while Puma migration from the Americas to Eurasia may have further influenced its genetic variation (175). Furthermore, the faunal exchange with South America and the formation of the Panamanian land bridge likely played a role in the differentiation of the Leopardus lineage (175).

This study revealed that a large number of ERV-gamma4 proviruses contain tandem repeat sequences, with variations observed across different species. Previous studies have reported that proviruses with tandem repeats may function as enhancers, potentially promoting high transcription levels of oncogenes (176-178). On the other hand, tandem repeat sequences have also been used as markers for tracing ancient migrations and studying relationships between different host populations (179). Additionally, tandem repeats serve as a basis for forensic fingerprinting, as variations in repeat number are unique to individuals (180). Given these

roles, we speculate that, in addition to acting as oncogene enhancers, variations in tandem repeat length within ERV-gamma4 could serve as a useful tool for tracing the evolutionary history of this virus. However, further studies are required to clarify the specific functional roles of tandem repeat sequences in ERV-gamma4.

As described above, immune pressure can lead to the disruption of the env gene. Although we identified a full-length Fca D3-2 provirus in a domestic cat sample, it was inactive. We speculate that the presence of this provirus may contribute to disease progression when an exogenous retrovirus infects this species. This aligns with previous reports showing that the recombinant virus XR-FeLV causes more severe disease in domestic cats compared to FeLV infection alone (67). Furthermore, we demonstrated for the first time that the Gamma4 Env protein from Geoffroy's cat (Lge A1-4) could facilitate the production of infectious viral particles. However, we did not observe a replication-competent provirus in this study. Our results also revealed that Gamma4 is unable to infect monkeys, rats, or mice, suggesting that these species lack a functional Gamma4 receptor. Conversely, feline cell lines may contain a soluble factor that inhibits Gamma4 infection, although we did not test the supernatant of these cell lines in this study. In contrast, Fca D3-2 was observed in felis catus and was unable to form infectious particle. Fca D3-2 contains substitution and mutation in SU region that make the virus become inactive. Consistent with previous reports, the SU region constitutes a component of the envelope that plays a role in the attachment of the retroviruses to the host. In line, amino acid variation in SU region reduces the infectivity of FeLV-E (61).

In an extensive search, not only intact envelopes were identified, but also numerous truncated env. Existing research revealed that truncated env that contains at least signal peptide and N-terminal of SU as Receptor binding domain (RBD) will function as an antiviral molecule, preventing the binding of receptors. In addition, the truncated env form with lacking c-terminal region easily release from cell as a soluble protein. In cat, truncated env ERV-DC 7 and DC 16 (Refrex-1) inhibit FeLV D and truncated env enFeLV (FeLIX) inhibit FeLV-B (140, 141). In Human, SUPYN, a truncated Env derived from HERVH48 inhibit type D retrovirus (142). Taken together, the truncated form of ERV-gamma4 may have antiviral function.

This study also discovered functional truncated env protein, termed Refrex-2, as a soluble truncated env protein. The Refrex-2 is referred to truncated env FcERV-Gamma4 A1 and C1 that consist of Env SU that contain RBD, but lacking TM region due to premature stop codon. The structure was similar with previous restriction factor in domestic cat, Refrex-1 and FeLIX (140, 141). The absence of TM region make Refrex-

2 could not fuse into the cells, resulting in the release of the molecule as a soluble protein (140, 181). Moreover, Refrex-2 molecules was expressed in immune system (Table 3.5) indicating that Refrex-2 may act as immune system in host body. However, unlike Refrex-1, we were unable to reconstitute ancestral of Refrex-2 by removing premature stop codon (182).

In addition, the dN/dS for sequence of Refrex-2 are lower than 1 which indicated that Refrex-2 was identified under purifying selection across Felidae family. This finding reflect that Refrex-2 may has a beneficial function, including as restriction factors to suppress the infections. Purifying selection genes indicates they may play beneficial role in the host genome (142, 182). Existing reports demonstrated that ERV has natural function. SUPYN, a truncated Env derived from HERVH48 is demonstrated that involving in placentation (142). Moreover, Refrex-1 acts to control homeostasis cell death by regulating copper supply (183).

The inhibitory effects of Refrex-2 is not limited in domestic cat, but extended to Felidae family. Our analysis revealed that Refrex-2–like structure were identified in European wild cat, Jungle cat, Manul cat, Fishing cat, Leopard cat, Tsusushima cat, Iriomote cat, Canadian lynx, Bobcat, Cheetah, Jaguarundi, and Puma. Same as in domestic cats, Refrex-2–like structure was observed in two loci, namely ERV-gamma4-C1 and ERV-gamma4-A1. ERV-gamma4-C1 were found more conserved in Felidae genome compared to Felidae ERV-gamma4-A1 (Fig 3.8). Although the felidae The Felidae ERV-Gamma4-C1 and the Felidae ERV-Gamma4-A1 ancestor probably began to endogenize, around 12-9 mya and 9-6 mya. Therefore, the presence of Refrex-2 as a result evolutionary arm race between host and virus.

In addition, frameshifting in OmERV-gamma4-A1 led to a reduction in amino acid length. This may be due to mutations affecting the receptor-binding domain (RBD), causing OmERV-gamma4-A1 in the manul cat to lose its ability to block infection. As a result, the manul cat likely relies on OmERV-gamma4-C1 for antiviral defense.

Interestingly, we were unable to find ERV-Gamma4-A1 in genome database of Tsushusima and Iriomotes. Nevertheless, we obtain the Gamma4-A1 from subspecies of leopard cat, Tsushusima and Iriomotes cat by our sample. This finding suggests that Gamma4-like elements may be present in species that are currently undetected in genomic databases

Lastly, although we found the phenomenon of infectious protein env protein Gamma4 and Refrex-2 as antiviral by using *in vitro* system, the exact role of Refrex-2 *in vivo* system is unknown. This is the limitation of this study.

In conclusion, this study characterized the genotypes of ERV-gamma4 in Felidae, providing a valuable model for investigating viral evolutionary history. These genotypes offer critical insights into the endogenization of retroviruses, which began approximately 12 million years ago, predating the divergence of felid ancestors. Our findings suggest that ERV-gamma4 has undergone both inter-species and intra-species recombination throughout its evolutionary history.

Additionally, we identified intact envelope proteins capable of generating viral particles, raising the possibility of novel exogenous virus emergence within the Felidae family. We also characterized Refrex-2 as a soluble protein that functions as a restriction factor. Its high expression in immune tissues suggests a potential role in host defense against viral infections.

Overall, this study provides new insights into the co-evolution of ERV-gamma4 and its hosts. The ongoing conflict between host and retrovirus has driven the evolution of antiviral molecules as part of an acquired defense mechanism. These findings may contribute to the development of novel strategies for combating retroviral infections

3.6. TABLES, FIGURES, SUPPLEMENTARY DATA

Table 3.1. The presence of ERV-Gamma4 in the Felidae

Scientific name	Name	Lineage	Abbreviation	Copy number (n)	Accession number
Felis catus	Domestic cat	Domestic cat	Fca	15	GCA_016509815.2
Felis chaus	Jungle cat	Domestic cat	Fch	9	GCA_019924945.1
Prionailurus bengalensis	Leopard cat	Leopard cat	Pbe	11	GCA_016509475.1
Prionailurus viverrinus	Fishing cat	Leopard cat	Pvi	11	GCA_022837055.1
Puma yagouaroudi	Jaguarundi	Puma	Pya	8	GCA_014898765.1
Puma concolor	Puma	Puma	Pco	1	NW_020338243.1
Acinonyx jubatus	Cheetah	Puma	Aju	6	GCA_027475565.2
Lynx canadensis	Canadian lynx	Lynx	Lca	51	GCA_007474595.2
Lynx rufus	Bobcat	Lynx	Lru	35	GCA_022079265.1
Leopardus geoffroyi	Geoffroy's cat	Ocelot	Lge	95	GCA_018350155.1
Panthera leo	Lion	Panthera	Ple	19	GCA_018350215.1
Panthera pardus	Leopard	Panthera	Ppa	75	GCA_024362865.1, GCA_024362975.1
Panthera tigris	Tiger	Panthera	Pti	14	GCA_018350195.2
Panthera onca	Jaguar	Panthera	Pon	1	GCA_004023805.1

Table 3.2. The presence of ERVGamma4 were identified by PCR method

Scientific name	Name	Lineage	Abbreviation	Copy number (n)
Felis silvestris	European wild cat	Domestic cat	Fsi	9
Otocolobus manul	Manul cat	Leopard cat	Oma	4
Prionailurus bengalensis euptilurus	Tsushima Leopard cat	Leopard cat	Peu	4
Prionailurus bengalensis iriomotensis	Iriomote cat	Leopard cat	Pir	4

Table 3.3. Intact provirus of Felidae ERV-gamma4

Scientific name	Intact Provirus	Provirus position	TSD	3'LTR/ 5'LTR (%)	Genotype	Accession number
Leopardus geoffroyi	Lge D2-2	D2:4438322..4447647	AAGC	572/572 (100)	9	NC_059334.1
Leopardus geoffroyi	Lge D1-1	D1:95869655..95879196	TTAG	584/584 (100)	9	NC_059329.1
Leopardus geoffroyi	Lge X-4	X:95017374..95026891	ATCT	572/572 (100)	9	NC_059343.1
Leopardus geoffroyi	Lge A2-2	A2:141450650..141460140	GTCT	569/569 (100)	9	NC_059331.1
Leopardus geoffroyi	Lge A1-5	A1:207158376..207167676	TTTA	570/570 (100)	9	NC_059326.1
Leopardus geoffroyi	Lge C1-3	C1:177840960..177850290	TAGG	575/575 (100)	9	NC_059328.1
Leopardus geoffroyi	Lge B1-4	B1:174963536..174972964	GTGAC	569/569 (100)	9	NC_059327.1
Leopardus geoffroyi	Lge A3-3	A3:126528445..126537979	GTCAG	581/582 (99.8)	9	NC_059336.1
Leopardus geoffroyi	Lge C3-1	C3:56001562..56010913	TAGG	580/580 (100)	2	NC_059338.1
Leopardus geoffroyi	Lge B2-1	B2:132218859..132228466	GTCAT	583/583 (100)	2	NC_059332.1
Leopardus geoffroyi	Lge B1-3	B1:103951138..103960748	GTGAC	583/583 (100)	2	NC_059327.1
Leopardus geoffroyi	Lge A3-2	A3:130130508..130139928	GTGAC	584/584 (100)	2	NC_059336.1
Leopardus geoffroyi	Lge A1-4	A1:194722361..194731164	GAGG	586/586 (100)	2	NC_059326.1
Leopardus geoffroyi	Lge A1-2	A1:16783412..16793110	GTAT	627/630 (99.5)	6	NC_059326.1
Lynx canadensis	Lca Unk-2	unk:43575..53159	CCTGG	623/623 (100)	1	VHLF02011566.1
Lynx canadensis	Lca E1-1	E1:44114020..44123584	GCCT	623/623 (100)	1	NC_044316.2
Lynx canadensis	Lca C2-1	C2:62993690..63003274	GGGC	623/623 (100)	1	NC_044311.2
Lynx canadensis	Lca B1-1	B1:198345552..198355136	CTAG	623/623 (100)	1	NC_044306.2
Felis catus	Fca D3-2	D3:88351199..88361026	ATCA	626/626 (100)	1	CM028209.1
Panthera pardus	Ppa Unk-79	unk:480694..491253	GACT	501/501 (100)	1	JANFAS010000494
Panthera leo	Ple A3-1	A3:25456879..25466268	AATG	503/503 (100)	1	NC_056681.1
Panthera pardus	Ppa Unk-2	unk:2770717..2779985	TCTT	501/501 (100)	1	JANFAO010000059.1

Table 2.3.6.4. Lge and reconstructed Fca D3-2 infections tropism in mammalian cell lines

Species	Cell lines	Mean viral titer (IU/mL) ± SD		
		Lge A1-4	**Mutant_3**	**Mutant_5**
Human	293T	$(1.0 \pm 0.1) \times 10^4$	$(1.9 \pm 0.1) \times 10^2$	$(8.9 \pm 0.1) \times 10^3$
	HeLa	$(1.4 \pm 0.2) \times 10^3$	$(0.5 \pm 0.3) \times 10^2$	$(9.2 \pm 0.3) \times 10^3$
Cat	AH927	0	0	0
	CRFK	$(3.2 \pm 1.0) \times 10^2$	0	0
Mouse	MDTF	0	0	0
	NIH3T3	0	0	0
Hamster	CHO	$(2.3 \pm 0.5) \times 10^3$	0	$(2.2 \pm 0.3) \times 10^2$
Dog	Canine liver cancer	$(9.4 \pm 0.8) \times 10^3$	$(1.6 \pm 0.1) \times 10^2$	$(7.1 \pm 1.4) \times 10^3$
	MDCK	0	0	0
	KWDM	$(1,1 \pm 0.1) \times 10^3$	$(7.0 \pm 0.5) \times 10^2$	$(4.2 \pm 0.7) \times 10^4$
Monkey	Vero	0	0	0
Rat	208F	$(4.5 \pm 0.6) \times 10^2$	0	0

Table 3.5. Refrex-2 expression in tissues

Tissue type	FcERV-Gamma4-A1 expression	FcERV-Gamma4-C1 expression
Stomach	-	+
PBMC	-	+
Spleen	-	+
Thymus	-	+
Bone Marrow	-	+
Lung	-	-
Liver	+	+
Kidney	+	-
Uterus	-	+
Ovary	-	+
Cerebellum	-	+
Cerebrum	-	+
Pancreas	+	+
Small intestine	-	+
Large intestine	+	+
Mandibular lymph node	+	+
Mesenteric lymph node	-	-
Mandibular Gland	-	+
Placenta	+	+

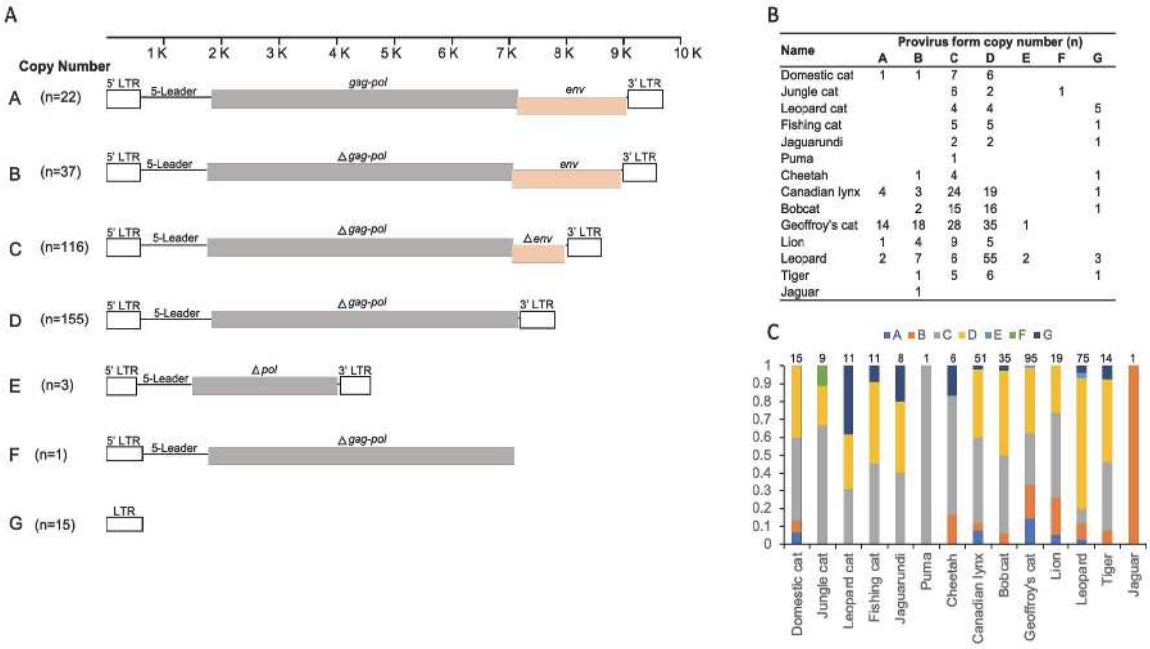

Name	Provirus form copy number (n)						
	A	B	C	D	E	F	G
Domestic cat	1	1	7	6			
Jungle cat			6	2		1	
Leopard cat			4	4			5
Fishing cat			5	5			1
Jaguarundi			2	2			1
Puma			1				
Cheetah		1	4				1
Canadian lynx	4	3	24	19			1
Bobcat		2	15	16			1
Geoffroy's cat	14	18	28	35	1		
Lion	1	4	9	5			
Leopard	2	7	6	55	2		3
Tiger		1	5	6			1
Jaguar		1					

Fig. 3.1. Schematic structure of Gamma4. The general schematic figure was made by comparing each nucleotide length of gamma4. (A) Gamma4 was then classified into 7 type form; type A: Intact provirus, type B: intact env provirus, type C: truncated env provirus, type D: *env*-less provirus, type E: *pol* provirus, type F: provirus lacking env and 3'LTR, and type G: solo-LTR. (B) and (C) Gamma4 form distribution across all species.

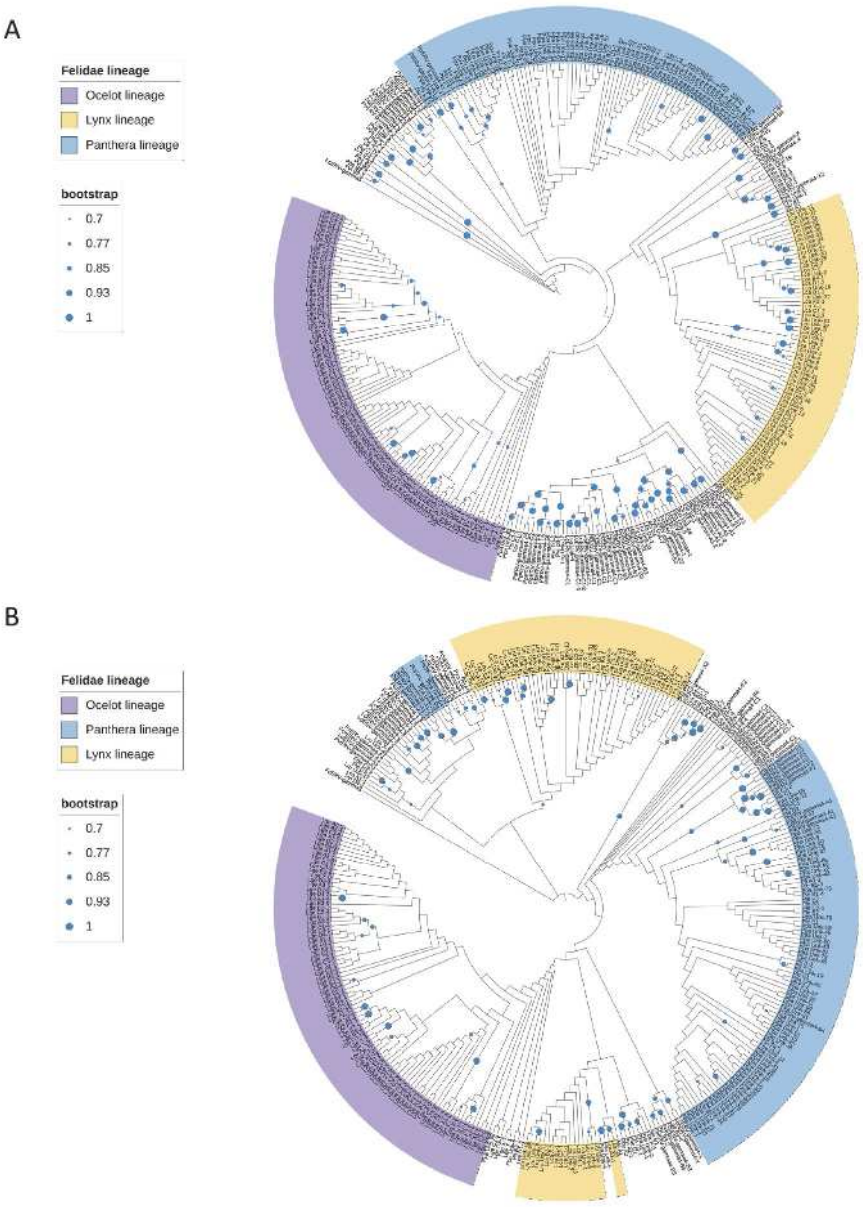

Fig. 3.2. Phylogenetic tree analysis of gag and pol gamma4 proviruses. The phylogenetic tree was constructed using Maximum Likelihood and GTR+G for *Gag* and *Pol* phylogenetic tree. The percentage of trees in which the associated taxa clustered together is shown next to the branches. The tree is drawn to scale, with branch lengths measured by the number of substitutions per site. Phylogenetic tree were made by (A) *Gag* nucleotide and (B) *Pol* nucleotide.

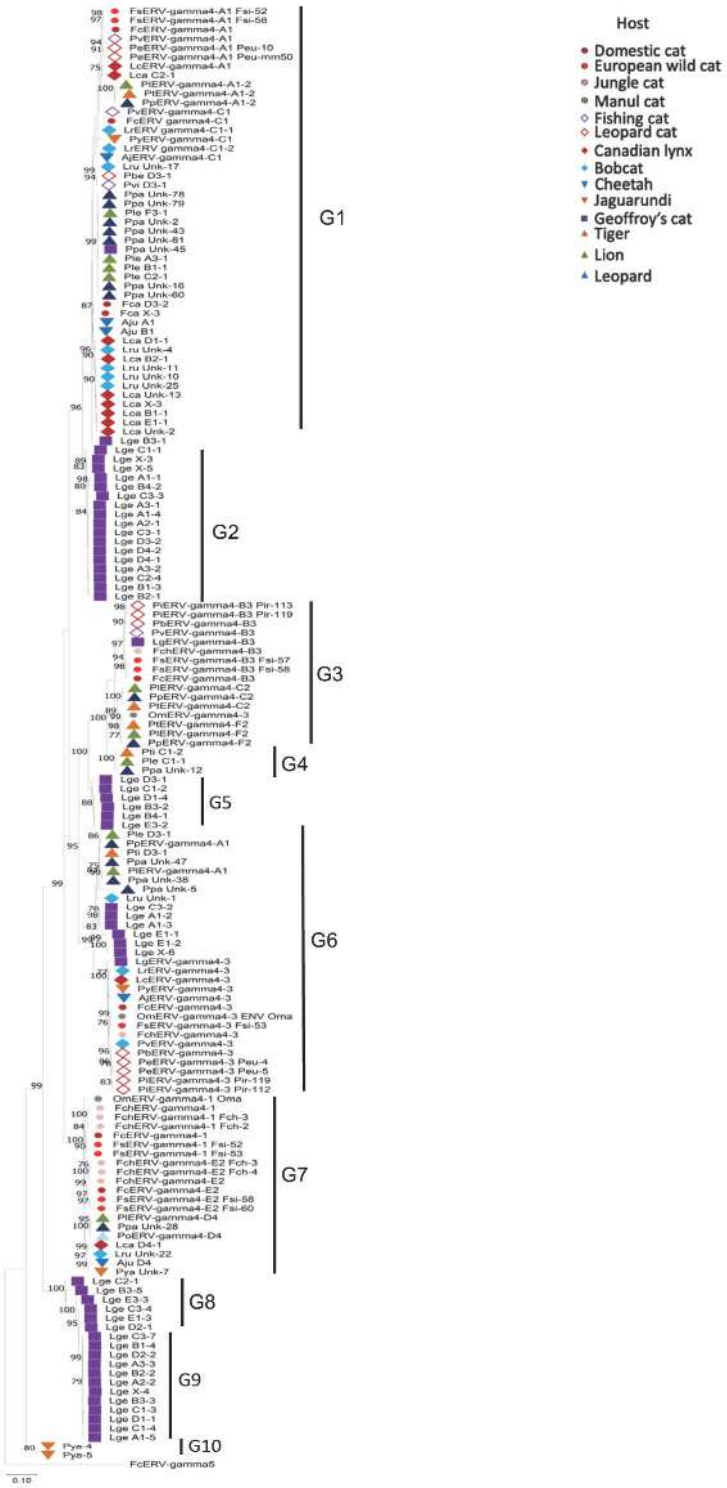

Fig. 3.3. Phylogenetic tree analysis based on nucleotide of Env SU region**.** The phylogenetic tree was constructed using Maximum Likelihood phylogenetic tree based on the HKY+G model. The percentage of trees in which the associated taxa clustered together is shown next to the branches. The tree is drawn to scale, with branch lengths measured by the number of substitutions per site. This analysis involved (check) nucleotide sequences.

Host	Lineage	Source	Genotype									
			1	2	3	4	5	6	7	8	9	10
Domestic cat	Domestic cat	NCBI	●		●			●	●			
European wild cat	Domestic cat	PCR	●		●			●	●			
Jungle cat	Domestic cat	NCBI	●		●			●	●			
Manul cat	Leopard cat	PCR	●					●	●			
Fishing cat	Leopard cat	NCBI	●		●			●				
Leopard cat	Leopard cat	NCBI, PCR	●		●			●	●			
Canadian lynx	Lynx	NCBI	●					●	●			
Bobcat	Lynx	NCBI	●					●	●			
Cheetah	Puma	NCBI	●					●	●			
Jaguarundi	Puma	NCBI						●	●			●
Puma	Puma	NCBI							●			
Geoffroy's cat	Ocelot	NCBI	●	●			●	●		●	●	
Tiger	Panthera	NCBI	●		●	●			●			
Jaguar	Panthera	NCBI							●			
Lion	Panthera	NCBI	●		●	●			●			
Leopard	Panthera	NCBI	●		●	●			●			

Fig. 3.4. Host and virus presence. Gamma4 proviruses from each genotype were diverse in each felidae. Of 10 genotypes were spread in 6 Felidae lineage (Domestic cat, Leopard cat, Lynx, Puma, Ocelot, Panthera). The color indicate genotype in each host.

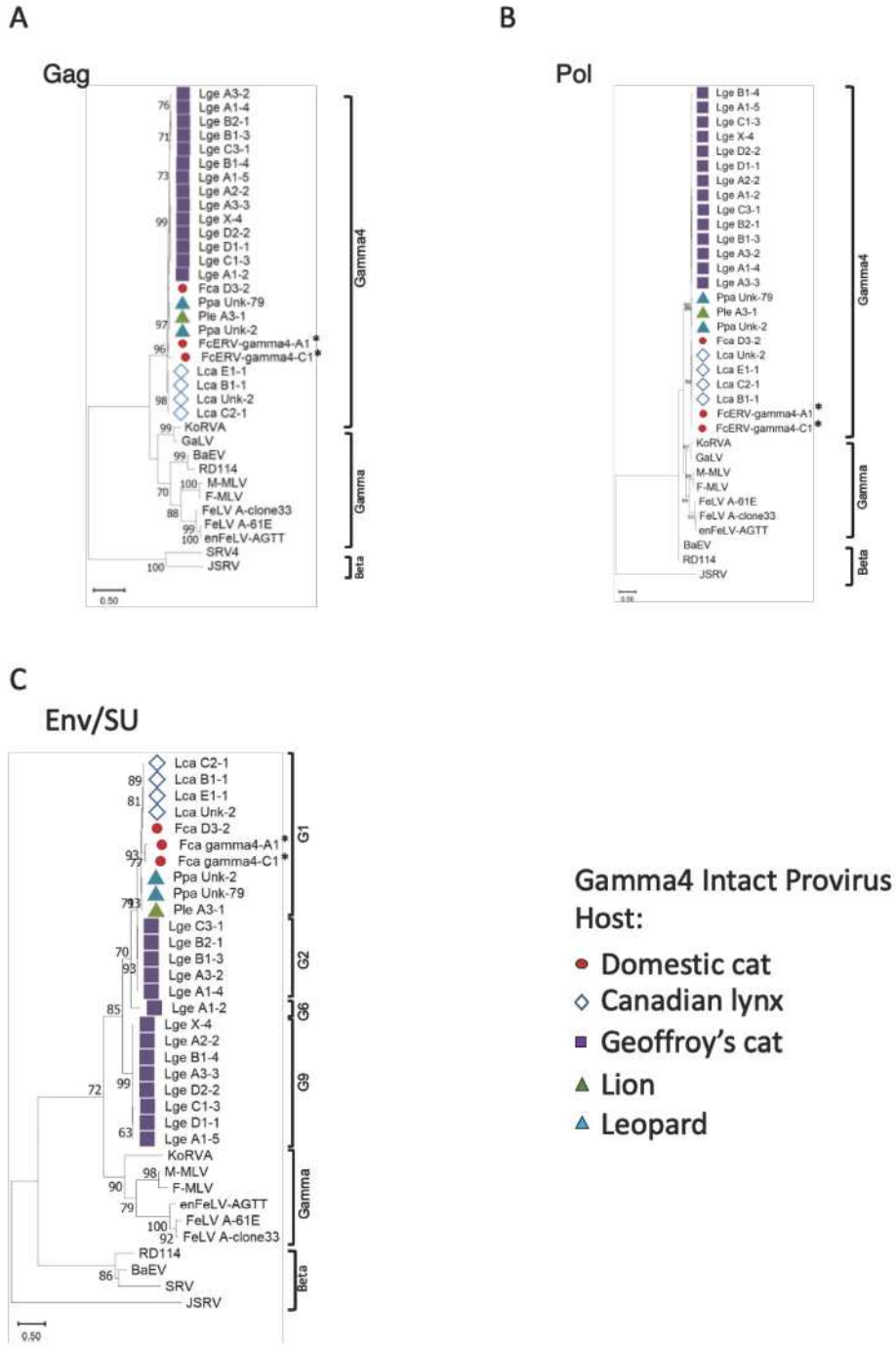

Fig. 3.5. Phylogenetic tree analysis of Intact provirus. The phylogenetic tree was constructed using Maximum Likelihood and JTT+G (*Gag*), rtREV+G (*Pol*), and WAG+G (Env) phylogenetic tree. The percentage of trees in which the associated taxa clustered together is shown next to the branches. The tree is drawn to scale, with branch lengths measured by the number of substitutions per site. Phylogenetic tree were made by (A) Gag amino acid, (B) Pol amino acid, and (C) Env SU amino acid.

A

Name	Lineage	5'leader length (bp)	X-region Size (bp)	Direct repeat
Domestic cat	Domestic cat	1494	522	25
Jungle cat	Domestic cat	1261	83	4
Leopard cat	Leopard cat	1494	84	4
Fishing cat	Leopard cat	1495	83	4
Jaguarundi	Puma	1229	105	5
Cheetah	Puma	1145	105	5
Canadian lynx	Lynx	1698	541	26
Bobcat	Lynx	1519	394	19
Geoffroy's cat	Ocelot	1576	375	18
Lion	Panthera	1362	149	7
Leopard	Panthera	1441	232	11
Tiger	Panthera	1441	274	12

B

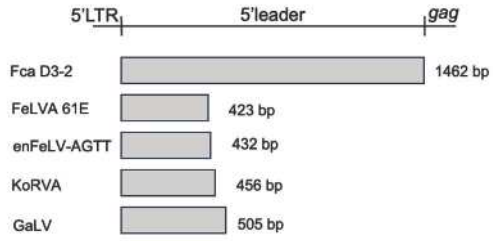

Fig. 3.6. 5'leader sequence characteristic. (A) Consensus of 5'leader sequence in Felidae species. (B) 5'leader sequence comparison between Gamma4 and another retrovirus.

Host	Lineage	Source	Fca-gamma4									Ple- Gamma4				
			X2	X	B4	E2	1	A1	C1	B3	3	C2	D4	C1	F2	A1
Domestic cat	Domestic cat	NCBI	●	●	●	●	●	●	●	●	●					
European wild	Domestic cat	PCR		●	●	●	●	●	●	●	●					
Jungle cat	Domestic cat	NCBI				●	●	●	●	●	●					
Manul cat	Leopard cat	PCR					●	●	●		●					
Fishing cat	Leopard cat	NCBI						●	●	●	●					
Leopard cat	Leopard cat	NCBI, PCR							●	●						
Canadian lynx	Lynx	NCBI						●	●	●	●					
Bobcat	Lynx	NCBI						●	●	●	●					
Cheetah	Puma	NCBI							●	●	●					
Jaguarundi	Puma	NCBI							●	●	●					
Puma	Puma	NCBI							●							
Geoffroy's cat	Ocelot	NCBI								●	●					
Tiger	Panthera	NCBI										●				
Jaguar	Panthera	NCBI											●			
Lion	Panthera	NCBI										●	●	●	●	●
Leopard	Panthera	NCBI										●	●	●	●	●
Integration time (mya)			<2.98	1.65	1.65	5.13	6.5	7.35	8.94	12	12	6.77	4.06	2.96	2.96	2.96

Fig 3.7. Integration time of gamma4 in felidae species. Each color indicates each ortholog gamma4 form in several species. Time integration is presented in million years age (mya).

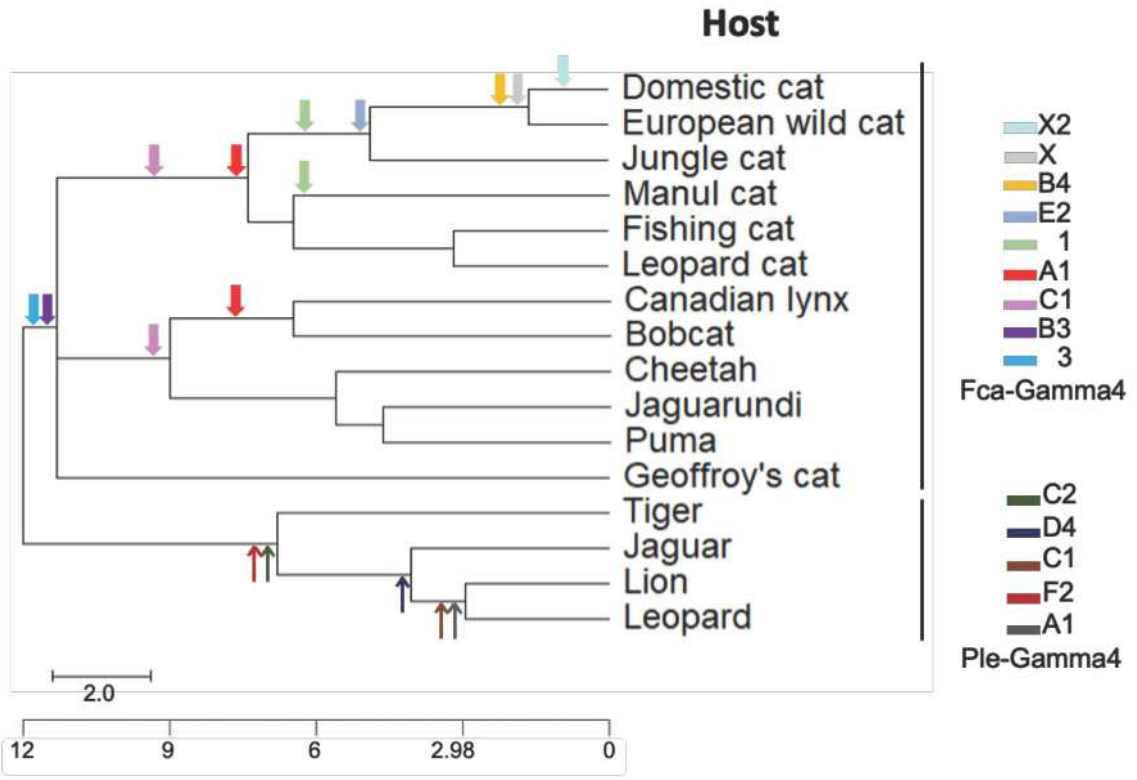

Fig. 3.8. Integration time of Felidae Gamma4. Integration time of Felidae gamma4 using ortholog dating method for predicting endogenization time of the virus to the host. The trees and divergence times were generated using TIMETREE (Ref). Down arrow indicates the insertion of FcERV-gamma4, up arrow indicates the insertion of Panthera-gamma4 in mya. The colour indicate each gamma4 virus.

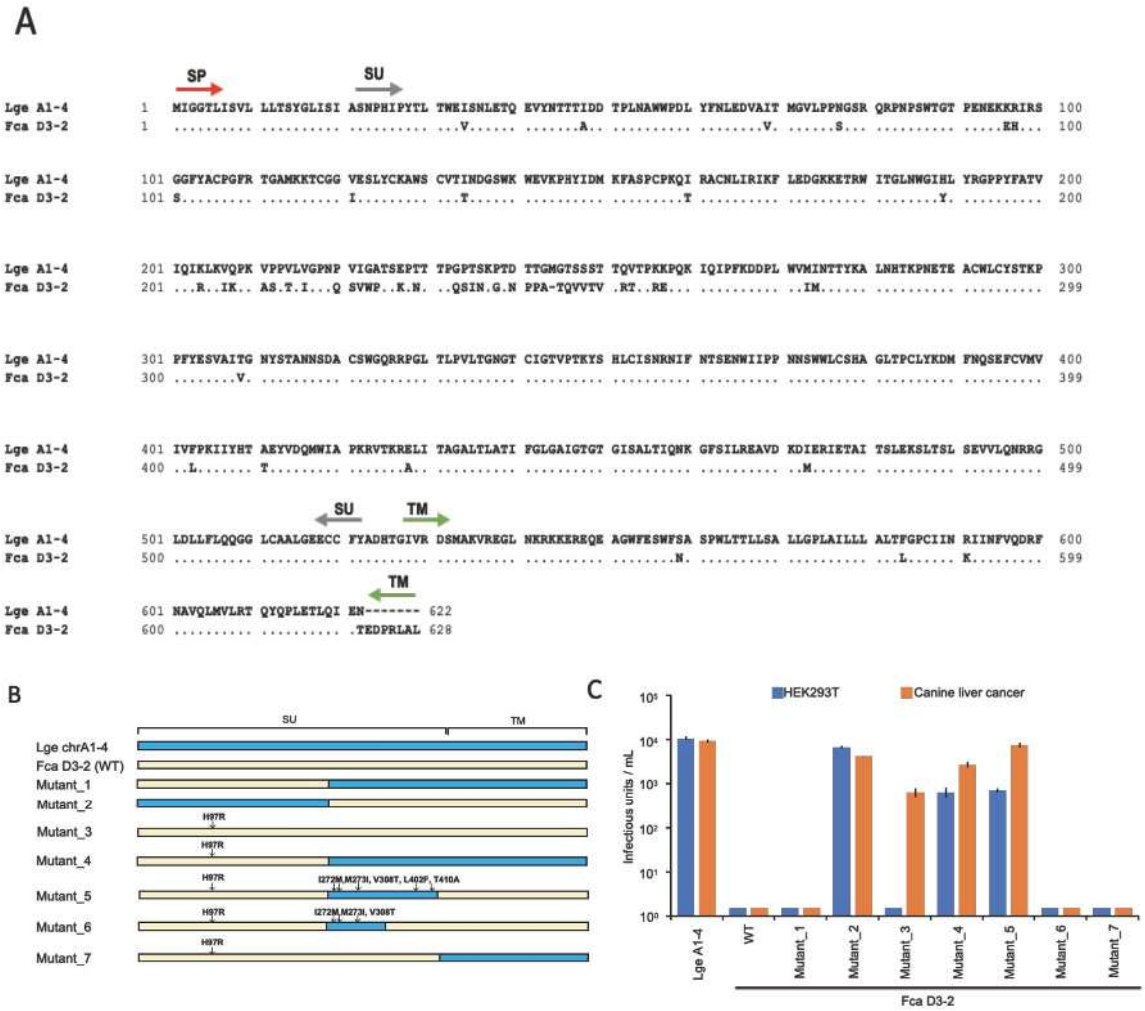

Fig. 3.9. Reconstruct the extinct domestic cat virus. (A) amino acid alignment Lge A1-4, Fca D3-2 and other mutants. (B) Schematic figure of mutants construction based on Lge A1-4 amino acid. (C) Virus titer of all mutant.

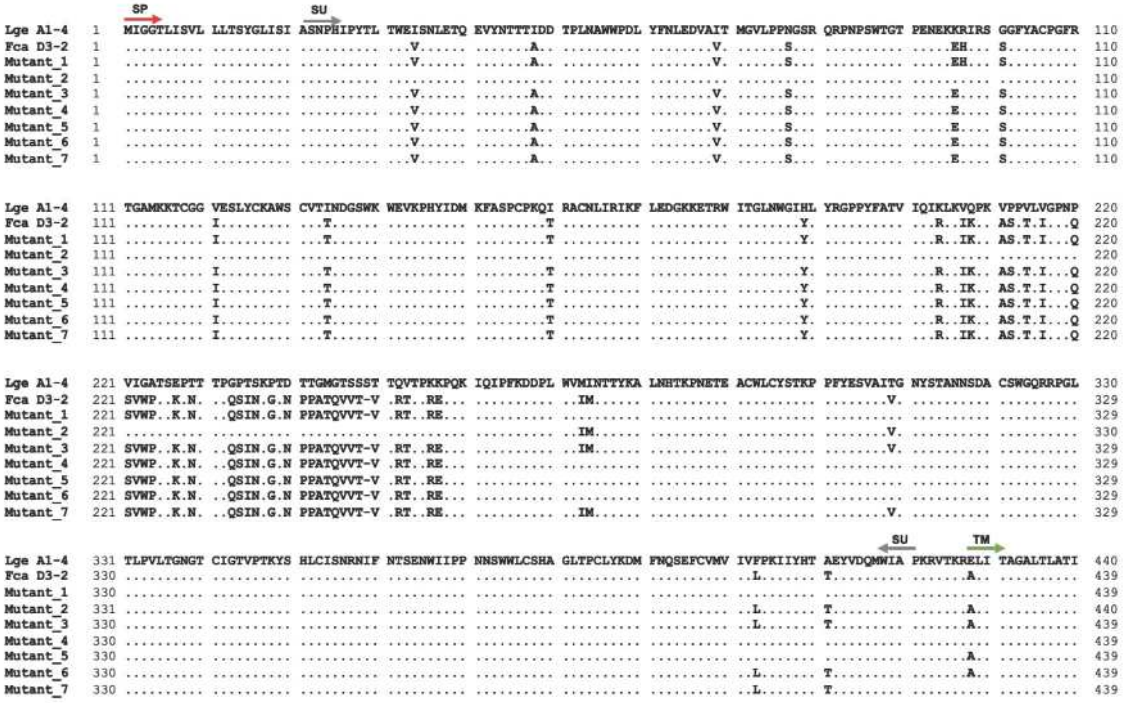

Fig. 3.10. Sequence comparison all mutants, Lge A1-4, and Fca D3-2 envelope. Red arrow indicates signal peptide (SP), gray color indicates surface unit region (SU), and green color indicates transmembrane region (TM).

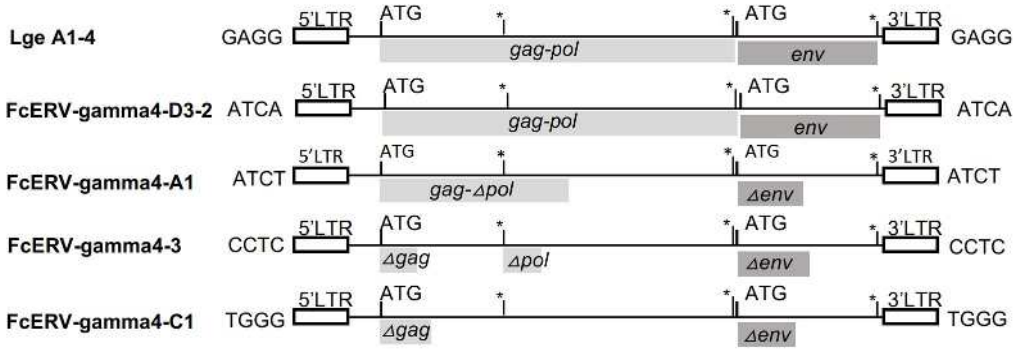

Fig. 3.11. Schematic figure of truncated gamma4(-A1, -C1, -3), Lge A1-4, and Fca D3-2. Light gray color indicates gag pol open reading frame and dark gray color indicates envelope open reading frame. Target site duplication is mentioned before 5'LTR and after 3'LTR.

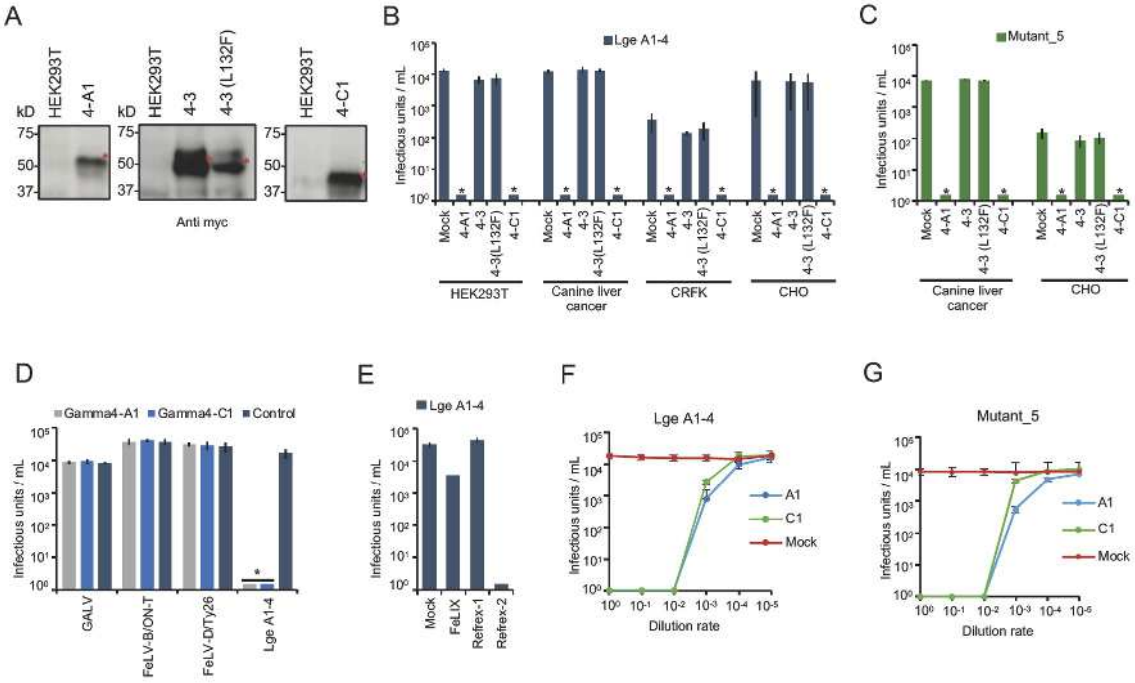

Fig. 3.12. Identification function of Truncated Gamma4. (A) Detection of truncated Gamma4 in supernatant of indicated cell. Red asterisks indicate truncated Env proteins. All truncated were analyzed via immunoprecipitation (IP) using an anti-Myc antibody. (B-C) Inhibitory effect of truncated gamma4 in cell lines. (D-E) Specificity of Refrex-2 against different viruses. (F-G) Dose dependent manner of Refrex-2. Each supernatant was added to the culture for 2 h. Subsequently, cells were infected with the Env-pseudotyped virus. The infectious units (IU) shown on the x-axis were determined by counting the number of log10-galactosidase (LacZ)-positive cells per milliliter (mL) of virus indicated on the y-axis. Virus infection titers with standard deviations represent the means of three independent infection experiments. Comparisons were performed using Student's t-test (*$P < 0.01$).

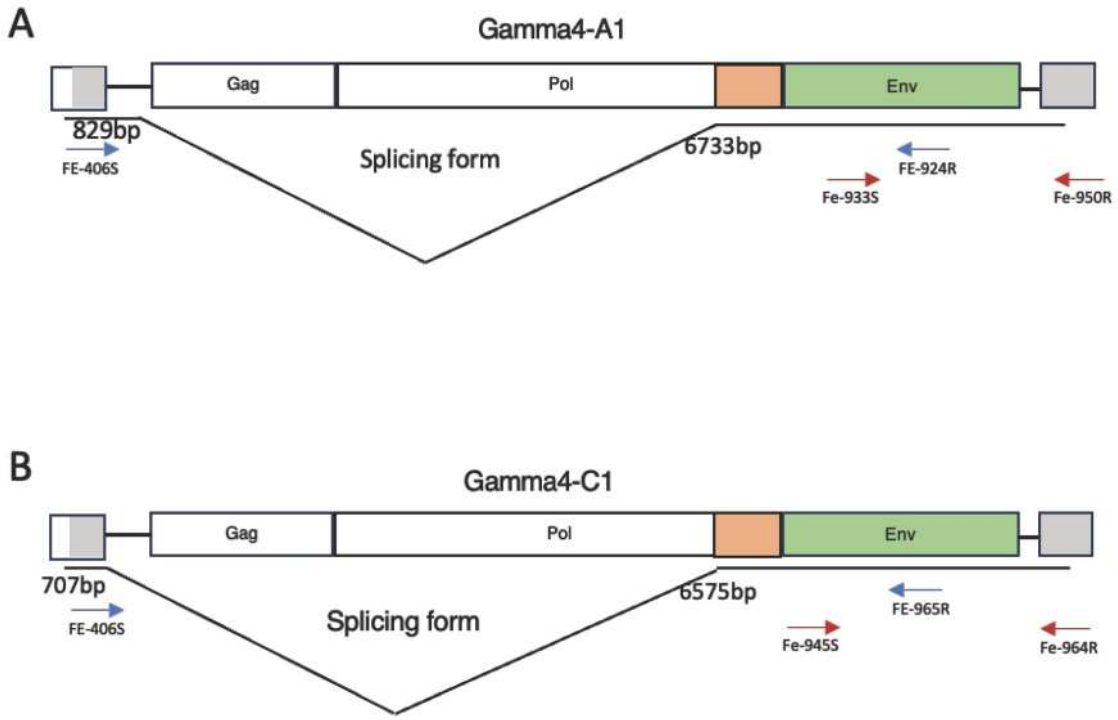

Fig. 3.13. Schematic figure of truncated gamma4-A1 (A) and -C1 (B) transcript. Orange color indicates pol orf, green color indicates envelope orf, gray color indicates LTR sequences.

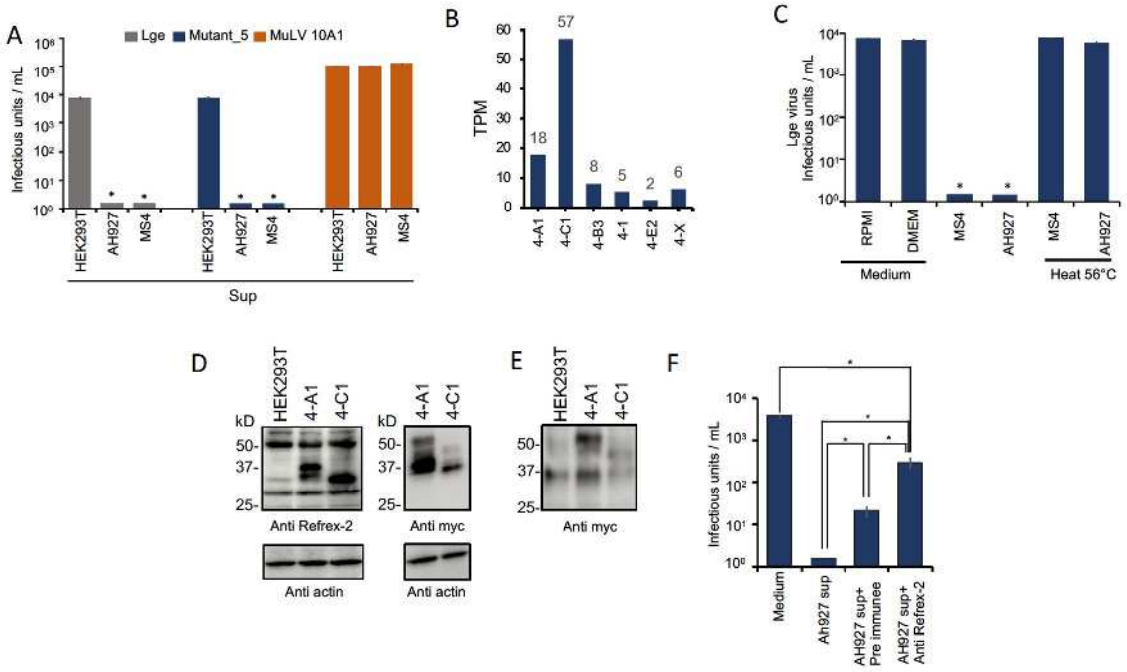

Fig. 3.14. Inhibitory effect of Refrex-2 from AH927 against Gamma4. (A) Inhibitory effect of cultured supernatant cell lines against gamma4. (B) RNA seq expression in AH927 cell lines. (C) Heat inactivation of cultured supernatant of AH927 and MS4. (D) antibody protein expression of Refrex-2 in cells transfected with gamma4-A1 and -C1. (E) Immunoprecipitation of cells supernatants expressed gamma4-A1 and -C1 using anti Refrex-2. (F) The culture supernatants from the AH927 cells were treated with either rabbit anti-Refrex-2 antibody or rabbit preimmune serum (control), after which the culture supernatant from which Refrex-2 was removed and used for the inhibition assays for Gamma4. The infectious units (IU) were determined by counting the number of log10-galactosidase (LacZ)-positive cells per milliliter (mL) of virus (x-axis). Virus infection titers with standard deviations represent the means of three independent experiments. Medium represents the negative control. Comparisons were performed using Student's t-test (*$P < 0.05$).

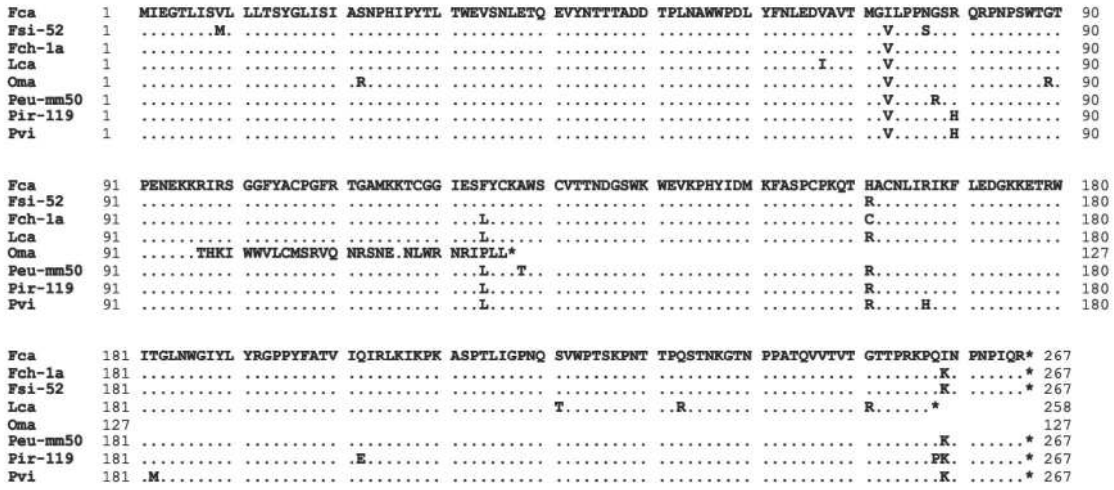

Fig. 3.15. Nucleotide sequence information of truncated gamma4-A1 in felidae genome. Asterisk indicates the stop codon.

```
Fca          1   MIEGTL-SVL LLTSYGLISI ASNPHIPY-- TWEVSNLETQ EVYNTTTADD TPLNAWWPDL YFNLEDVAVT MGVLPPNGSR QRPNPSWTGT 87
Fsi-52       1   ......-... .......... ........TL .......... .......... .......... .......... .......... .......... 89
Fch (JC4)    1   ......I... .......... ........TL .......... .......... .......... .......... .......... .......... 90
Oma          1   ......I... .......... ........TL .......... .......... .......... ........I. .......... .......... 90
Pvi          1   ......I... .......... ........TL .......... .......... .......... .......... .......... .......... 90
Pbe          1   ......I... .......... ........IL .......... .......... .......... .......... .....S.... .......... 90
Peu (TWC4)   1   ......I... .......... ........IL .......... .......... .......... .......... .......... ...D...... 90
Pir-119      1   ......I... .......... ........IL .......... .......... .......... .......... .......... ...D...... 90
Lca          1   ......I... .......... ........TL .......... .......... .......... .......... .......... .......... 90
Lru          1   ......I... .......... ........TL .......... .......... .......... .......... .......... .......... 90
Aju          1   ..G...I... .......... ........TL .......... .......... .......... .......... .......... .......... 90
Pya          1   ......I... .......... ........TL .......... .......... .......... .......... .......... .......... 90
Pco          1   ......I... .......... ........TL .......... .......... .......... .......... .......... .......... 90

Fca         88   PENEKKRIRS GGFYACPGFR TGAMKKTCGG IESLYCKAWS CVTTNDGNWK WEVKPHYIDM KFASPCPKQT RACNLIRIKF LEDGKKETRW 177
Fsi-52      90   .......... .......... .......... .......... .......... .......... .......... .......... .......... 179
Fch (JC4)   91   .......... .......... .......... ...F...... .......... .......... .......... .......... .......... 180
Oma         91   .......... .......... .......... .......... .......S.. .......... .......... .......... .......... 180
Pvi         91   .......... .......... .......... ...F...... .......S.. .......... .......... .......... .......... 180
Pbe         91   .......... .......... .......... ...F...... .......S.. .......... .......... .......... .......... 180
Peu (TWC4)  91   .......... .......... .......... ...F...... .......S.. .......... .......... .......... .......... 180
Pir-119     91   .......... .......... .......... ...F...... .......S.. .......... .......... .......... .......... 180
Lca         91   .......... .......... .......... .......... .......S.. .......... .......... .......... .......... 180
Lru         91   .......... .......... .......... .......... .......S.. .......... .......... .......... .......... 180
Aju         91   .......... .......... .......... .......... .......S.. .......... .......... .......... .......... 180
Pya         91   .......... .......... .......... ......R... .......S.. .......... .......... .......... .......... 180
Pco         91   .......... .......... .......... .......... .......S.. .......... .......... .......... .......... 180

Fca        178   ITGLNWGIYL YRGPPYFATV IQIRLKIKPK ASPTLIGPNQ SVWPTSKPNT TPRSTNKGGL NPGSTRPLG* 246
Fsi-52     180   .......... .......... .......... .......... .......... .......... .........* 248
Fch (JC4)  181   .......... .......... .......... .......... .......... ....QIRVV*           239
Oma        181   .......... F......... .......... .........H .......... .......... .........* 249
Pvi        181   .......... .......... .......... .......... ...S...... ..W....... .........* 249
Pbe        181   .......... .......... .......... .......... .......... ..W....... .....H...* 249
Peu (TWC4) 181   .......... .......... .......... .......... .......... ..W....... .....H...* 249
Pir-119    181   .......... .......... .......... .......... .......... ..W....... .....H...* 249
Lca        181   .......... .......... .......... .....T.... .......... .......... .........* 249
Lru        181   .......... .......... .......... .......... .......... .......... .........* 249
Aju        181   .......... .......... .......... .......... .......... .......... .........* 249
Pya        181   .......... .......... .......... .......... .......... .......... .........* 249
Pco        181   .......... .......... .......... .......... .......... .......... .........* 249
```

Fig. 3.16. Nucleotide sequence information of truncated gamma4-C1 in felidae genome. Asterisk indicates the stop codon.

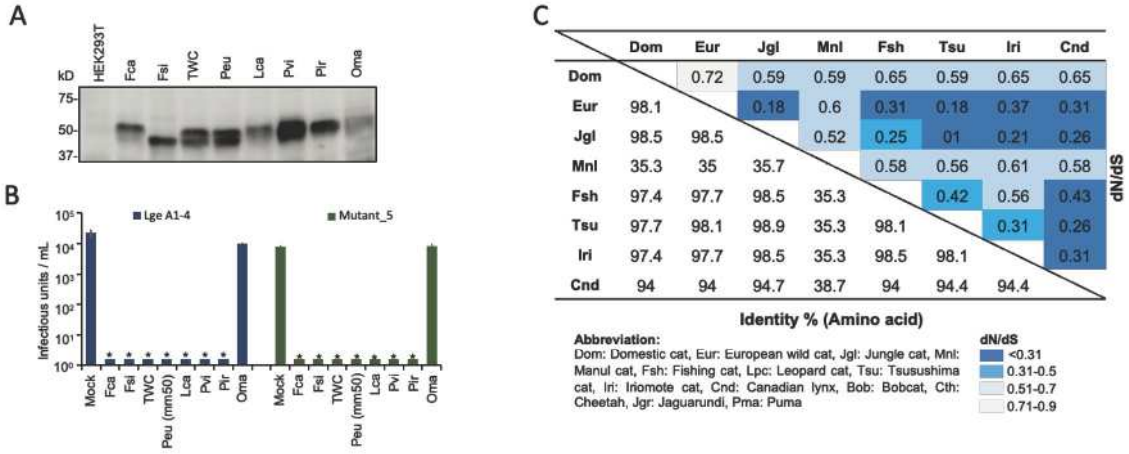

Fig. 3.17. Expression, inhibitory, and selective pressure of Felidae Gamma4-A1. (A) Detection of truncated Gamma4 from different species in supernatant of indicated cell. Red asterisks indicate truncated Env proteins. All truncated were analyzed via immunoprecipitation (IP) using an anti-Myc antibody. (B) Inhibitory effect of Felinae ERV-Gamma4-A1. (C) Sequence conservation and evidence for purifying selection of Felinae ERV-Gamma4-A1 in Felidae. The table shows the pairwise percentages of amino acid sequence identity between Felinae ERV-Gamma4-A1 and the indicated species in the upper triangular area, along with the non-synonymous/synonymous (dN/dS) rate. The pairwise Nei–Gojobori method (168) was used to construct the table.. Color codes are provided below the table for both series of values.

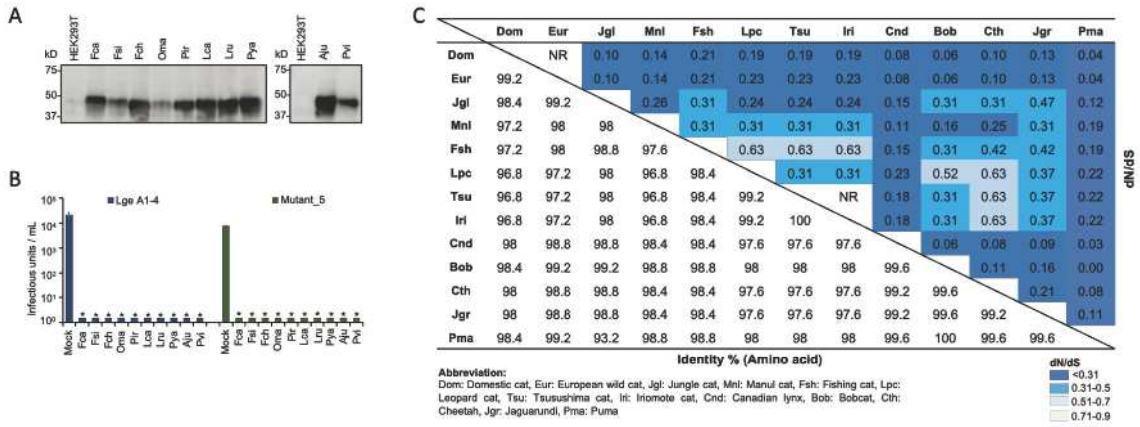

	Dom	Eur	Jgl	Mnl	Fsh	Lpc	Tsu	Iri	Cnd	Bob	Cth	Jgr	Pma
Dom		NR	0.10	0.14	0.21	0.19	0.19	0.19	0.08	0.06	0.10	0.13	0.04
Eur	99.2		0.10	0.14	0.21	0.23	0.23	0.23	0.08	0.06	0.10	0.13	0.04
Jgl	98.4	99.2		0.26	0.31	0.24	0.24	0.24	0.15	0.31	0.31	0.47	0.12
Mnl	97.2	98	98		0.31	0.31	0.31	0.31	0.11	0.16	0.25	0.31	0.19
Fsh	97.2	98	98.8	97.6		0.63	0.63	0.63	0.15	0.31	0.42	0.42	0.19
Lpc	96.8	97.2	98	96.8	98.4		0.31	0.31	0.23	0.52	0.63	0.37	0.22
Tsu	96.8	97.2	98	96.8	98.4	99.2		NR	0.18	0.31	0.63	0.37	0.22
Iri	96.8	97.2	98	96.8	98.4	99.2	100		0.18	0.31	0.63	0.37	0.22
Cnd	98	98.8	98.8	98.4	98.4	97.6	97.6	97.6		0.06	0.08	0.09	0.03
Bob	98.4	99.2	99.2	98.8	98.8	98	98	98	99.6		0.11	0.16	0.00
Cth	98	98.8	98.8	98.4	98.4	97.6	97.6	97.6	99.2	99.6		0.21	0.08
Jgr	98	98.8	98.8	98.4	98.4	97.6	97.6	97.6	99.2	99.6	99.2		0.11
Pma	98.4	99.2	93.2	98.8	98.8	98	98	98	99.6	100	99.6	99.6	

Fig. 3.18. Expression, inhibitory, and selective pressure of Felidae Gamma4-C1. (A) Detection of truncated Gamma4 from different species in supernatant of indicated cell. Red asterisks indicate truncated Env proteins. All truncated were analyzed via immunoprecipitation (IP) using an anti-Myc antibody. (B) Inhibitory effect of Felidae ERV-Gamma4-C1. (C) Sequence conservation and evidence for purifying selection of Felidae ERV-Gamma4-C1 in Felidae. The table shows the pairwise percentages of amino acid sequence identity between Felidae ERV-Gamma4-C1 and the indicated species in the upper triangular area, along with the non-synonymous/ synonymous (dN/dS) rate. The pairwise Nei–Gojobori method (168) was used to construct the table.. Color codes are provided below the table for both series of values.

Supplementary table 3.1. Primer used for PCR isolation FcERV-gamma4 orthologues

Provirus locus	Primer name	Sense	Primer Sequence (5'-3')
FcERV-gamma4-1	Fe-672S	Forward	CTGCATCGAAAACCTGACCC
	Fe-242R	Reverse	CACGTGAGAGGCTTGAACAAAT
FcERV-gamma4-B3	Fe-672S	Forward	CTGCATCGAAAACCTGACCC
	Fe-244R	Reverse	CCCTTTTCCAGAGGAGCCTTAT
FcERV-gamma4-3	Fe-307S	Forward	CCTTGAGGGAACTCCAGCAC
	Fe-250R	Reverse	AAGCCCTGCTCTGCCACTC
FcERV-gamma4-A1	Fe-672S	Forward	CTGCATCGAAAACCTGACCC
	Fe-272R	Reverse	CGCCTCTCACCTCTCTCTCA
FcERV-gamma4-C1	Fe-672S	Forward	CTGCATCGAAAACCTGACCC
	Fe-271R	Reverse	TGCTCCACCACTAGCCTCTTT
FcERV-gamma4-E2	Fe-672S	Forward	CTGCATCGAAAACCTGACCC
	Fe-274R	Reverse	CCGCGCAAACATATTGAATG

Supplementary table 3.2. Primer used for Mutant and truncated env construction

Primer name	Primer Sequence (5'-3')
Fe-771S	GCATTTTGCTTTGAATCAGTGGCTC
Fe-796R	ACCGTCAAGTGTTTTTGCACCTAAC
Fe-797S	GGATCCGGATCCAGCATGATCGGAGGAACACTCATTA
Fe-819R	GAAGATCCAAGATTGGCTCTTGAACAGAAGCTGATTAGTGAGGAAGATCTTTAATAGCTAGCGCTAGC
Fe-828S	TTGATGAGTTTGGACAAACCA
Fe-864R	CAAAAAATTCAAATCCCATTC
Fe-833S	ATTCAAATCCCATTCAAAGATGACCCTCTGTGGGTGAT
PFU-1R	TTGATGAGTTTGGACAAACCA
Fe-951R	GATTCAGATTCCCTTCAAAGATG
Fe-934S	GATTCCCTTCAAAGATGACCCCTTATGGGTAATAATGA
FE-867S	CAGAAAATGAAAAAGAGCGCATAAGATCTAGTGGGTT
Fe-897R	CAGAAAATGAAAAAGAGCGCATAAGATCTAGTGGGTT
Fe-848S	ATTCAGATTCCCTTCAAA
Fe-913R	ATTGCCCCTAAGAGAGTGAC
Fe-892S	ATTGCCCCTAAGAGAGTGACTAAGAGAGCACTCATTACT
Fe-879R	CCAAGAGAACCCCAAAAAATTCAGATTCCCTTCAAA
Fe-917R	GAGAATTGGATTATTCCACC
Fe-893S	GAGAATTGGATTATTCCACC
Fe-910R	GAGTATGTAGACCAGATGTGG
Fe-885S	GAGTATGTAGACCAGATGTGGATTGCCCCTAAGAGAGTGAC
Fe-406S	GCYRCTTGGCTTTGACTTA
Fe-924R	AGATGACCCCTTATGGGTAATGATA
Fe-933S	AGAAAACCCCAAATAAATCCAAATCC
Fe-950R	ACTTACGACTCTGGTGGTCTTCTGTG
Fe-965R	CGTGCCTGTAACCTTATTCGTATCA
Fe-945S	ATGATCGAAGGAACACTCAGC
Fe-964R	GCCGCTTGGCTTTGACTTAC
Fe-941S	ACCTGGATCCGCCACCATGATCGAAGGAACACTCAGTGTG
Fe-957R	CTGGTTCAACGCATCCCCTTGGTGAGCAGAAGCTGATCTCCGAGGAGGATCTGTAAGAATTCTGCA
Fe-912S	ACCTGGATCCGCCACCATGATCGAAGGAACACTCA
Fe-935R	ATCCAAATCCCATTCAAAGAGAGCAGAAGCTGATCTCCGAGGAGGATCTGTGAGAATTCTGCA
Fe-946S	ACCTGGATCCGCCACCATGATCGAAGGAACACTCATTAGC
Fe-968R	GTCACAAATAAGGGTGGTTGAGCAGAAGCTGATCTCCGAGGAGGATCTGTGAGAATTCTGCA
Fe-969R	GAGGAATCGAATCCCTCTACTGGAGCAGAAGCTGATCTCCGAGGAGGATCTGTAAGCTAGCTGCA
Fe-947S	GGATCCAGCATGATTGGAGGGACATTGATCTCTGTG
Fe-970R	GGATCCAGCATGATTGGAGGGACATTGATCTCTGTG
Fe-948S	CCCAAAGCTAGTCCCACTCTCACAGGGCCCAATCAGTCCGTATGG
Fe-971R	CCCAAAGCTAGTCCCACTCTCACAGGGCCCAATCAGTCCGTATGG
Fe-949S	ATAGAGTCACTGTACTGCCGAGCCTGGTCATGTGTGACCAC
Fe-927R	ATAGAGTCACTGTACTGCCGAGCCTGGTCATGTGTGACCAC
Fe-961S	ACCTGGATCCGCCACCATGATCGAAGGAACACTCATTAGC
Fe-1001R	CTGGTTCAACGCGTCCCCTTGGTGAGCAGAAGCTGATCTCCGAGGAGGATCTGTAAGAATTCTGCA
Fe-960S	ACCTGGATCCGCCACCATGATCGAAGGAACACTCAGCGTGC
Fe-981R	CTGGTTCAACGCGTCCCCTTGGTTAAGAGCAGAAGCTGATCTCCGAGGAGGATCTGTGAGAATTCTGCA

Supplementary table 3. Primer used for expression of FcERV-Gamma4-C1 and -A1

Primer name	Primer Sequence (5'-3')
Fe-989S	GCATTTTGCTTTGAATCAGTGGCTC
Fe-954R	ACCGTCAAGTGTTTTTGCACCTAAC
Fe-962S	TACTACCAACGATGGAAACTGAA
Fe-982R	TAAGGTTACAGGCACGGGTTT

GENERAL DISCUSSIONS AND CONCLUSIONS

Studying the interaction between viral elements and host systems is important in biomedical research, as these interactions can influence both the endocrine and immune systems. The anterior pituitary (AP) plays a central role in regulating hormone secretion. Both aging and viral infections can disrupt hormone regulation. Compared to humans, the bovine AP is more accessible for study, as it can be collected from slaughterhouses. However, age-related changes in hormone profiles in the bovine AP are not yet well understood. Therefore, investigating AP hormone profiles using RNA-seq can provide valuable insights into the effects of aging. Additionally, viral infections such as SARS-CoV-2 may affect hormone regulation, as its receptor, ACE2, is expressed in the AP, testes, and other reproductive organs. However, the impact of SARS-CoV-2 on hormone regulation in cattle remains poorly documented. To explore this, the spike (S) protein of SARS-CoV-2 was used to examine its effect on hormone secretion in the bovine AP.

Endogenous retroviruses (ERVs) are heritable viral elements integrated into the host genome through germline infection. They are widely recognized as molecular remnants of ancient exogenous retroviruses, providing valuable insights into the long-term co-evolution between viruses and their hosts. This study underscores the remarkable strategies by which ERVs preserve their presence in host genomes through mechanisms such as recombination, reinfection, and replication, and further reveals their potential to be co-opted as functional antiviral elements. Notably, a truncated variant known as Refrex-2 is broadly conserved across the genomes of most Felidae species, suggesting a possible adaptive advantage conferred by this element. This study was designed with two primary objectives. First, I investigated the effects of aging and viral infection using cattle as a model. Second, I explored the evolutionary relationship between endogenous retroviruses (ERV-gamma4 and FeLV) and their hosts in Felidae species, providing insights into host–virus co-evolution.

In Chapter One, I investigated age-associated changes in gene expression in the anterior pituitary (AP) of female Japanese Black cattle revealed that aging significantly alters the transcriptional landscape of the AP. Genes involved in hormone production, immune regulation, and cellular maintenance were differentially expressed between young and old cows. Notably, genes related to gonadotropin secretion, such as LHB and FSHB, showed decreased expression in older animals, suggesting that aging impairs reproductive hormone

synthesis at the AP level. These findings provide new insights hormone profile underlying age-related declines in endocrine function in cattle.

In Chapter Two, I demonstrated that the spike (S) protein of SARS-CoV-2 suppresses gonadotropin secretion in bovine AP explants. The AP expresses ACE2, the cellular receptor for SARS-CoV-2, indicating that it may be a direct target of viral infection or its components. Treatment with spike protein led to reduced secretion of LH and FSH, implicating the S protein in the disruption of pituitary hormone regulation. This suggests that viral proteins can directly influence endocrine function, and highlights a potential mechanism by which SARS-CoV-2 may affect reproductive physiology in mammals, including livestock.

In Chapter Three, In addition, this study also explored the evolutionary and functional roles of endogenous retroviruses (ERVs), particularly FcERV-gamma4, found exclusively in the Felidae lineage. Recombination events involving FcERV-gamma4 may contribute to the emergence of infectious variants like XR-FeLV, which pose a threat to feline health despite their endogenous origin. A key discovery was Refrex-2, a truncated, soluble Env-derived protein likely acting as an antiviral restriction factor across Felidae. Refrex-2 shows structural similarity to known antiviral proteins and is expressed in immune tissues, with evidence of purifying selection supporting its functional importance. These findings highlight a complex interplay between ERVs and host evolution, revealing how ancient viral elements have been repurposed to enhance host antiviral defenses and influence the genomic architecture of modern species.

In conclusion, investigating virus-host interactions using cattle and cats as animal models offers unique advantages for understanding how viruses impact host physiology and evolution. Cattle provide a practical and accessible model for investigating endocrine responses to viral components, such as the SARS-CoV-2 spike protein, which has been shown to alter hormone secretion in the anterior pituitary. Similarly, domestic cats serve as a valuable model for exploring retrovirus dynamics, particularly the evolution and pathogenicity of feline leukemia virus (FeLV) and the role of endogenous retroviruses like FcERV-gamma4. These models enable researchers to examine both acute and long-term effects of viral infection, including immune modulation, viral recombination, and the emergence of host antiviral factors such as Refrex-2. Together, cows and cats offer complementary systems for dissecting virus-host interactions in both physiological and evolutionary contexts, contributing to broader insights relevant to veterinary and comparative biomedical research.

REFERENCES

1. Chen H. 2004. Gene expression by the anterior pituitary gland: effects of age and caloric restriction. Molecular and Cellular Endocrinology 222:21-31.
2. Gunes S, Hekim GN, Arslan MA, Asci R. 2016. Effects of aging on the male reproductive system. J Assist Reprod Genet 33:441-54.
3. van den Beld AW, Kaufman JM, Zillikens MC, Lamberts SWJ, Egan JM, van der Lely AJ. 2018. The physiology of endocrine systems with ageing. Lancet Diabetes Endocrinol 6:647-658.
4. Epelbaum J, Terrien J. 2020. Mini-review: Aging of the neuroendocrine system: Insights from nonhuman primate models. Prog Neuropsychopharmacol Biol Psychiatry 100:109854.
5. Kadokawa H, Kotaniguchi M, Kereilwe O, Kitamura S. 2021. Reduced gonadotroph stimulation by ethanolamine plasmalogens in old bovine brains. Scientific Reports 11:4757.
6. He W, Dai X, Chen X, He J, Yin Z. 2014. Zebrafish pituitary gene expression before and after sexual maturation. J Endocrinol 221:429-40.
7. Ho Y, Hu P, Peel MT, Chen S, Camara PG, Epstein DJ, Wu H, Liebhaber SA. 2020. Single-cell transcriptomic analysis of adult mouse pituitary reveals sexual dimorphism and physiologic demand-induced cellular plasticity. Protein Cell 11:565-583.
8. Wang C, Ma W. 2019. Hypothalamic and pituitary transcriptome profiling using RNA-sequencing in high-yielding and low-yielding laying hens. Scientific Reports 9:10285.
9. Cánovas A, Reverter A, DeAtley KL, Ashley RL, Colgrave ML, Fortes MR, Islas-Trejo A, Lehnert S, Porto-Neto L, Rincón G, Silver GA, Snelling WM, Medrano JF, Thomas MG. 2014. Multi-tissue omics analyses reveal molecular regulatory networks for puberty in composite beef cattle. PLoS One 9:e102551.
10. Dias MM, Cánovas A, Mantilla-Rojas C, Riley DG, Luna-Nevarez P, Coleman SJ, Speidel SE, Enns RM, Islas-Trejo A, Medrano JF, Moore SS, Fortes MR, Nguyen LT, Venus B, Diaz IS, Souza FR, Fonseca LF, Baldi F, Albuquerque LG, Thomas MG, Oliveira HN. 2017. SNP detection using RNA-sequences of candidate genes associated with puberty in cattle. Genet Mol Res 16.
11. Li M, Lu X, Xia H, Zhang C, Wang X, Chen Z, Zhang H, Qu K, Huang B, Moore S, Mao Y, Yang Z. 2019. In-depth characterization of the pituitary transcriptome in Simmental and Chinese native cattle. Domest Anim Endocrinol 66:35-42.
12. Weber KL, Welly BT, Van Eenennaam AL, Young AE, Porto-Neto LR, Reverter A, Rincon G. 2016. Identification of Gene Networks for Residual Feed Intake in Angus Cattle Using Genomic Prediction and RNA-seq. PLoS One 11:e0152274.
13. Pareek CS, Smoczyński R, Kadarmideen HN, Dziuba P, Błaszczyk P, Sikora M, Walendzik P, Grzybowski T, Pierzchała M, Horbańczuk J, Szostak A, Ogluszka M, Zwierzchowski L, Czarnik U, Fraser L, Sobiech P, Wąsowicz K, Gelfand B, Feng Y, Kumar D. 2016. Single Nucleotide Polymorphism Discovery in Bovine Pituitary Gland Using RNA-Seq Technology. PLOS ONE 11:e0161370.

14. Pandey K, Mizukami Y, Watanabe K, Sakaguti S, Kadokawa H. 2017. Deep sequencing of the transcriptome in the anterior pituitary of heifers before and after ovulation. J Vet Med Sci 79:1003-1012.
15. Jamison Jr DA, Anand Narayanan S, Trovão NS, Guarnieri JW, Topper MJ, Moraes-Vieira PM, Zaksas V, Singh KK, Wurtele ES, Beheshti A. 2022. A comprehensive SARS-CoV-2 and COVID-19 review, Part 1: Intracellular overdrive for SARS-CoV-2 infection. European Journal of Human Genetics 30:889-898.
16. Beyerstedt S, Casaro EB, Rangel É B. 2021. COVID-19: angiotensin-converting enzyme 2 (ACE2) expression and tissue susceptibility to SARS-CoV-2 infection. Eur J Clin Microbiol Infect Dis 40:905-919.
17. Sharma GT, Chandra V, Mankuzhy P, Thirupathi Y, Swain DK, Pillai H, Patel SK, Pathak M, Guttula S. 2021. Physiological implications of COVID-19 in reproduction: angiotensin-converting enzyme 2 a key player. Reprod Fertil Dev 33:381-391.
18. Agolli A, Yukselen Z, Agolli O, Patel MH, Bhatt KP, Concepcion L, Halpern J, Alvi S, Abreu R. 2021. SARS-CoV-2 effect on male infertility and its possible pathophysiological mechanisms. Discoveries (Craiova) 9:e131.
19. Moshrefi M, Ghasemi-Esmailabad S, Ali J, Findikli N, Mangoli E, Khalili MA. 2021. The probable destructive mechanisms behind COVID-19 on male reproduction system and fertility. J Assist Reprod Genet 38:1691-1708.
20. Takano H, Suhara T. 2013. [Imaging blood-brain barrier function by using positron emission tomography to evaluate drug penetration into the brain]. Brain Nerve 65:137-43.
21. Pal R. 2020. COVID-19, hypothalamo-pituitary-adrenal axis and clinical implications. Endocrine 68:251-252.
22. Kadokawa H. 2020. Discovery of new receptors regulating luteinizing hormone and follicle-stimulating hormone secretion by bovine gonadotrophs to explore a new paradigm for mechanisms regulating reproduction. Journal of Reproduction and Development 66:291-297.
23. Gu WT, Zhou F, Xie WQ, Wang S, Yao H, Liu YT, Gao L, Wu ZB. 2021. A potential impact of SARS-CoV-2 on pituitary glands and pituitary neuroendocrine tumors. Endocrine 72:340-348.
24. Zhang S, Liu Y, Wang X, Yang L, Li H, Wang Y, Liu M, Zhao X, Xie Y, Yang Y, Zhang S, Fan Z, Dong J, Yuan Z, Ding Z, Zhang Y, Hu L. 2020. SARS-CoV-2 binds platelet ACE2 to enhance thrombosis in COVID-19. J Hematol Oncol 13:120.
25. Greenwood AD, Ishida Y, O'Brien SP, Roca AL, Eiden MV. 2018. Transmission, Evolution, and Endogenization: Lessons Learned from Recent Retroviral Invasions. Microbiol Mol Biol Rev 82.
26. Coffin JM, Hughes SH, Varmus H. 1997. Retroviruses. Cold Spring Harbor Laboratory Press.
27. Coffin JM. 1992. Structure and Classification of Retroviruses, p 19-49. *In* Levy JA (ed), The Retroviridae doi:10.1007/978-1-4615-3372-6_2. Springer US, Boston, MA.
28. Boeke JD, Stoye JP. 1997. Retrotransposons, Endogenous Retroviruses, and the Evolution of Retroelements. *In* Coffin JM, Hughes SH, Varmus HE (ed), Retroviruses, Cold Spring Harbor (NY).

29. Waterston RH, Lindblad-Toh K, Birney E, Rogers J, Abril JF, Agarwal P, Agarwala R, Ainscough R, Alexandersson M, An P, Antonarakis SE, Attwood J, Baertsch R, Bailey J, Barlow K, Beck S, Berry E, Birren B, Bloom T, Bork P, Botcherby M, Bray N, Brent MR, Brown DG, Brown SD, Bult C, Burton J, Butler J, Campbell RD, Carninci P, Cawley S, Chiaromonte F, Chinwalla AT, Church DM, Clamp M, Clee C, Collins FS, Cook LL, Copley RR, Coulson A, Couronne O, Cuff J, Curwen V, Cutts T, Daly M, David R, Davies J, Delehaunty KD, Deri J, Dermitzakis ET, et al. 2002. Initial sequencing and comparative analysis of the mouse genome. Nature 420:520-62.

30. Pontius JU, Mullikin JC, Smith DR, Lindblad-Toh K, Gnerre S, Clamp M, Chang J, Stephens R, Neelam B, Volfovsky N, Schäffer AA, Agarwala R, Narfström K, Murphy WJ, Giger U, Roca AL, Antunes A, Menotti-Raymond M, Yuhki N, Pecon-Slattery J, Johnson WE, Bourque G, Tesler G, O'Brien SJ. 2007. Initial sequence and comparative analysis of the cat genome. Genome Res 17:1675-89.

31. Lander ES, Linton LM, Birren B, Nusbaum C, Zody MC, Baldwin J, Devon K, Dewar K, Doyle M, FitzHugh W, Funke R, Gage D, Harris K, Heaford A, Howland J, Kann L, Lehoczky J, LeVine R, McEwan P, McKernan K, Meldrim J, Mesirov JP, Miranda C, Morris W, Naylor J, Raymond C, Rosetti M, Santos R, Sheridan A, Sougnez C, Stange-Thomann Y, Stojanovic N, Subramanian A, Wyman D, Rogers J, Sulston J, Ainscough R, Beck S, Bentley D, Burton J, Clee C, Carter N, Coulson A, Deadman R, Deloukas P, Dunham A, Dunham I, Durbin R, French L, Grafham D, et al. 2001. Initial sequencing and analysis of the human genome. Nature 409:860-921.

32. Xu X, Zhao H, Gong Z, Han GZ. 2018. Endogenous retroviruses of non-avian/mammalian vertebrates illuminate diversity and deep history of retroviruses. PLoS Pathog 14:e1007072.

33. Johnson WE. 2019. Origins and evolutionary consequences of ancient endogenous retroviruses. Nature Reviews Microbiology 17:355-370.

34. Kozak CA. 2014. Origins of the endogenous and infectious laboratory mouse gammaretroviruses. Viruses 7:1-26.

35. Malfavon-Borja R, Feschotte C. 2015. Fighting fire with fire: endogenous retrovirus envelopes as restriction factors. J Virol 89:4047-50.

36. Lavialle C, Cornelis G, Dupressoir A, Esnault C, Heidmann O, Vernochet C, Heidmann T. 2013. Paleovirology of 'syncytins', retroviral env genes exapted for a role in placentation. Philos Trans R Soc Lond B Biol Sci 368:20120507.

37. Redelsperger F, Raddi N, Bacquin A, Vernochet C, Mariot V, Gache V, Blanchard-Gutton N, Charrin S, Tiret L, Dumonceaux J, Dupressoir A, Heidmann T. 2016. Genetic Evidence That Captured Retroviral Envelope syncytins Contribute to Myoblast Fusion and Muscle Sexual Dimorphism in Mice. PLoS Genet 12:e1006289.

38. Pastuzyn ED, Day CE, Kearns RB, Kyrke-Smith M, Taibi AV, McCormick J, Yoder N, Belnap DM, Erlendsson S, Morado DR, Briggs JAG, Feschotte C, Shepherd JD. 2018. The Neuronal Gene Arc Encodes a Repurposed Retrotransposon Gag Protein that Mediates Intercellular RNA Transfer. Cell 173:275.

39. Ashley J, Cordy B, Lucia D, Fradkin LG, Budnik V, Thomson T. 2018. Retrovirus-like Gag Protein Arc1 Binds RNA and Traffics across Synaptic Boutons. Cell 172:262-274.e11.
40. Heidmann O, Béguin A, Paternina J, Berthier R, Deloger M, Bawa O, Heidmann T. 2017. HEMO, an ancestral endogenous retroviral envelope protein shed in the blood of pregnant women and expressed in pluripotent stem cells and tumors. Proc Natl Acad Sci U S A 114:E6642-e6651.
41. Tarlinton RE, Meers J, Young PR. 2006. Retroviral invasion of the koala genome. Nature 442:79-81.
42. Hanger JJ, Bromham LD, McKee JJ, O'Brien TM, Robinson WF. 2000. The nucleotide sequence of koala (Phascolarctos cinereus) retrovirus: a novel type C endogenous virus related to Gibbon ape leukemia virus. J Virol 74:4264-72.
43. Wilson CA, Wong S, Muller J, Davidson CE, Rose TM, Burd P. 1998. Type C retrovirus released from porcine primary peripheral blood mononuclear cells infects human cells. J Virol 72:3082-7.
44. Kuse K, Ito J, Miyake A, Kawasaki J, Watanabe S, Makundi I, Ngo MH, Otoi T, Nishigaki K. 2016. Existence of Two Distinct Infectious Endogenous Retroviruses in Domestic Cats and Their Different Strategies for Adaptation to Transcriptional Regulation. J Virol 90:9029-45.
45. Anai Y, Ochi H, Watanabe S, Nakagawa S, Kawamura M, Gojobori T, Nishigaki K. 2012. Infectious endogenous retroviruses in cats and emergence of recombinant viruses. J Virol 86:8634-44.
46. Fábryová H, Hron T, Kabíčková H, Poss M, Elleder D. 2015. Induction and characterization of a replication competent cervid endogenous gammaretrovirus (CrERV) from mule deer cells. Virology 485:96-103.
47. Aaronson SA, Stephenson JR. 1976. Endogenous type-C RNA viruses of mammalian cells. Biochim Biophys Acta 458:323-54.
48. Willett BJ, Hosie MJ. 2013. Feline leukaemia virus: half a century since its discovery. Vet J 195:16-23.
49. Hartmann K, Hofmann-Lehmann R. 2020. What's New in Feline Leukemia Virus Infection. Vet Clin North Am Small Anim Pract 50:1013-1036.
50. Hoover EA, Olsen RG, Hardy WD, Jr., Schaller JP, Mathes LE. 1976. Feline leukemia virus infection: age-related variation in response of cats to experimental infection. J Natl Cancer Inst 57:365-9.
51. Grant CK, Essex M, Gardner MB, Hardy WD, Jr. 1980. Natural feline leukemia virus infection and the immune response of cats of different ages. Cancer Res 40:823-9.
52. Jarrett O, Laird HM, Hay D. 1973. Determinants of the Host Range of Feline Leukaemia Viruses. Journal of General Virology 20:169-175.
53. Sarma PS, Log T. 1973. Subgroup classification of feline leukemia and sarcoma viruses by viral interference and neutralization tests. Virology 54:160-169.
54. Takeuchi Y, Vile RG, Simpson G, O'Hara B, Collins MK, Weiss RA. 1992. Feline leukemia virus subgroup B uses the same cell surface receptor as gibbon ape leukemia virus. J Virol 66:1219-22.

55. Tailor CS, Willett BJ, Kabat D. 1999. A Putative Cell Surface Receptor for Anemia-Inducing Feline Leukemia Virus Subgroup C Is a Member of a Transporter Superfamily. Journal of Virology 73:6500-6505.
56. Anderson MM, Lauring AS, Burns CC, Overbaugh J. 2000. Identification of a cellular cofactor required for infection by feline leukemia virus. Science 287:1828-30.
57. Quigley JG, Burns CC, Anderson MM, Lynch ED, Sabo KM, Overbaugh J, Abkowitz JL. 2000. Cloning of the cellular receptor for feline leukemia virus subgroup C (FeLV-C), a retrovirus that induces red cell aplasia. Blood 95:1093-9.
58. Anderson MM, Lauring AS, Robertson S, Dirks C, Overbaugh J. 2001. Feline Pit2 functions as a receptor for subgroup B feline leukemia viruses. J Virol 75:10563-72.
59. Mendoza R, Anderson MM, Overbaugh J. 2006. A putative thiamine transport protein is a receptor for feline leukemia virus subgroup A. J Virol 80:3378-85.
60. Shalev Z, Duffy SP, Adema KW, Prasad R, Hussain N, Willett BJ, Tailor CS. 2009. Identification of a feline leukemia virus variant that can use THTR1, FLVCR1, and FLVCR2 for infection. J Virol 83:6706-16.
61. Miyake A, Kawasaki J, Ngo H, Makundi I, Muto Y, Khan AH, Smith DJ, Nishigaki K. 2019. Reduced Folate Carrier: an Entry Receptor for a Novel Feline Leukemia Virus Variant. J Virol 93.
62. Miyake A, Ngo MH, Wulandari S, Shimojima M, Nakagawa S, Kawasaki J, Nishigaki K. 2022. Convergent evolution of antiviral machinery derived from endogenous retrovirus truncated envelope genes in multiple species. Proc Natl Acad Sci U S A 119:e2114441119.
63. Moser M, Burns CC, Boomer S, Overbaugh J. 1998. The Host Range and Interference Properties of Two Closely Related Feline Leukemia Variants Suggest That They Use Distinct Receptors. Virology 242:366-377.
64. Overbaugh J, Riedel N, Hoover EA, Mullins JI. 1988. Transduction of endogenous envelope genes by feline leukaemia virus in vitro. Nature 332:731-4.
65. Stewart MA, Warnock M, Wheeler A, Wilkie N, Mullins JI, Onions DE, Neil JC. 1986. Nucleotide sequences of a feline leukemia virus subgroup A envelope gene and long terminal repeat and evidence for the recombinational origin of subgroup B viruses. J Virol 58:825-34.
66. Erbeck K, Gagne RB, Kraberger S, Chiu ES, Roelke-Parker M, VandeWoude S. 2021. Feline Leukemia Virus (FeLV) Endogenous and Exogenous Recombination Events Result in Multiple FeLV-B Subtypes during Natural Infection. J Virol 95:e0035321.
67. Ngo MH, AbuEed L, Kawasaki J, Oishi N, Pramono D, Kimura T, Sakurai M, Watanabe K, Mizukami Y, Ochi H, Anai Y, Odahara Y, Umehara D, Kawamura M, Watanabe S, Miyake A, Nishigaki K. 2024. Multiple recombination events between endogenous retroviral elements and feline leukemia virus. J Virol 98:e0140023.
68. Jarrett O, Hardy WD, Jr., Golder MC, Hay D. 1978. The frequency of occurrence of feline leukaemia virus subgroups in cats. Int J Cancer 21:334-7.

69. Watanabe S, Kawamura M, Odahara Y, Anai Y, Ochi H, Nakagawa S, Endo Y, Tsujimoto H, Nishigaki K. 2013. Phylogenetic and structural diversity in the feline leukemia virus env gene. PLoS One 8:e61009.

70. Sheets RL, Pandey R, Jen WC, Roy-Burman P. 1993. Recombinant feline leukemia virus genes detected in naturally occurring feline lymphosarcomas. Journal of Virology 67:3118-3125.

71. Coelho FM, Bomfim MRQ, de Andrade Caxito F, Ribeiro NA, Luppi MM, Costa ÉA, Oliveira ME, Da Fonseca FG, Resende M. 2008. Naturally occurring feline leukemia virus subgroup A and B infections in urban domestic cats. Journal of General Virology 89:2799-2805.

72. Sarma PS, Log T. 1971. Viral interference in feline leukemia-sarcoma complex. Virology 44:352-358.

73. Nakamura M, Sato E, Miura T, Baba K, Shimoda T, Miyazawa T. 2010. Differential diagnosis of feline leukemia virus subgroups using pseudotype viruses expressing green fluorescent protein. J Vet Med Sci 72:787-90.

74. Kawasaki J, Kawamura M, Ohsato Y, Ito J, Nishigaki K. 2017. Presence of a Shared 5'-Leader Sequence in Ancestral Human and Mammalian Retroviruses and Its Transduction into Feline Leukemia Virus. J Virol 91.

75. Malhi PS, Adams GP, Pierson RA, Singh J. 2006. Bovine model of reproductive aging: Response to ovarian synchronization and superstimulation. Theriogenology 66:1257-1266.

76. Xu W, Seok J, Mindrinos MN, Schweitzer AC, Jiang H, Wilhelmy J, Clark TA, Kapur K, Xing Y, Faham M, Storey JD, Moldawer LL, Maier RV, Tompkins RG, Wong WH, Davis RW, Xiao W, Inflammation t, Program HRtIL-SCR, Toner M, Warren S, Schoenfeld DA, Rahme LG, McDonald-Smith GP, Hayden DL, Mason PH, Fagan S, Yu Y-M, Cobb JP, Remick DG, Mannick JA, Lederer JA, Gamelli RL, Silver GM, West MA, Shapiro MB, Smith RD, Camp DG, Qian W, Tibshirani R, Lowry SF, Calvano SE, Chaudry I, Cohen M, Moore EE, Johnson JL, Baker HV, Efron PA, Balis UGJ, Billiar TR, et al. 2011. Human transcriptome array for high-throughput clinical studies. Proceedings of the National Academy of Sciences 108:3707-3712.

77. Nakamura S, Noda K, Miwa M, Minabe S, Hagiwara T, Hirasawa A, Matsuyama S, Moriyama R. 2020. Colocalization of GPR120 and anterior pituitary hormone-producing cells in female Japanese Black cattle. J Reprod Dev 66:135-141.

78. Hoffman JM, Valencak TG. 2020. A short life on the farm: aging and longevity in agricultural, large-bodied mammals. Geroscience 42:909-922.

79. Miyamoto Y, Skarzynski DJ, Okuda K. 2000. Is tumor necrosis factor alpha a trigger for the initiation of endometrial prostaglandin F(2alpha) release at luteolysis in cattle? Biol Reprod 62:1109-15.

80. Harada K, Ferdous T, Watanabe K, Mizukami Y, Mishima K. 2021. Effects of an elemental diet, Elental®, may differ between healthy oral cells and oral cancer cells. Oncol Rep 45:738-751.

81. Wagner GP, Kin K, Lynch VJ. 2012. Measurement of mRNA abundance using RNA-seq data: RPKM measure is inconsistent among samples. Theory in Biosciences 131:281-285.

82. Shimizu F, Ogawa R, Mizukami Y, Watanabe K, Hara K, Kadono C, Takahashi T, Misu T, Takeshita Y, Sano Y, Fujisawa M, Maeda T, Nakashima I, Fujihara K, Kanda T. 2022. GRP78 Antibodies Are Associated With Blood-Brain Barrier Breakdown in Anti-Myelin Oligodendrocyte Glycoprotein Antibody-Associated Disorder. Neurol Neuroimmunol Neuroinflamm 9.

83. Zhou Y, Zhou B, Pache L, Chang M, Khodabakhshi AH, Tanaseichuk O, Benner C, Chanda SK. 2019. Metascape provides a biologist-oriented resource for the analysis of systems-level datasets. Nature Communications 10:1523.

84. Freeman ME, Kanyicska B, Lerant A, Nagy G. 2000. Prolactin: structure, function, and regulation of secretion. Physiol Rev 80:1523-631.

85. Grattan DR. 2015. 60 YEARS OF NEUROENDOCRINOLOGY: The hypothalamo-prolactin axis. J Endocrinol 226:T101-22.

86. Welch JE, Barbee RR, Roberts NL, Suarez JD, Klinefelter GR. 1998. SP22: a novel fertility protein from a highly conserved gene family. J Androl 19:385-93.

87. Benoit AM, McCoy GL, Blake CA. 2005. Localization of fertility factor SP22 to specific cell types within the anterior pituitary gland. Exp Biol Med (Maywood) 230:721-30.

88. Hossain MS, Mineno K, Katafuchi T. 2016. Neuronal Orphan G-Protein Coupled Receptor Proteins Mediate Plasmalogens-Induced Activation of ERK and Akt Signaling. PLoS One 11:e0150846.

89. Nakagawa S, Nguyen Pham KT, Shao X, Doi M. 2020. Time-Restricted G-Protein Signaling Pathways via GPR176, G(z), and RGS16 Set the Pace of the Master Circadian Clock in the Suprachiasmatic Nucleus. Int J Mol Sci 21.

90. Bottoni A, Piccin D, Tagliati F, Luchin A, Zatelli MC, degli Uberti EC. 2005. miR-15a and miR-16-1 down-regulation in pituitary adenomas. J Cell Physiol 204:280-5.

91. Kim J, Kang S, Kwon H, Moon H, Park MC. 2019. Dual functional bioactive-peptide, AIMP1-derived peptide (AdP), for anti-aging. J Cosmet Dermatol 18:251-257.

92. Gore AJ, Philips DP, Miller WL, Bernard DJ. 2005. Differential regulation of follicle stimulating hormone by activin A and TGFB1 in murine gonadotropes. Reproductive Biology and Endocrinology 3:73.

93. Sarkar DK, Kim KH, Minami S. 1992. Transforming growth factor-beta 1 messenger RNA and protein expression in the pituitary gland: its action on prolactin secretion and lactotropic growth. Molecular Endocrinology 6:1825-1833.

94. Boutillier AL, Gaiddon C, Lorang D, Roberts JL, Loeffler JP. 1998. Transcriptional activation of the proopiomelanocortin gene by cyclic AMP-responsive element binding protein. Pituitary 1:33-43.

95. Mayer SI, Willars GB, Nishida E, Thiel G. 2008. Elk-1, CREB, and MKP-1 regulate Egr-1 expression in gonadotropin-releasing hormone stimulated gonadotrophs. J Cell Biochem 105:1267-78.

96. Miller RS, Wolfe A, He L, Radovick S, Wondisford FE. 2012. CREB binding protein (CBP) activation is required for luteinizing hormone beta expression and normal fertility in mice. Mol Cell Biol 32:2349-58.

97. Davis TL, Whitesell JD, Cantlon JD, Clay CM, Nett TM. 2011. Does a Nonclassical Signaling Mechanism Underlie an Increase of Estradiol-Mediated Gonadotropin-Releasing Hormone Receptor Binding in Ovine Pituitary Cells?1. Biology of Reproduction 85:770-778.

98. Fujiwara K, Maliza R, Tofrizal A, Batchuluun K, Ramadhani D, Tsukada T, Azuma M, Horiguchi K, Kikuchi M, Yashiro T. 2014. In situ hybridization analysis of the temporospatial expression of the midkine/pleiotrophin family in rat embryonic pituitary gland. Cell Tissue Res 357:337-44.

99. Koks G, Pfaff AL, Bubb VJ, Quinn JP, Koks S. 2021. At the dawn of the transcriptomic medicine. Exp Biol Med (Maywood) 246:286-292.

100. Ben-Shlomo A, Melmed S. 2022. Hypothalamic Regulation of Anterior Pituitary Function, p 27-50 doi:10.1016/B978-0-323-99899-4.00021-4.

101. Pandey K, Nahar A, Kadokawa H. 2016. Method for isolating pure bovine gonadotrophs from anterior pituitary using magnetic nanoparticles and anti-gonadotropin-releasing hormone receptor antibody. J Vet Med Sci 78:1699-1702.

102. Szarek E, Farrand K, McMillen IC, Young IR, Houghton D, Schwartz J. 2008. Hypothalamic input is required for development of normal numbers of thyrotrophs and gonadotrophs, but not other anterior pituitary cells in late gestation sheep. The Journal of Physiology 586:1185-1194.

103. Hoffmann M, Kleine-Weber H, Schroeder S, Krüger N, Herrler T, Erichsen S, Schiergens TS, Herrler G, Wu NH, Nitsche A, Müller MA, Drosten C, Pöhlmann S. 2020. SARS-CoV-2 Cell Entry Depends on ACE2 and TMPRSS2 and Is Blocked by a Clinically Proven Protease Inhibitor. Cell 181:271-280.e8.

104. Rudolf FO, Kadokawa H. 2015. Cytoplasmic kinases downstream of GPR30 suppress GnRH-induced LH secretion from bovine anterior pituitary cells. Journal of Reproduction and Development advpub.

105. Kereilwe O, Pandey K, Kadokawa H. 2018. Influence of brain plasmalogen changes on gonadotropin secretion from the cultured bovine anterior pituitary cells. Domest Anim Endocrinol 64:77-83.

106. Kereilwe O, Pandey K, Borromeo V, Kadokawa H. 2018. Anti-Müllerian hormone receptor type 2 is expressed in gonadotrophs of postpubertal heifers to control gonadotrophin secretion. Reprod Fertil Dev 30:1192-1203.

107. Luan J, Jin X, Lu Y, Zhang L. 2020. SARS-CoV-2 spike protein favors ACE2 from Bovidae and Cricetidae. J Med Virol 92:1649-1656.

108. Di Teodoro G, Valleriani F, Puglia I, Monaco F, Di Pancrazio C, Luciani M, Krasteva I, Petrini A, Marcacci M, D'Alterio N, Curini V, Iorio M, Migliorati G, Di Domenico M, Morelli D, Calistri P, Savini G, Decaro N, Holmes EC, Lorusso A. 2021. SARS-CoV-2 replicates in respiratory ex vivo organ cultures of domestic ruminant species. Veterinary Microbiology 252:108933.

109. Kadokawa H, Pandey K, Nahar A, Nakamura U, Rudolf FO. 2014. Gonadotropin-releasing hormone (GnRH) receptors of cattle aggregate on the surface of gonadotrophs and are increased by elevated GnRH concentrations. Anim Reprod Sci 150:84-95.

110. Nett TM, Cermak D, Braden T, Manns J, Niswender G. 1987. Pituitary receptors for GnRH and estradiol, and pituitary content of gonadotropins in beef cows. I. Changes during the estrous cycle. Domest Anim Endocrinol 4:123-32.

111. Alhenc-Gelas F, Drueke TB. 2020. Blockade of SARS-CoV-2 infection by recombinant soluble ACE2. Kidney Int 97:1091-1093.

112. Matteri RL, Roser JF, Baldwin DM, Lipovetsky V, Papkoff H. 1987. Characterization of a monoclonal antibody which detects luteinizing hormone from diverse mammalian species. Domestic Animal Endocrinology 4:157-165.

113. Borromeo V, Amsterdam A, Berrini A, Gaggioli D, Dantes A, Secchi C. 2004. Characterization of biologically active bovine pituitary FSH purified by immunoaffinity chromatography using a monoclonal antibody. General and Comparative Endocrinology 139:179-189.

114. Iqbal J, Latchoumanin O, Sari IP, Lang RJ, Coleman HA, Parkington HC, Clarke IJ. 2009. Estradiol-17beta inhibits gonadotropin-releasing hormone-induced Ca2+ in gonadotropes to regulate negative feedback on luteinizing hormone release. Endocrinology 150:4213-20.

115. Sherman EJ, Emmer BT. 2021. ACE2 protein expression within isogenic cell lines is heterogeneous and associated with distinct transcriptomes. Scientific Reports 11:15900.

116. Young JM, Juengel JL, Dodds KG, Laird M, Dearden PK, McNeilly AS, McNatty KP, Wilson T. 2008. The activin receptor-like kinase 6 Booroola mutation enhances suppressive effects of bone morphogenetic protein 2 (BMP2), BMP4, BMP6 and growth and differentiation factor-9 on FSH release from ovine primary pituitary cell cultures. J Endocrinol 196:251-61.

117. Manders EMM, Verbeek FJ, Aten JA. 1993. Measurement of co-localization of objects in dual-colour confocal images. J Microsc 169:375-382.

118. Sviridov D, Miller YI, Ballout RA, Remaley AT, Bukrinsky M. 2020. Targeting Lipid Rafts—A Potential Therapy for COVID-19. Frontiers in Immunology Volume 11 - 2020.

119. Wehmeyer L, Du Toit A, Lang DM, Hapgood JP. 2014. Lipid raft- and protein kinase C-mediated synergism between glucocorticoid- and gonadotropin-releasing hormone signaling results in decreased cell proliferation. J Biol Chem 289:10235-51.

120. Kadihasanoglu M, Aktas S, Yardimci E, Aral H, Kadioglu A. 2021. SARS-CoV-2 Pneumonia Affects Male Reproductive Hormone Levels: A Prospective, Cohort Study. J Sex Med 18:256-264.

121. Han T, Kang J, Li G, Ge J, Gu J. 2020. Analysis of 2019-nCoV receptor ACE2 expression in different tissues and its significance study. Ann Transl Med 8:1077.

122. Sengupta P, Dutta S. 2023. COVID-19 and hypogonadism: secondary immune responses rule-over endocrine mechanisms. Hum Fertil (Camb) 26:182-185.

123. Falkenberg S, Buckley A, Laverack M, Martins M, Palmer MV, Lager K, Diel DG. 2021. Experimental Inoculation of Young Calves with SARS-CoV-2. Viruses 13.

124. Palmer MV, Martins M, Falkenberg S, Buckley A, Caserta LC, Mitchell PK, Cassmann ED, Rollins A, Zylich NC, Renshaw RW, Guarino C, Wagner B, Lager K, Diel DG. 2021. Susceptibility of white-tailed deer (Odocoileus virginianus) to SARS-CoV-2. J Virol 95.

125. Deschepper CF, Crumrine DA, Ganong WF. 1986. Evidence that the gonadotrophs are the likely site of production of angiotensin II in the anterior pituitary of the rat. Endocrinology 119:36-43.

126. D'Onofrio N, Scisciola L, Sardu C, Trotta MC, De Feo M, Maiello C, Mascolo P, De Micco F, Turriziani F, Municinò E, Monctti P, Lombardi A, Napolitano MG, Marino FZ, Ronchi A, Grimaldi V, Hermenean A, Rizzo MR, Barbieri M, Franco R, Campobasso CP, Napoli C, Municinò M, Paolisso G, Balestrieri ML, Marfella R. 2021. Glycated ACE2 receptor in diabetes: open door for SARS-COV-2 entry in cardiomyocyte. Cardiovascular Diabetology 20:99.

127. Rabilloud T. 2009. Membrane proteins and proteomics: love is possible, but so difficult. Electrophoresis 30 Suppl 1:S174-80.

128. Chen Z, Chen X, Bai Y, Diao Z, Liu W. 2020. Angiotensin-converting enzyme-2 improves diabetic nephropathy by targeting Smad7 for ubiquitin degradation. Mol Med Rep 22:3008-3016.

129. Bohaczuk SC, Cassin J, Slaiwa TI, Thackray VG, Mellon PL. 2021. Distal Enhancer Potentiates Activin- and GnRH-Induced Transcription of FSHB. Endocrinology 162.

130. Yang F, Chung AC, Huang XR, Lan HY. 2009. Angiotensin II induces connective tissue growth factor and collagen I expression via transforming growth factor-beta-dependent and -independent Smad pathways: the role of Smad3. Hypertension 54:877-84.

131. Wang LA, de Kloet AD, Smeltzer MD, Cahill KM, Hiller H, Bruce EB, Pioquinto DJ, Ludin JA, Katovich MJ, Raizada MK, Krause EG. 2018. Coupling corticotropin-releasing-hormone and angiotensin converting enzyme 2 dampens stress responsiveness in male mice. Neuropharmacology 133:85-93.

132. Xu W, Stadler CK, Gorman K, Jensen N, Kim D, Zheng H, Tang S, Switzer WM, Pye GW, Eiden MV. 2013. An exogenous retrovirus isolated from koalas with malignant neoplasias in a US zoo. Proc Natl Acad Sci U S A 110:11547-52.

133. Hleihel R, Skayneh H, de Thé H, Hermine O, Bazarbachi A. 2023. Primary cells from patients with adult T cell leukemia/lymphoma depend on HTLV-1 Tax expression for NF-κB activation and survival. Blood Cancer Journal 13:67.

134. Tsatsanis C, Fulton R, Nishigaki K, Tsujimoto H, Levy L, Terry A, Spandidos D, Onions D, Neil JC. 1994. Genetic determinants of feline leukemia virus-induced lymphoid tumors: patterns of proviral insertion and gene rearrangement. Journal of Virology 68:8296-8303.

135. McAllister RM, Nicolson M, Gardner MB, Rongey RW, Rasheed S, Sarma PS, Huebner RJ, Hatanaka M, Oroszlan S, Gilden RV, Kabigting A, Vernon L. 1972. C-Type Virus Released from Cultured Human Rhabdomyosarcoma Cells. Nature New Biology 235:3-6.

136. Martinelli SC, Goff SP. 1990. Rapid reversion of a deletion mutation in moloney murine leukemia virus by recombination with a closely related endogenous provirus. Virology 174:135-144.

137. Stoye JP, Moroni C, Coffin JM. 1991. Virological events leading to spontaneous AKR thymomas. J Virol 65:1273-85.
138. Britten RJ, Davidson EH. 1969. Gene Regulation for Higher Cells: A Theory. Science 165:349-357.
139. Sugimoto J, Schust DJ, Kinjo T, Aoki Y, Jinno Y, Kudo Y. 2019. Suppressyn localization and dynamic expression patterns in primary human tissues support a physiologic role in human placentation. Scientific Reports 9:19502.
140. Ito J, Watanabe S, Hiratsuka T, Kuse K, Odahara Y, Ochi H, Kawamura M, Nishigaki K. 2013. Refrex-1, a soluble restriction factor against feline endogenous and exogenous retroviruses. J Virol 87:12029-40.
141. Pramono D, Takeuchi D, Katsuki M, AbuEed L, Abdillah D, Kimura T, Kawasaki J, Miyake A, Nishigaki K. 2024. FeLIX is a restriction factor for mammalian retrovirus infection. J Virol 98:e0177123.
142. Frank JA, Singh M, Cullen HB, Kirou RA, Benkaddour-Boumzaouad M, Cortes JL, Garcia Pérez J, Coyne CB, Feschotte C. 2022. Evolution and antiviral activity of a human protein of retroviral origin. Science 378:422-428.
143. Bjerregaard B, Talts JF, Larsson L-I. 2011. The endogenous envelope protein syncytin is involved in myoblast fusion. Cell fusions: regulation and control:267-275.
144. Cohen CJ, Lock WM, Mager DL. 2009. Endogenous retroviral LTRs as promoters for human genes: a critical assessment. Gene 448:105-14.
145. Ikeda H, Laigret F, Martin MA, Repaske R. 1985. Characterization of a molecularly cloned retroviral sequence associated with Fv-4 resistance. Journal of Virology 55:768-777.
146. Jung YT, Lyu MS, Buckler-White A, Kozak CA. 2002. Characterization of a polytropic murine leukemia virus proviral sequence associated with the virus resistance gene Rmcf of DBA/2 mice. J Virol 76:8218-24.
147. Wu T, Yan Y, Kozak CA. 2005. Rmcf2, a xenotropic provirus in the Asian mouse species Mus castaneus, blocks infection by polytropic mouse gammaretroviruses. J Virol 79:9677-84.
148. Miyake A, Watanabe S, Hiratsuka T, Ito J, Ngo MH, Makundi I, Kawasaki J, Endo Y, Tsujimoto H, Nishigaki K. 2016. Novel Feline Leukemia Virus Interference Group Based on the env Gene. Journal of Virology 90:4832-4837.
149. Miyake A, Ngo MH, Wulandari S, Shimojima M, Nakagawa S, Kawasaki J, Nishigaki K. 2022. Convergent evolution of antiviral machinery derived from endogenous retrovirus truncated envelope genes in multiple species. Proceedings of the National Academy of Sciences 119:e2114441119.
150. Song N, Jo H, Choi M, Kim JH, Seo HG, Cha SY, Seo K, Park C. 2013. Identification and classification of feline endogenous retroviruses in the cat genome using degenerate PCR and in silico data analysis. J Gen Virol 94:1587-1596.
151. Zhu H, Gifford R, Murcia P. 2018. Distribution, Diversity, and Evolution of Endogenous Retroviruses in Perissodactyl Genomes. Journal of Virology 92.

152. DuBridge RB, Tang P, Hsia HC, Leong P-M, Miller JH, Calos MP. 1987. Analysis of mutation in human cells by using an Epstein-Barr virus shuttle system. Molecular and cellular biology 7:379-387.
153. Lander MR, Chattopadhyay SK. 1984. A Mus dunni cell line that lacks sequences closely related to endogenous murine leukemia viruses and can be infected by ectropic, amphotropic, xenotropic, and mink cell focus-forming viruses. J Virol 52:695-8.
154. Puck TT, Cicciura SJ, Robinson A. 1958. Genetics of somatic mammalian cells. III. Long-term cultivation of euploid cells from human and animal subjects. J Exp Med 108:945-56.
155. Hardy WD, Essex M, McClelland AJ. 1980. Feline Leukemia Virus: Proceedings of the Third International Feline Leukemia Virus Meeting, St. Thomas, United States Virgin Islands, May 5-9, 1980. Elsevier/North-Holland.
156. Crandell RA, Fabricant CG, Nelson-Rees WA. 1973. Development, characterization, and viral susceptibility of a feline (Felis catus) renal cell line (CRFK). In Vitro 9:176-85.
157. Gey G. 1952. Tissue culture studies of the proliferative capacity of cervical carcinoma and normal epithelium. Cancer research 12:264-265.
158. Jainchill JL, Aaronson SA, Todaro GJ. 1969. Murine sarcoma and leukemia viruses: assay using clonal lines of contact-inhibited mouse cells. J Virol 4:549-53.
159. Yasumura Y. 1963. Studies on SV40 virus in tissue culture cells. Nippon Rinsho 21:1201-1215.
160. Quade K. 1979. Transformation of mammalian cells by avian myelocytomatosis virus and avian erythroblastosis virus. Virology 98:461-465.
161. Galtier N, Gouy M, Gautier C. 1996. SEAVIEW and PHYLO_WIN: two graphic tools for sequence alignment and molecular phylogeny. Comput Appl Biosci 12:543-8.
162. Hall T A. 1999. BioEdit : a user-friendly biological sequence alignment editor and analysis program for Windows 95/98/NT. Nucleic Acids Symp Ser 41:95-98.
163. Tamura K, Stecher G, Kumar S. 2021. MEGA11: Molecular Evolutionary Genetics Analysis Version 11. Molecular Biology and Evolution 38:3022-3027.
164. Nei M, Kumar S. 2000. Molecular evolution and phylogenetics. Oxford university press.
165. Aiewsakun P, Katzourakis A. 2015. Endogenous viruses: Connecting recent and ancient viral evolution. Virology 479-480:26-37.
166. Kumar S, Stecher G, Suleski M, Hedges SB. 2017. TimeTree: A Resource for Timelines, Timetrees, and Divergence Times. Molecular Biology and Evolution 34:1812-1819.
167. Edgar RC. 2004. MUSCLE: multiple sequence alignment with high accuracy and high throughput. Nucleic Acids Res 32:1792-7.
168. Nei M, Gojobori T. 1986. Simple methods for estimating the numbers of synonymous and nonsynonymous nucleotide substitutions. Mol Biol Evol 3:418-26.
169. Tamura K, Stecher G, Kumar S. 2021. MEGA11: Molecular Evolutionary Genetics Analysis Version 11. Mol Biol Evol 38:3022-3027.

170. Pramono D, Sugimoto K, Kimura T, Miyake A, Nishigaki K. 2024. Characterization of the endogenous retrovirus-derived placenta-specific soluble protein EnvV-Fca from domestic cats. FEBS Lett 598:1792-1806.
171. Johnson WE, Eizirik E, Pecon-Slattery J, Murphy WJ, Antunes A, Teeling E, O'Brien SJ. 2006. The late Miocene radiation of modern Felidae: a genetic assessment. Science 311:73-7.
172. Stoye JP. 2009. Proviral protein provides placental function. Proc Natl Acad Sci U S A 106:11827-8.
173. Mathes LE, Olsen RG, Hebebrand LC, Hoover EA, Schaller JP, Adams PW, Nichols WS. 1979. Immunosuppressive properties of a virion polypeptide, a 15,000-dalton protein, from feline leukemia virus. Cancer Res 39:950-5.
174. Magiorkinis G, Gifford RJ, Katzourakis A, De Ranter J, Belshaw R. 2012. Env-less endogenous retroviruses are genomic superspreaders. Proceedings of the National Academy of Sciences 109:7385-7390.
175. Marshall LG, Webb SD, Sepkoski JJ, Jr., Raup DM. 1982. Mammalian evolution and the great american interchange. Science 215:1351-7.
176. Levinson B, Khoury G, Vande Woude G, Gruss P. 1982. Activation of SV40 genome by 72-base pair tandem repeats of Moloney sarcoma virus. Nature 295:568-572.
177. Nishigaki K, Hanson C, Thompson D, Yugawa T, Hisasue M, Tsujimoto H, Ruscetti S. 2002. Analysis of the Disease Potential of a Recombinant Retrovirus Containing Friend Murine Leukemia Virus Sequences and a Unique Long Terminal Repeat from Feline Leukemia Virus. Journal of Virology 76:1527-1532.
178. Arrigo S, Yun M, Beemon K. 1987. cis-acting regulatory elements within gag genes of avian retroviruses. Mol Cell Biol 7:388-97.
179. Xie N. 2024. Building a catalogue of short tandem repeats in diverse populations. Nature Reviews Genetics 25:457-457.
180. Anonymous. 2024. Tandem repeats in the long-read sequencing era. Nature Reviews Genetics 25:449-449.
181. Faix PH, Feldman SA, Overbaugh J, Eiden MV. 2002. Host range and receptor binding properties of vectors bearing feline leukemia virus subgroup B envelopes can be modulated by envelope sequences outside of the receptor binding domain. J Virol 76:12369-75.
182. Ito J, Baba T, Kawasaki J, Nishigaki K. 2016. Ancestral Mutations Acquired in Refrex-1, a Restriction Factor against Feline Retroviruses, during its Cooption and Domestication. Journal of Virology 90:1470-1485.
183. Tury S, Chauveau L, Lecante A, Courgnaud V, Battini JL. 2023. A co-opted endogenous retroviral envelope promotes cell survival by controlling CTR1-mediated copper transport and homeostasis. Cell Rep 42:113065.